

UCSF

UC San Francisco Electronic Theses and Dissertations

Title

Developing Covalent Biologics through Genetic Code Expansion for Cancer Therapeutics

Permalink

<https://escholarship.org/uc/item/4h4104s0>

Author

Klauser, Paul Chuang

Publication Date

2023

Peer reviewed|Thesis/dissertation

Developing Covalent Biologics through Genetic Code Expansion for Cancer Therapeutics

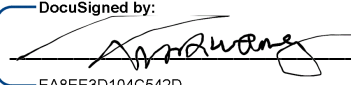
by
Paul Chuang Klauser

DISSERTATION
Submitted in partial satisfaction of the requirements for degree of
DOCTOR OF PHILOSOPHY

in
Chemistry and Chemical Biology

in the
GRADUATE DIVISION
of the
UNIVERSITY OF CALIFORNIA, SAN FRANCISCO

Approved:

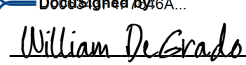
DocuSigned by:

EA8EE3D104C542D...
Lei Wang
Chair

DocuSigned by:

Michael Evans

DocuSigned by:

Roshanak Irannejad

DocuSigned by:

582727E949C7441...
William DeGrado

Committee Members

Copyright 2023

By

Paul Chuang Klauser

Acknowledgements

I am so grateful to everyone at UCSF and the broader scientific community who've supported me during my time in graduate school. First, I would like to thank my Ph.D. advisor, Professor Lei Wang. His guidance and support has allowed me to pursue interesting and impactful scientific questions and for that I owe my deepest gratitude. Your enthusiasm for science and making new discoveries has been a daily inspiration for me.

Thank you to my thesis committee members, Professor Mike Evans, Professor Bill DeGrado, and Professor Roshanak Irannejad. My discussions with all of you have been helpful and informative to push my research forward and to keep me focused. Thank you, Professor Evans, for introducing and welcoming me to the field of radiopharmaceuticals. Your experience and expertise guided me through an exciting collaboration.

I've had the privilege of working with some of the friendliest and patient lab members throughout the years. Thank you to Nanxi Wang and Jun Liu for mentoring me early in my graduate career and helping me design experiments. Thank you to Li Cao, Shanshan Li, and Qingke Li for your helpful scientific discussions. Thank you Bingchen Yu for your patients with me and mentoring me in organic synthesis. Thank you Wei Sun for helping with cloning and molecular biology techniques – my discussions with you, whether science-related or basketball-related, have always been a joy.

A special thank you to my collaborator Shalini Chopra who taught me so much about radiopharmaceuticals and mouse work. Thank you for being patient with me on days where the radiolabeling didn't work, the injections went poorly, or the PET scan failed.

I would also like to acknowledge my CCB cohort and the CCB graduate program community who have been nothing but supportive during my graduate school journey. I am excited to see

where the future takes each and every one of us. Thank you to CCB director, Jason Gestwicki for giving me career advice and helping me navigate my next steps.

I want to thank my parents, Ruth and Tung, for their continuous love and support as I navigate my scientific career. Thank you for pushing me to pursue my dreams and being there for me during highs and lows. Finally, thank you Viktoriya for your love, support, and extraordinary patience. I am very excited for our next steps and new adventures!

Contributions

Portions of chapter 1 of this thesis are a reprint of the material as it appears in:

V. Y. Berdan, † P. C. Klauser, † L. Wang, “Covalent peptides and proteins for therapeutics”, *Bioorg. Med. Chem.* 2021, 29, 115896. DOI: 10.1016/j.bmc.2020.115896

† V.Y.B and P.C.K. are co-first authors of this manuscript.

Chapter 2 of this thesis is a reprint of the material as it appears in:

P. C. Klauser, V. Y. Berdan, L. Cao, L. Wang, “Encoding latent SuFEx reactive meta-fluorosulfate tyrosine to expand covalent bonding of proteins”. *Chem. Commun.* **2022**, 58, 6861-6864. DOI: 10.1039/D2CC01902G

Chapter 3 of this thesis is a reprint of the material as it appears in:

P. C. Klauser, S. Chopra, L. Cao, B. Yu, M. J. Evans, L. Wang, “Covalent Proteins as Targeted Radionuclide Therapies Enhance Antitumor Effects”. *ACS Cent. Sci.* 2023, 9, 1241-1251. DOI: 10.1021/acscentsci.3c00288

Chapter 4 is a manuscript in preparation. The following authors contributed to the study: Devan Diwanji M.D., Ph.D.; Raphael Trenker Ph.D.; Sheamin Khyeam; Rosie Chen; Kliment A. Verba Ph.D.; Guo Huang, Ph.D.; and Natalia Jura, Ph.D.

Developing Covalent Biologics through Genetic Code Expansion for Cancer

Therapeutics

Paul Chuang Klauser

Abstract

Targeted covalent inhibitors have had a major impact on human health and disease. In the past decade, several drugs with a covalent mechanism of action have been approved for the treatment of various cancers. Unfortunately, due to the lack of chemical diversity found naturally in protein biologics, we have been limited to designing covalent inhibitors that are small molecules or peptides. In recent years, however, through the use of genetic code expansion, we have been able to genetically encode new functionalities into proteins. These new functionalities include incorporating bioreactive unnatural amino acids (Uaas) into proteins, which allow for the formation of covalent bonds between binding proteins and their targets. Developing covalent biologics has great implications for the development of novel therapeutics and diagnostic tools. Chapter 1 introduces the reader to the recent chemical advancement of encoding bioreactive Uaas into proteins as well as successful development of anticancer and antiviral covalent protein drugs.

Here, we describe the development of a new electrophilic bioreactive Uaa as well as two applications of protein binders with covalent mechanisms. In chapter 2, we describe the development of genetically encoding a SuFEx reactive meta-fluorosulfate tyrosine (mFSY) into proteins to expand the toolbox of bioreactive Uaas. mFSY has the ability to covalently target different side chain orientations as compared to known fluorosulfate Uaas fluorosulfate-L-tyrosine (FSY) and fluorosulfonyloxy-benzoyl-L-lysine (FSK). Chapter 3 describes the application of covalent biologics for targeted radionuclide therapies. We develop a covalent nanobody that binds to its target irreversibly, achieving exceptional tumor uptake, fast blood clearance, and low

background. This radiolabeled covalent nanobody markedly increases radioisotope levels in tumors and extends tumor residence time while maintaining systematic clearance. Finally, in chapter 4 we demonstrate the selectivity a covalent mechanism of action contributes to protein binding by developing a covalent neuregulin capable of specifically crosslinking with HER4; this covalent binding alters the signaling axis of HER4 in a novel and unexpected manner.

Table of Contents

1. Introduction	1
1.1 Abstract	1
1.2 Overview on Bioreactive Unnatural Amino Acids	1
1.3 Advances in Genetically Encoded Covalent Protein Drugs	6
1.4 References	9
2. Encoding Latent SuFEx Reactive meta-Fluorosulfate Tyrosine to Expand Covalent Bonding of Proteins	15
2.1 Abstract	15
2.2 Introduction	15
2.3 Results	17
2.4 Discussion	26
2.5 Materials and Methods	28
2.6 Supplemental Figures	36
2.7 References	40
3. Covalent Proteins as Targeted Radionuclide Therapies Enhance Antitumor Effects	45
3.1 Abstract	45
3.2 Introduction	46
3.3 Results	49
3.4 Discussion	62
3.5 Materials and Methods	66

3.6 Supplemental Figures	73
3.7 References	80
4. Engineered Covalent Neuregulin Ligand Modulates HER4 Signaling	89
4.1 Abstract	89
4.2 Introduction	89
4.3 Results	91
4.4 Discussion	99
4.5 Material and Methods	102
4.6 Supplemental Figures	107
4.7 References	108

List of Figures

Figure 1.1: Bioreactive Uaas	6
Figure 2.1: mFSY incorporation into proteins in <i>E. coli</i> and mammalian cells via genetic code expansion.	20
Figure 2.2: mFSY facilitates crosslinking between affibody dimer dZ _{HER2} and HER2 receptor.	22
Figure 2.3: mFSY-containing nanobodies crosslink their target proteins.	24
Figure 2.4: Incorporation of mFSY into TrasFab enables first shown instance of Fab-receptor crosslinking with HER2.	26
Figure 2.S1: Selection plates for mFSY-specific synthetase.	36
Figure 2.S2: Western blot analysis of WT-7D12, 7D12(44FSY), and 7D12(44mFSY) incubation with the EGFR receptor.	37
Figure 2.S3: Mass spectra for intact 2Rs15d(37mFSY).	38
Figure 2.S4: ¹ H NMR for mFSY.	39
Figure 2.S5: ¹³ C NMR for mFSY.	39
Figure 3.1: Covalent protein radiopharmaceuticals to enhance efficacy and safety for TRT.	51
Figure 3.2: Genetically encoding FSY in Nb _{HER2} to covalently crosslink HER2 irreversibly <i>in vitro</i>	53
Figure 3.3: Nb _{HER2} (FSY) covalently crosslinked native HER2 on cancer cells and on tumor <i>in vivo</i> .	55
Figure 3.4: Radiolabeled covalent nanobody ¹²⁴ I-Nb _{HER2} (FSY) prolonged tumor retention, increased tumor accumulation and	

exhibited low background in mice.	57
Figure 3.5: α -Emitter labeled covalent $^{225}\text{Ac-Nb}_{\text{HER2}}(\text{FSY})$ inhibited tumor growth in mice without tissue toxicity.	61
Figure 3.S1: Mass Spectrum of $\text{Nb}_{\text{HER2}}(\text{WT})$.	73
Figure 3.S2.: Biolayer interferometry of HER2 and $\text{Nb}_{\text{HER2}}(\text{WT})$ or $\text{Nb}_{\text{HER2}}(\text{FSY})$.	73
Figure 3.S3: Radiochemical yield and purity of $^{124}\text{I-Nb}_{\text{HER2}}(\text{WT})$ and $^{124}\text{I-Nb}_{\text{HER2}}(\text{FSY})$.	74
Figure 3.S4: $^{124}\text{I-Nb}_{\text{HER2}}(\text{WT})$ and $^{124}\text{I-Nb}_{\text{HER2}}(\text{FSY})$ both were cleared from blood rapidly	75
Figure 3.S5: $^{124}\text{I-Nb}_{\text{HER2}}(\text{WT})$ and $^{124}\text{I-Nb}_{\text{HER2}}(\text{FSY})$ showed similar biodistribution in normal organs.	76
Figure 3.S6: Radiochemical yield of $^{225}\text{Ac-Nb}_{\text{HER2}}(\text{WT})$ and $^{225}\text{Ac-Nb}_{\text{HER2}}(\text{FSY})$.	77
Figure 4.1: Selectively targeting HER2/HER4 heterodimer by installing a covalent mechanism in neuregulin.	92
Figure 4.2: Developing NRG1 β (H178FSY) to covalently crosslink HER2/HER4.	94
Figure 4.3: Characterizing receptor selectivity of NRG1 β (H178FSY).	95
Figure 4.4: NRG1 β (H178FSY) inhibits HER2/HER4 signaling.	97
Figure 4.5: NRG1 β (H178FSY) blocks HER2/HER4 activation and inhibits cardiomyocyte cell proliferation.	99
Figure 4.S1: Small mutant screen reveals NRG1 β (H178FSY) crosslinks HER2/HER4 but not HER2/HER3.	107

List of Tables

Table 3.T1: Primers used for cloning Nb _{HER2} (D54TAG)	77
Table 5.T2: Values in Figure 3.S3.	78

1. Introduction

1.1 Abstract

Drugs with a covalent mechanism of action benefit from enhanced potency, selectivity, and *in vivo* efficacy. Historically, the only covalent drugs on the market have been covalent small molecules. However, many proteins and protein-protein interactions cannot be targeted by small molecules due to their lack of small molecule binding pockets and are thus deemed “undruggable.” In order to drug the undruggable, protein therapeutics that can better bind to flat protein surfaces have been developed. Until recently, protein therapeutics have had noncovalent mechanisms of action. The recent advancement of unnatural amino acid chemistry, along with the development of better and more specific electrophilic warheads, has allowed for the application of covalent mechanisms to protein drugs. Covalent protein therapeutics have the potential to benefit from the same advantages that covalent small molecules have over their noncovalent counterparts. Here we provide a brief overview of the chemistry that makes this advancement possible, as well as examples of anticancer and antiviral covalent protein drugs. These examples successfully crosslink their target proteins and have beneficial therapeutic effects.

1.2 Overview on Bioreactive Unnatural Amino Acids

In recent years, there have been major efforts in the fields of drug discovery and chemical biology to develop covalent small molecule drugs.¹⁻³ These drugs provide a unique mechanism of action that gives them certain added advantages when compared to conventional noncovalent binders. Covalent drugs possess a two-step binding mechanism: first, the drug binds to the target through reversible, noncovalent interactions; then, the drug reacts with a residue on the target and

forms a covalent bond, resulting in the final covalent complex.⁴ This additional step of covalent bond formation results in an increased residence time of the drug and a possible off-rate of zero, driving *in vivo* efficacy and more desirable pharmacodynamics.⁵ Furthermore, compared to their noncovalent counterparts, covalent drugs are typically more potent, have higher selectivity, and can potentially avoid certain resistance mechanisms.^{6,7}

Traditionally, only small molecules have been developed into covalent drugs due to their potential for infinite chemical diversity.^{8,9} Strategies to covalently target a protein with a small molecule are only limited by the reactivity of the protein, not the small molecule. Most covalent small molecule drugs target cysteine or lysine residues that are buried in protein pockets or active sites.^{10,11} However, small molecule drugs are generally not suited for binding to smooth and flat protein surfaces or for inhibiting protein-protein interactions (PPIs), which account for the majority of biological activity and interactions in cells. Protein-protein interactions occur across interfaces that can span hundreds of angstroms in area. Small molecule drugs are more apt for binding specifically in distinct pockets than to these vast surfaces.^{9,12} In order to address this gap in the field, many have started to develop protein drugs instead, where protein drugs are able to bind specifically to large surface areas.^{13,14} While progress continues to be made in the fields of protein drug development, protein therapeutics could benefit from the potential advantages of having a covalent mechanism. Protein therapeutics that can bind covalently to their target of interest could have improved pharmacodynamic properties that make them desirable drug candidates.

The development of covalent protein therapeutics can, in theory, provide the same advantages as covalent small molecule and peptide drugs. These potential advantages include ‘infinitely high’ affinity, better selectivity, and enhanced pharmacodynamic properties.⁴ Antibodies can form covalent bonds with small molecule antigens when the latter contain or are modified with warheads

to react with natural residues of the antibody,^{15,16} yet this approach cannot enable covalent binding of protein antigens, because target proteins usually cannot be modified *in vivo* in therapeutics. In a reverse manner, Holm et al. were able to conjugate a weakly electrophilic acrylamide onto an affibody,¹⁷ and showed that the affibody forms a covalent complex with its substrate protein ZSPA through the reaction of the attached acrylamide with either a Cys, His, or Lys residue on ZSPA. The covalent affibody has good specificity towards the target protein both *in vitro* and on mammalian cell surfaces expressing the target protein, improving the detection sensitivity of ELISA and stability in cell surface imaging. Unfortunately, the covalent bond formation with Lys and His has a slow rate and a low yield, and introduction of the electrophilic warhead via Cys conjugation is not generally applicable to other proteins. Moreover, the specificity and performance of the covalent affibody *in vivo*, which are critical to drug development, have not been evaluated.

A general site-specific method for incorporating unnatural amino acids (Uaas) into proteins in live systems is genetic code expansion, which uses an orthogonal pair of tRNA and aminoacyl-tRNA synthetase (aaRS) to translationally incorporate the desired Uaa into proteins.¹⁸⁻²⁰ To be compatible with live cells or systems, Uaas genetically incorporated in the past have contained functional groups that are either chemically inert, bio-orthogonal, or caged, that is, they are non-bioreactive.²¹⁻²³ Genetically encoding a bioreactive Uaa itself is a conundrum:²⁴ to form a new covalent bond between the side chains of a Uaa and a natural amino acid, the Uaa must be reactive toward the target natural amino acid. However, the ubiquitous presence of the natural amino acid in proteins and inside cells could result in nonspecific linkages, which may trap the Uaa during translation and/or cause cytotoxicity.

This impasse of bioreactivity and selectivity has been overcome elegantly through the concept of proximity-enabled bioreactivity initially proposed and demonstrated by Xiang et al.²⁵ Specifically, the reactivity of the Uaa is fine-tuned so that it does not react with free natural amino acids and other biomolecules under physiological conditions, thereby permitting genetic incorporation *in vivo* via endogenous translational machinery. When the Uaa comes into proximity to its target natural residue in proteins while in the appropriate orientation, the increased local effective concentration then facilitates the Uaa to selectively react with the side chain of the target natural residue to create a covalent bond. Xiang et al. designed and incorporated the first bioreactive Uaa, p-2'-fluoroacetyl-phenylalanine (Ffact), to target Cys.²⁵ When introduced at the binding interface of an affibody and its substrate protein, Ffact specifically reacts with a proximal Cys to generate a covalent complex of the two proteins. Ffact has also been incorporated into fluorescent proteins to generate covalent bonds with Cys intramolecularly in live cells, improving the photon output and photostability of the proteins, and into a GPCR expressed on live mammalian cell surfaces in order to pinpoint receptor-peptide ligand interactions.

The work of Xiang et al. opens the gate to the incorporation of bioreactive Uaas into proteins via genetic code expansion. A range of bioreactive Uaas have subsequently been incorporated to covalently target different natural residues, such as Uaas containing haloalkanes, perfluorobenzene, or fluoroacetamide to target Cys,^{26,27-31} vinyl sulphonamide or phenyl isothiocyanate to target Lys,^{32,33} and aryl carbamate to target Lys/Cys/Tyr³⁴. These bioreactive Uaas have largely been used to study protein-protein interactions *in vitro* and in cells.

To develop covalent protein drugs, the bioreactive Uaa needs to meet more stringent requirements: these Uaas must be chemically inert *in vivo*; they must efficiently react with the target residue before target dissociation; and they must have no cytotoxicity and no cytotoxic

reaction products or metabolic byproducts. A milestone toward this goal was the design and genetic incorporation of the latent bioreactive Uaa fluorosulfate-L-tyrosine (FSY) by Wang et al.³⁵ Aryl fluorosulfonate installed on small molecules has been shown to be essentially unreactive toward the proteome.³⁶ Wang et al. showed that FSY is nontoxic to mammalian cells, remains inert in proteins inside cells, and is able to react with residues Tyr, His, or Lys in proximity efficiently via SuFEx, generating stable linkages resistant to hydrolysis. Furthermore, FSY has been shown to be able to chemically crosslink RNA when incorporated into an RNA binding protein.³⁷ In addition, the byproduct of the reaction, the fluoride ion, is found in fluoridated salt, milk, and toothpaste, and is excreted through the kidneys, which means it should be nontoxic *in vivo*. Interestingly, the reaction of FSY with Ser and Thr in proximity results in the conversion of the latter into dehydroalanine and dehydrobutyrine, respectively.³⁸

Since the initial development of FSY, several other Uaas have been developed using SuFEx chemistry to crosslink their target residue. Fluorosulfonyloxybenzoyl-L-lysine (FSK) contains a long and flexible linker to target residues unreachable by FSY.³⁹ In addition to protein-protein crosslinking, bioactive Uaa, o-sulfonyl fluoride-O-methyltyrosine (SFY) that bears a sulfonyl fluoride functional group was able to crosslink carbohydrates or RNA when genetically encoded into a sugar binding protein or RNA-binding protein, respectively.^{37,40} Lastly, a fluorine-substituted fluorosulfate-L-tyrosine (FFY) was genetically encoded and enhanced the crosslinking rate over FSY.⁴¹ Chapter 2 will describe the advancement of *meta*-fluorosulfate-L-tyrosine (mFSY) accommodating different target side chain orientations, expanding the range of proteins covalently targetable by latent bioreactive Uaas. Overall, a lot of new bioreactive chemical functionalities have been encoded into proteins for the development of covalent protein drugs (**Fig. 1.1**)

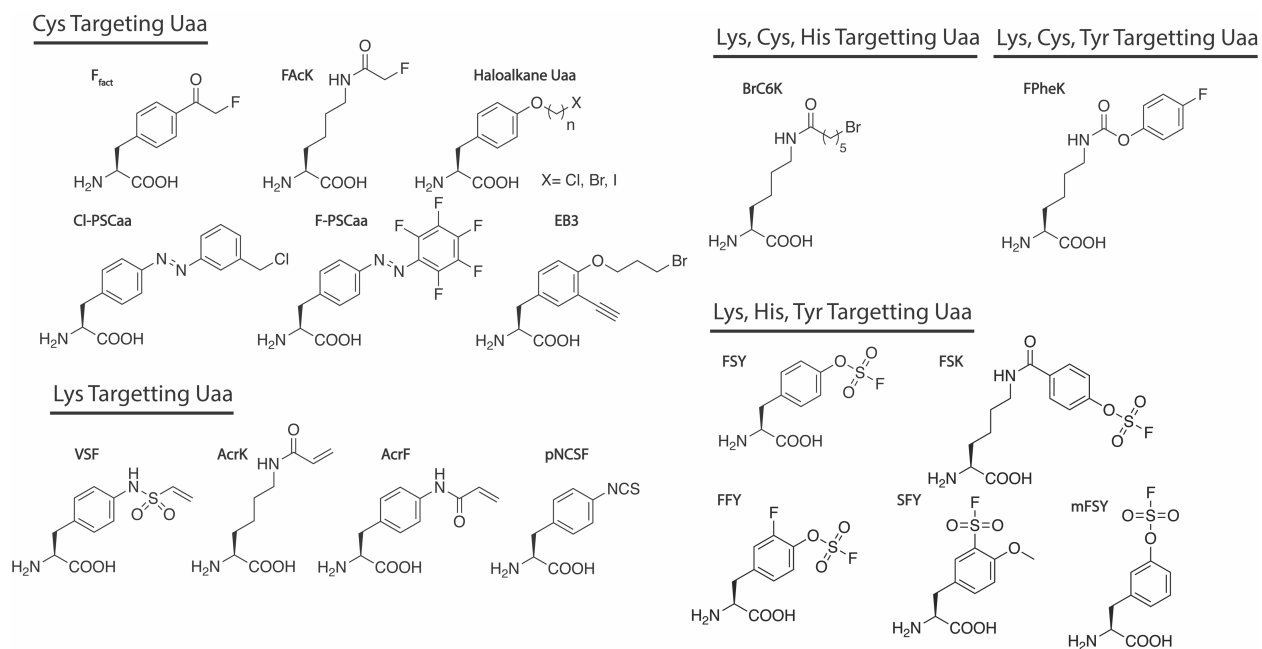


Figure 1.1: Bioreactive Uaas. Latent bioreactive unnatural amino acids that have been successfully incorporated into proteins via genetic code expansion and used to target specific nucleophilic natural residues.

1.3 Advances in Genetically Encoded Covalent Protein Drugs

With the advances in bioreactive Uaas development, several covalent protein drugs have been developed as cancer therapeutics. Li et al.⁴² demonstrated the first successful example of a covalent protein drug by incorporating FSY into the human programmed cell death protein-1 (PD-1) through a general platform technology termed PERx (Proximity-Enabled Reactive Therapeutics). The latent bioreactive Uaa FSY was genetically incorporated into protein PD-1, and, upon PD-1 binding to PD-L1, the Uaa reacted with a natural His residue of the target PD-L1 via proximity-enabled reactivity. This highly specific reactivity resulted in irreversible binding of the PD-1(FSY) drug to the target PD-L1 selectively *in vitro*, on cancer cell surface, and in tumors *in vivo*. The PD-1/PD-L1 interaction inhibited T-lymphocyte proliferation and activity, resulting in exhaustion and apoptosis of tumor-specific T cells. As PD-L1 is often overexpressed in different tumors, Li et al. used PD-1(FSY) to block the PD-1/PD-L1 interaction as cancer immunotherapy. Compared with

the noncovalent PD-1(WT), the covalent PD-1(FSY) significantly enhanced the functional activities of human T cells and CAR-T cells *in vitro*. When administered in tumor xenograft mouse models immune-humanized with human peripheral blood mononuclear cells (PBMCs), human CAR-T cells, or with the advanced systematic bone marrow-liver-thymus humanization, in all cases the covalent protein drug PD-1(FSY) showed an antitumor effect that is markedly more potent than PD-1(WT), with a therapeutic effect equivalent to or better than the anti-PD-L1 monoclonal antibody atezolizumab. In addition, the covalent binding of PD-1(FSY) to PD-L1 showcased that covalent reactivity in PERx necessitates both drug-target binding and Uaa-natural residue pairing, thus uniquely affording unusual specificity and target selectivity. Moreover, irreversible binding through PERx also enabled the direct use of small proteins *in vivo* as protein drugs without worrying about their half-lives. In an alternative strategy to blocking the PD-1/PD-L1 interaction, Zhang et al.⁴³ developed a covalent nanobody chimeras for targeted protein degradation (GlueTac), specifically triggering the internalization and degradation of PD-L1 on cancer cells. The covalent nanobody was conjugated with a cell-penetrating peptide and lysosome-sorting sequence to enhance the lysosomal degradation of the PD-L1 target protein. The GlueTac demonstrate higher PD-L1 degradation over the non-covalent counterpart and higher *in vivo* efficacy.

In another example of covalent protein drugs for immuno-oncology, Li et al.⁴⁰ incorporated SFY into Siglec-7v forming Siglec-7v(127SFY) that can covalently target sialic acids on the cell surface. Sialic acids are upregulated on the cancer cell surface and evade immune surveillance through binding interaction with Siglec-7 on natural killer (NK) cells. By irreversibly crosslinking cell surface sialoglycan, Siglec-7v(127SFY) can block the sialoglycan/Siglec-7 interactions enhancing the NK cell killing of the cancer cells. When hypersialylated cells lines where treated

with Siglec-7v(127SFY), NK-92 cells had enhanced killing of the cancer cells over WT Siglec-7v.

Yu et al.⁴¹ and Han et al.⁴⁴ demonstrated the first example of covalent protein drug as an antiviral agent by developing a covalent nanobody and a covalent minibinder respectively that targets the spike receptor binding domain of severe acute respiratory syndrome coronavirus 2 (SARS-CoV-2). The covalent protein binders enhanced the neutralization efficacy against wild-type SARS-CoV-2 and the Alpha, Delta, Epsilon, Lambda, and Omicron variants. The protein binders with a covalent mechanism displayed several folds higher potency as compared to the noncovalent binder. This work opens the possibility of developing other covalent protein therapeutic for viral infections such as influenza, hepatitis, and AIDS.

Chapter 3 of the present work describes the use of covalent proteins drugs as a radiopharmaceutical that targets human epidermal growth factor receptor (HER2) positive cancers. The covalent nanobody described stays on the tumor much longer compared with the noncovalent counterpart and delivers more radioactivity to the tumor over time. Developing protein drugs has the potential to improve on existing therapeutics and lead to a new generation of biological therapeutics working in the covalent mode.

1.4 References

- (1) Bauer, R. A. Covalent Inhibitors in Drug Discovery: From Accidental Discoveries to Avoided Liabilities and Designed Therapies. *Drug Discov Today* 2015, 20 (9), 1061–1073. <https://doi.org/10.1016/j.drudis.2015.05.005>.
- (2) Johnson, D. S.; Weerapana, E.; Cravatt, B. F. Strategies for Discovering and Derisking Covalent, Irreversible Enzyme Inhibitors. *Future Med Chem* 2010, 2 (6), 949–964. <https://doi.org/10.4155/fmc.10.21>.
- (3) Baillie, T. A. Targeted Covalent Inhibitors for Drug Design. *Angewandte Chemie Int Ed* 2016, 55 (43), 13408–13421. <https://doi.org/10.1002/anie.201601091>.
- (4) Singh, J.; Petter, R. C.; Baillie, T. A.; Whitty, A. The Resurgence of Covalent Drugs. *Nat. Rev. Drug Discov.* 2011, 10 (4), 307–317. <https://doi.org/10.1038/nrd3410>.
- (5) Copeland, R. A. The Drug–Target Residence Time Model: A 10-Year Retrospective. *Nat Rev Drug Discov* 2016, 15 (2), 87–95. <https://doi.org/10.1038/nrd.2015.18>.
- (6) Smith, A. J. T.; Zhang, X.; Leach, A. G.; Houk, K. N. Beyond Picomolar Affinities: Quantitative Aspects of Noncovalent and Covalent Binding of Drugs to Proteins. *J Med Chem* 2009, 52 (2), 225–233. <https://doi.org/10.1021/jm800498e>.
- (7) Hagel, M.; Niu, D.; Martin, T. S.; Sheets, M. P.; Qiao, L.; Bernard, H.; Karp, R. M.; Zhu, Z.; Labenski, M. T.; Chaturvedi, P.; Nacht, M.; Westlin, W. F.; Petter, R. C.; Singh, J. Selective Irreversible Inhibition of a Protease by Targeting a Noncatalytic Cysteine. *Nat Chem Biol* 2011, 7 (1), 22–24. <https://doi.org/10.1038/nchembio.492>.
- (8) Cuesta, A.; Taunton, J. Lysine-Targeted Inhibitors and Chemoproteomic Probes. *Annu Rev Biochem* 2016, 88 (1), 1–17. <https://doi.org/10.1146/annurev-biochem-061516-044805>.

- (9) Gehring, M.; Laufer, S. A. Emerging and Re-Emerging Warheads for Targeted Covalent Inhibitors: Applications in Medicinal Chemistry and Chemical Biology. *J Med Chem* 2018, 62 (12), 5673–5724. <https://doi.org/10.1021/acs.jmedchem.8b01153>.
- (10) Laskowski, R. A.; Luscombe, N. M.; Swindells, M. B.; Thornton, J. M. Protein Clefts in Molecular Recognition and Function. *Protein Sci Publ Protein Soc* 1996, 5 (12), 2438–2452.
- (11) Potashman, M. H.; Duggan, M. E. Covalent Modifiers: An Orthogonal Approach to Drug Design. *J Med Chem* 2009, 52 (5), 1231–1246. <https://doi.org/10.1021/jm8008597>.
- (12) Jones, S.; Thornton, J. M. Principles of Protein-Protein Interactions. *Proc National Acad Sci* 1996, 93 (1), 13–20. <https://doi.org/10.1073/pnas.93.1.13>.
- (13) Milroy, L.-G.; Grossmann, T. N.; Hennig, S.; Brunsveld, L.; Ottmann, C. Modulators of Protein-Protein Interactions. *Chem Rev* 2014, 114 (9), 4695–4748. <https://doi.org/10.1021/cr400698c>.
- (14) Leader, B.; Baca, Q. J.; Golan, D. E. Protein Therapeutics: A Summary and Pharmacological Classification. *Nat Rev Drug Discov* 2008, 7 (1), 21–39. <https://doi.org/10.1038/nrd2399>.
- (15) Barbas, C. F.; Heine, A.; Zhong, G.; Hoffmann, T.; Gramatikova, S.; Björnstedt, R.; List, B.; Anderson, J.; Stura, E. A.; Wilson, I. A.; Lerner, R. A. Immune Versus Natural Selection: Antibody Aldolases with Enzymic Rates But Broader Scope. *Science* 1997, 278 (5346), 2085–2092. <https://doi.org/10.1126/science.278.5346.2085>.
- (16) Chmura, A. J.; Orton, M. S.; Meares, C. F. Antibodies with Infinite Affinity. *Proc National Acad Sci* 2001, 98 (15), 8480–8484. <https://doi.org/10.1073/pnas.151260298>.
- (17) Holm, L.; Moody, P.; Howarth, M. Electrophilic Affibodies Forming Covalent Bonds to Protein Targets. *J Biol Chem* 2009, 284 (47), 32906–32913. <https://doi.org/10.1074/jbc.m109.034322>.

- (18) Wang, L.; Brock, A.; Herberich, B.; Schultz, P. G. Expanding the Genetic Code of *Escherichia Coli*. *Science* 2001, 292 (5516), 498–500. <https://doi.org/10.1126/science.1060077>.
- (19) Wang, L.; Schultz, P. G. Expanding the Genetic Code. *Angewandte Chemie Int Ed* 2004, 44 (1), 34–66. <https://doi.org/10.1002/anie.200460627>.
- (20) Wang, L. Engineering the Genetic Code in Cells and Animals: Biological Considerations and Impacts. *Accounts Chem Res* 2017, 50 (11), 2767–2775. <https://doi.org/10.1021/acs.accounts.7b00376>.
- (21) Liu, C. C.; Schultz, P. G. Adding New Chemistries to the Genetic Code. *Annu Rev Biochem* 2010, 79 (1), 413–444. <https://doi.org/10.1146/annurev.biochem.052308.105824>.
- (22) Liu, J.; Zheng, F.; Cheng, R.; Li, S.; Rozovsky, S.; Wang, Q.; Wang, L. Site-Specific Incorporation of Selenocysteine Using an Expanded Genetic Code and Palladium-Mediated Chemical Deprotection. *J Am Chem Soc* 2018, 140 (28), 8807–8816. <https://doi.org/10.1021/jacs.8b04603>.
- (23) Liu, J.; Li, S.; Aslam, N. A.; Zheng, F.; Yang, B.; Cheng, R.; Wang, N.; Rozovsky, S.; Wang, P. G.; Wang, Q.; Wang, L. Genetically Encoding Photocaged Quinone Methide to Multitarget Protein Residues Covalently in Vivo. *J Am Chem Soc* 2019, 141 (24), 9458–9462. <https://doi.org/10.1021/jacs.9b01738>.
- (24) Wang, L. Genetically Encoding New Bioreactivity. *New Biotechnol* 2017, 38 (Pt A), 16–25. <https://doi.org/10.1016/j.nbt.2016.10.003>.
- (25) Xiang, Z.; Ren, H.; Hu, Y. S.; Coin, I.; Wei, J.; Cang, H.; Wang, L. Adding an Unnatural Covalent Bond to Proteins through Proximity-Enhanced Bioreactivity. *Nat Methods* 2013, 10 (9), 885–888. <https://doi.org/10.1038/nmeth.2595>.

- (26) Hoppmann, C.; Lacey, V. K.; Louie, G. V.; Wei, J.; Noel, J. P.; Wang, L. Genetically Encoding Photoswitchable Click Amino Acids in Escherichia Coli and Mammalian Cells. *Angewandte Chemie Int Ed* 2014, 53 (15), 3932–3936. <https://doi.org/10.1002/anie.201400001>.
- (27) Xiang, Z.; Lacey, V. K.; Ren, H.; Xu, J.; Burban, D. J.; Jennings, P. A.; Wang, L. Proximity-Enabled Protein Crosslinking through Genetically Encoding Haloalkane Unnatural Amino Acids. *Angewandte Chemie Int Ed* 2014, 53 (8), 2190–2193. <https://doi.org/10.1002/anie.201308794>.
- (28) Yang, B.; Tang, S.; Ma, C.; Li, S.-T.; Shao, G.-C.; Dang, B.; DeGrado, W. F.; Dong, M.-Q.; Wang, P. G.; Ding, S.; Wang, L. Spontaneous and Specific Chemical Cross-Linking in Live Cells to Capture and Identify Protein Interactions. *Nat Commun* 2017, 8 (1), 2240. <https://doi.org/10.1038/s41467-017-02409-z>.
- (29) Chen, X.-H.; Xiang, Z.; Hu, Y. S.; Lacey, V. K.; Cang, H.; Wang, L. Genetically Encoding an Electrophilic Amino Acid for Protein Stapling and Covalent Binding to Native Receptors. *Acs Chem Biol* 2014, 9 (9), 1956–1961. <https://doi.org/10.1021/cb500453a>.
- (30) Hoppmann, C.; Maslennikov, I.; Choe, S.; Wang, L. In Situ Formation of an Azo Bridge on Proteins Controllable by Visible Light. *J Am Chem Soc* 2015, 137 (35), 11218–11221. <https://doi.org/10.1021/jacs.5b06234>.
- (31) Kobayashi, T.; Hoppmann, C.; Yang, B.; Wang, L. Using Protein-Confined Proximity To Determine Chemical Reactivity. *J Am Chem Soc* 2016, 138 (45), 14832–14835. <https://doi.org/10.1021/jacs.6b08656>.
- (32) Furman, J. L.; Kang, M.; Choi, S.; Cao, Y.; Wold, E. D.; Sun, S. B.; Smider, V. V.; Schultz, P. G.; Kim, C. H. A Genetically Encoded Aza-Michael Acceptor for Covalent Cross-Linking of Protein–Receptor Complexes. *J Am Chem Soc* 2014, 136 (23), 8411–8417. <https://doi.org/10.1021/ja502851h>.

- (33) Xuan, W.; Li, J.; Luo, X.; Schultz, P. G. Genetic Incorporation of a Reactive Isothiocyanate Group into Proteins. *Angewandte Chemie Int Ed* 2016, 55 (34), 10065–10068. <https://doi.org/10.1002/anie.201604891>.
- (34) Xuan, W.; Shao, S.; Schultz, P. G. Protein Crosslinking by Genetically Encoded Noncanonical Amino Acids with Reactive Aryl Carbamate Side Chains. *Angewandte Chemie Int Ed* 2017, 56 (18), 5096–5100. <https://doi.org/10.1002/anie.201611841>.
- (35) Wang, N.; Yang, B.; Fu, C.; Zhu, H.; Zheng, F.; Kobayashi, T.; Liu, J.; Li, S.; Ma, C.; Wang, P. G.; Wang, Q.; Wang, L. Genetically Encoding Fluorosulfate-1-Tyrosine To React with Lysine, Histidine, and Tyrosine via SuFEx in Proteins in Vivo. *J Am Chem Soc* 2018, 140 (15), 4995–4999. <https://doi.org/10.1021/jacs.8b01087>.
- (36) Chen, W.; Dong, J.; Plate, L.; Mortenson, D. E.; Brighty, G. J.; Li, S.; Liu, Y.; Galmozzi, A.; Lee, P. S.; Hulce, J. J.; Cravatt, B. F.; Saez, E.; Powers, E. T.; Wilson, I. A.; Sharpless, K. B.; Kelly, J. W. Arylfluorosulfates Inactivate Intracellular Lipid Binding Protein(s) through Chemoselective SuFEx Reaction with a Binding Site Tyr Residue. *J Am Chem Soc* 2016, 138 (23), 7353–7364. <https://doi.org/10.1021/jacs.6b02960>.
- (37) Sun, W.; Wang, N.; Liu, H.; Yu, B.; Jin, L.; Ren, X.; Shen, Y.; Wang, L. Genetically Encoded Chemical Crosslinking of RNA in Vivo. *Nat. Chem.* 2023, 15 (1), 21–32. <https://doi.org/10.1038/s41557-022-01038-4>.
- (38) Yang, B.; Wang, N.; Schnier, P. D.; Zheng, F.; Zhu, H.; Polizzi, N. F.; Ittuveetil, A.; Saikam, V.; DeGrado, W. F.; Wang, Q.; Wang, P. G.; Wang, L. Genetically Introducing Biochemically Reactive Amino Acids Dehydroalanine and Dehydrobutyrine in Proteins. *J Am Chem Soc* 2019, 141 (19), 7698–7703. <https://doi.org/10.1021/jacs.9b02611>.

- (39) Liu, J.; Cao, L.; Klauser, P. C.; Cheng, R.; Berdan, V. Y.; Sun, W.; Wang, N.; Ghelichkhani, F.; Yu, B.; Rozovsky, S.; Wang, L. A Genetically Encoded Fluorosulfonyloxybenzoyl-L-lysine for Expansive Covalent Bonding of Proteins via SuFEx Chemistry. *J Am Chem Soc* 2021, 143 (27), 10341–10351. <https://doi.org/10.1021/jacs.1c04259>.
- (40) Li, S.; Wang, N.; Yu, B.; Sun, W.; Wang, L. Genetically Encoded Chemical Crosslinking of Carbohydrate. *Nat. Chem.* 2023, 15 (1), 33–42. <https://doi.org/10.1038/s41557-022-01059-z>.
- (41) Yu, B.; Li, S.; Tabata, T.; Wang, N.; Cao, L.; Kumar, G. R.; Sun, W.; Liu, J.; Ott, M.; Wang, L. Accelerating PERx Reaction Enables Covalent Nanobodies for Potent Neutralization of SARS-CoV-2 and Variants. *Chem* 2022, 8 (10), 2766–2783. <https://doi.org/10.1016/j.chempr.2022.07.012>.
- (42) Li, Q.; Chen, Q.; Klauser, P. C.; Li, M.; Zheng, F.; Wang, N.; Li, X.; Zhang, Q.; Fu, X.; Wang, Q.; Xu, Y.; Wang, L. Developing Covalent Protein Drugs via Proximity-Enabled Reactive Therapeutics. *Cell* 2020, 182 (1), 85-97.e16. <https://doi.org/10.1016/j.cell.2020.05.028>.
- (43) Zhang, H.; Han, Y.; Yang, Y.; Lin, F.; Li, K.; Kong, L.; Liu, H.; Dang, Y.; Lin, J.; Chen, P. R. Covalently Engineered Nanobody Chimeras for Targeted Membrane Protein Degradation. *J. Am. Chem. Soc.* 2021, 143 (40), 16377–16382. <https://doi.org/10.1021/jacs.1c08521>.
- (44) Han, Y.; Yang, Z.; Hu, H.; Zhang, H.; Chen, L.; Li, K.; Kong, L.; Wang, Q.; Liu, B.; Wang, M.; Lin, J.; Chen, P. R. Covalently Engineered Protein Minibinders with Enhanced Neutralization Efficacy against Escaping SARS-CoV-2 Variants. *J. Am. Chem. Soc.* 2022, 144 (13), 5702–5707. <https://doi.org/10.1021/jacs.1c11554>.

2. Encoding Latent SuFEx Reactive *meta*-Fluorosulfate Tyrosine to Expand Covalent Bonding of Proteins

2.1 Abstract

Introduction of new covalent bonds in proteins is affording novel avenues for protein research and applications, yet it remains difficult to generate covalent linkages at all possible sites and across diverse protein classes. Herein, we genetically encoded *meta*-fluorosulfate-L-tyrosine (mFSY) to selectively react with lysine, tyrosine, and histidine via proximity-enabled SuFEx reaction. mFSY was able to target residues elusive to previous Uaas, and permitted engineering of various proteins including affibody, nanobody, and Fab into covalent binders that irreversibly cross-linked EGFR and HER2 receptors. mFSY is thus valuable for developing covalent proteins for biological research, synthetic biology, and biotherapeutics.

2.2 Introduction

Adding new covalent bonding capability to proteins would offer diverse properties unattainable with natural proteins, and would enable novel avenues for researching and engineering proteins and protein-involved biological processes.¹ In recent years, latent bioreactive unnatural amino acids (Uaas) have been designed and site-specifically incorporated into proteins through genetic code expansion.²⁻⁵ These latent bioreactive Uaas react with natural amino acid residues through proximity-enabled reactivity, generating covalent linkages within or between

proteins specifically. The resultant covalent linkages have been harnessed to enhance protein properties, to probe protein interactions, and to develop covalent protein drugs.⁶⁻¹¹ The most challenging aspect of developing a latent bioreactive Uaa is to finely balance its biocompatibility and reactivity.¹² The Uaa should not react with any biomolecules inside cells to avoid off-target reactions and cytotoxicity, while simultaneously being able to react with the target residue in high efficiency under mild cellular conditions.

In fulfilling these demanding requirements, aryl fluorosulfate has emerged as one of the most attractive warheads to use in latent bioreactive Uaas.¹³ Aryl fluorosulfates are quite stable and inert in cells, but become reactive toward weak nucleophiles only when brought into close proximity, proceeding via the sulfur fluoride exchange (SuFEx) click reaction in water, at physiological pH, and without any catalyst or additive needed.¹⁴⁻¹⁶ We previously genetically encoded the first aryl fluorosulfate-containing Uaa, fluorosulfate-L-tyrosine (FSY), demonstrating its ability to selectively crosslink proteins *in vitro* and in cells through SuFEx reaction with proximal Lys, His, or Tyr residues.¹⁷ FSY has been subsequently used to study protein-protein interactions in cells and to develop covalent protein therapeutics.^{9,18} Most recently, we further developed and genetically encoded fluorosulfonyloxybenzoyl-L-lysine (FSK), which has a longer side chain than FSY to achieve a larger radius of reactivity.¹⁹ Nonetheless, we discovered many situations where FSK was too long to be accommodated and FSY's rigid *para*-pointing warhead did not orient toward the target residue for reaction despite the close proximity. To date, only a few proteins have been covalently engineered with FSY and FSK;¹ the general applicability of a SuFEx warhead to diverse proteins still awaits demonstration.

To expand the proximity-enabled SuFEx reactivity to a broader range of proteins with greater site diversity, here we developed another aryl fluorosulfate Uaa, *meta*-fluorosulfate-L-

tyrosine (mFSY). A new orthogonal tRNA/synthetase pair was generated to genetically encode mFSY into proteins in *E. coli* and mammalian cells. Through the incorporation of mFSY, we engineered affibody and nanobody proteins into covalent binders for HER2 and EGFR. We further showcased the first example of generating a covalent Fab irreversibly crosslinked to HER2. Moreover, owing to the *meta* positioning of the fluorosulfate, mFSY was able to react with residues elusive to FSY. These results collectively indicate that mFSY can be generally incorporated into various proteins to expand the covalent engineering of proteins.

2.3 Results

We designed mFSY to complement FSY and FSK and further expand covalent targeting abilities (**Fig. 2.1a**). While FSK has a long and flexible side chain to reach target residues at further distances, FSY is similar to tyrosine in structure and side chain length. Thus, FSK is suitable for use at sites peripheral to a protein-protein binding interface, whereas FSY can be used inside the interface without disrupting the protein interaction. However, the rigid side chain of FSY and the often compact protein binding interface can make FSY unable to react with the target residue when its *para*-fluorosulfate warhead is not oriented toward the target residue despite their close proximity. We reasoned that putting fluorosulfate at the *meta* position, as in mFSY, would allow for the targeting of residues that are unable to react with FSY due to orientation misalignment. In addition, the phenyl ring of mFSY or FSY could rotate around the C β -C γ bond, which would increase the reaction area of fluorosulfate when installed at the *meta* than the *para* position. Using the same warhead, mFSY should have similar reactivity as FSY to target multiple nucleophilic residues via proximity-enabled SuFEx reaction.

mFSY was efficiently synthesized using [4-(acetylamino)phenyl] imidodisulfuryl difluoride (AISF) in two steps.²⁰ To genetically encode mFSY, we evolved an orthogonal tRNA^{Pyl}/synthetase pair for mFSY incorporation in response to the amber stop codon. Using the small-intelligent mutagenesis approach,²¹ residues Ala302, Leu305, Tyr306, Leu309, Ile322, Asn346, Cys348, Tyr384, Val401, and Trp417 of the *Methanosarcina mazei* PylRS were mutated to create a PylRS mutant library, which was subjected to selection as described.^{22,23} A clone showing an mFSY-dependent phenotype was identified (**Fig. 2.S1**), and the synthetase was found to contain the following mutations L305M/I322T/N346G, herein called mFSYRS. To evaluate mFSY incorporation into proteins, we expressed tRNA^{Pyl}/mFSYRS together with the EGFP gene containing a TAG codon at the permissive site 182 in *E. coli*. In the absence of mFSY in the growth media, only background EGFP fluorescence was detected; when 1 mM of mFSY was added, strong EGFP fluorescence was measured with intensity increased over 100-fold (**Fig. 2.1b**), suggesting mFSY incorporation into EGFP. Using the tRNA^{Pyl}/mFSYRS pair, we also incorporated mFSY into a dimeric affibody dZ_{HER2} at site 37 in *E. coli*. Full-length dZ_{HER2} protein was obtained only when mFSY was added to growth media. The purified intact dZ_{HER2}(37mFSY) protein was analyzed by electrospray ionization high-resolution mass spectrometry (**Fig. 2.1c**). A peak observed at 14645.0 Da corresponds to intact dZ_{HER2} containing mFSY at site 37 (expected 14645.0 Da). Notably, no peaks corresponding to dZ_{HER2} containing other amino acids at site 37 were observed. The dZ_{HER2}(37mFSY) protein was further digested and analyzed by tandem MS (**Fig. 2.1d**). A series of b and y ions clearly indicated that mFSY was incorporated at site 37 specified by the TAG codon. These results showed that the evolved tRNA^{Pyl}/mFSYRS pair was able to incorporate mFSY into proteins with high efficiency and specificity in *E. coli*.

We further assessed the incorporation of mFSY in mammalian cells (**Fig. 2.1E**). mFSYRS and tRNA^{PyI} were cloned into a mammalian expression vector then transfected into HeLa-GFP(182TAG) cells, a stable cell line expressing genome-integrated GFP gene with a TAG codon at permissive site 182.²⁴ When 1 mM of mFSY was added to the cell culture, flow cytometric analysis showed that 54.70 % of cells became green fluorescent (**Fig. 2.1e**). Cells cultured without mFSY had negligible background fluorescence, whereas cells cultured with 1 mM mFSY showed 200-fold increase in fluorescence intensity (**Fig. 2.1f**). Fluorescence microscopic images further confirmed that fluorescent full-length GFP was produced in transfected HeLa-GFP(182TAG) cells only when mFSY was added to growth media (**Fig. 2.1g**). These results indicate that the tRNA^{PyI}/mFSYRS pair was able to efficiently incorporate mFSY into GFP in mammalian cells.

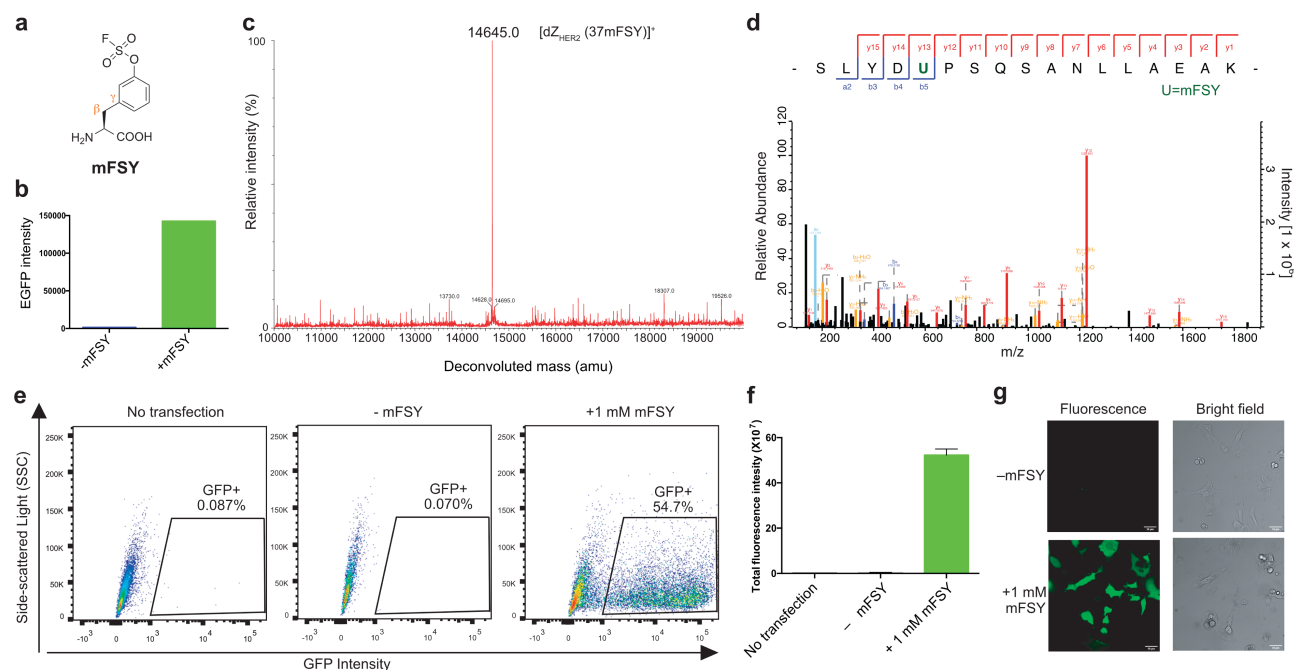


Figure 2.1: mFSY incorporation into proteins in *E. coli* and mammalian cells via genetic code expansion. (A) Structure of mFSY. (B) Fluorescence intensity of *E. coli* cells expressing tRNA^{Pyl}/mFSYRS and EGFP(182TAG) in the absence or presence of 1 mM mFSY. Same number of cells were compared. (C) Mass spectrum of the intact dZ_{HER2} (37mFSY) protein. (D) Tandem mass spectrometric analysis showing the dZ_{HER2} peptide with mFSY clearly incorporated at position 37 (indicated by the green U). (E) Flow cytometric analysis of mFSY incorporation into HeLa-GFP(182TAG) reporter cells. Data is representative of three biological replicates. (F) Total GFP fluorescence intensity from flow cytometric analysis of the same number of HeLa-GFP(182TAG) reporter cells. Error bar: s.d., n = 3. (G) Fluorescence and brightfield microscopic images of HeLa-GFP(182TAG) reporter cells with or without 1 mM mFSY added in cell culture.

To evaluate mFSY as a new latent bioreactive Uaa for creating covalent linkages in proteins, we incorporated it into various protein binders and tested the resultant protein binders' ability to crosslink their targets. First, we incorporated mFSY into an affibody Z_{HER2} specific for the tyrosine kinase receptor HER2. Affibodies are derived from staphylococcal protein A as antibody mimetics and can be evolved to bind different proteins. On the basis of the crystal structure of Z_{HER2} in complex with HER2,²⁵ two sites, D36 and D37, were chosen for mFSY incorporation to target the proximal nucleophilic residue H490 on the HER2 receptor (**Fig. 2.2a**). The dimeric form of Z_{HER2} (dZ_{HER2}) was used to increase the binding affinity ($K_D = 6$ pM),²⁶ and mFSY was incorporated in

the N-terminal Z_{HER2} monomer. mFSY-incorporated dZ_{HER2} proteins were expressed and purified from *E. coli* and incubated with HER2 extracellular domain (ECD) in PBS buffer to allow cross-linking for different time durations, followed by Western blot analysis (**Fig. 2.2b, 2.2c**). FSY was similarly incorporated into dZ_{HER2} for comparison. At both sites, mFSY was shown to efficiently crosslink with the HER2 receptor in a time-dependent manner (**Fig. 2c, 2.2c**). Cross-linking could be detected at 0.5 h. When compared with dZ_{HER2} mutants incorporating FSY at the same site, mFSY mutants crosslinked HER2 with a similar efficiency, suggesting that mFSY was as capable as FSY for certain protein crosslinking purposes. When WT-dZ_{HER2} was added to compete, the crosslinking efficiency of dZ_{HER2}(37mFSY) with HER2 ECD decreased with the increasing concentration of WT-dZ_{HER2} (**Fig. 2.2d**), indicating that the crosslinking was dependent on dZ_{HER2}/HER2 interaction. These results demonstrate that mFSY could be used to engineer affibody proteins into covalent binders.

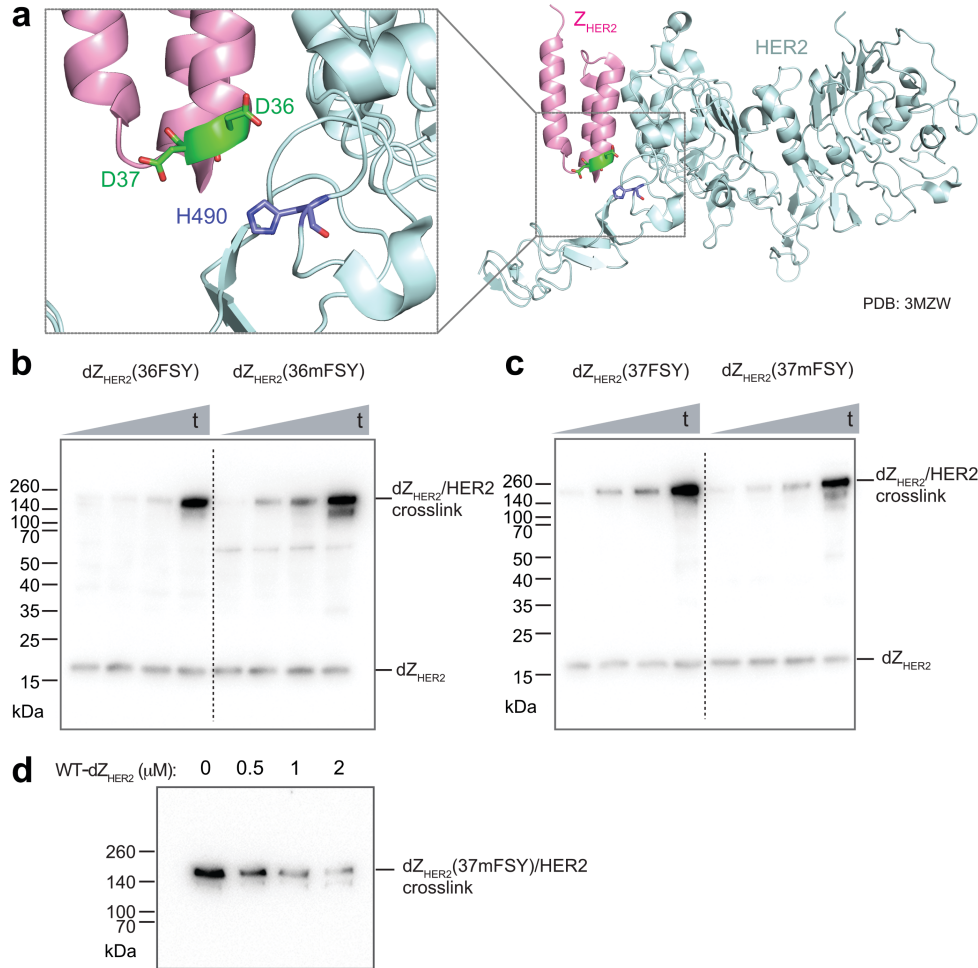


Figure 2.2: mFSY facilitates cross-linking between affibody dZ_{HER2} and HER2 receptor. (A) Structure of affibody Z_{HER2} in complex with the ECD of HER2, showing D36 and D37 on the affibody in proximity to H490 of HER2. (B) Western blot analysis of *in vitro* cross-linking between HER2 ECD and dZ_{HER2}-36FSY or -36mFSY mutant. t: 0.5, 2, 4, and 24 h. (C) Western blot analysis of *in vitro* crosslinking between HER2 ECD and dZ_{HER2}-37FSY or -37mFSY mutant. t: 0.5, 2, 4, and 24 h. (D) Western blot analysis showing that increasing WT-dZ_{HER2} decreased crosslinking between dZ_{HER2}(37mFSY) (1 μM) and HER2 ECD (1 μM).

We next incorporated mFSY into nanobodies, which are single-domain antibodies able to bind different antigens. In one example, we incorporated mFSY into nanobody 7D12, which specifically binds to the epidermal growth factor receptor (EGFR). The structure of 7D12-EGFR complex suggests that E44 of 7D12 is in close proximity to K443 of EGFR (Fig. 2.3a).²⁷ 7D12(44mFSY) mutant protein was purified in *E. coli* and showed robust crosslinking with EGFR

in a higher efficiency (47.3%) than the 7D12(44FSY) mutant (28.7%) and the 7D12(44FSK) mutant (22.3%) (**Fig. 2.3B**). In another example, we incorporated mFSY into nanobody 2Rs15d, which is specific for the HER2 receptor. On the basis of the crystal structure of 2Rs15d-HER2 complex, within the binding interface, Tyr37 of 2Rs15d has its *meta* position oriented toward the hydroxyl of Tyr112 of HER2, while its *para* hydroxyl is pointing away (**Fig. 2.3c**).²⁸ We reasoned that mFSY, but not FSY, incorporated at site 37 should be able to crosslink Tyr112 of HER2. We characterized the purified intact 2Rs15d(37mFSY) protein with mass spectrometry, which showed major monomeric and minor non-crosslinked dimeric 2Rs15d(37mFSY) species (**Fig. 2.S3**). As expected, 2Rs15d(37mFSY) led to crosslinking of the HER2 receptor, whereas 2Rs15d(37FSY) did not (**Fig. 2.3d**), demonstrating the mFSY could complement FSY in crosslinking side chains of different orientation as designed.

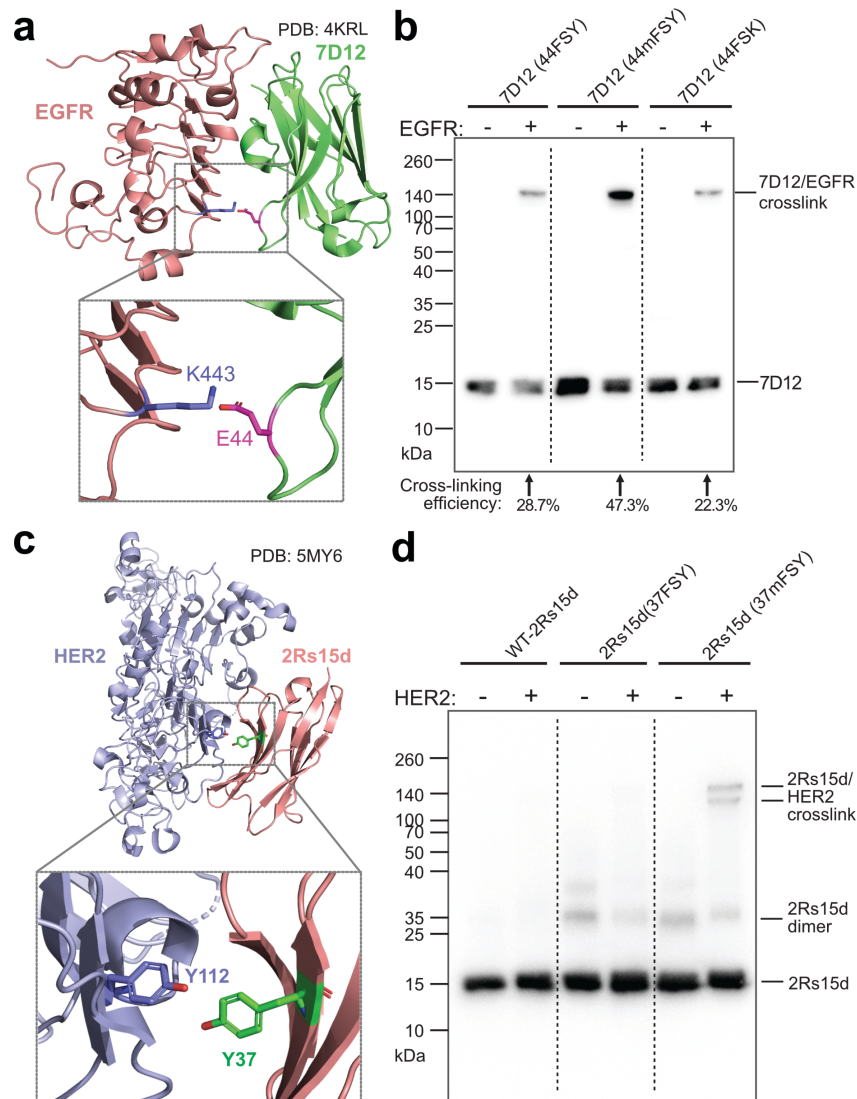


Figure 2.3: mFSY-containing nanobodies crosslink their target proteins. (A) Structure of nanobody 7D12 in complex with EGFR, showing E44 on 7D12 in proximity to K443 of EGFR. (B) Western blot analysis of 7D12(44FSY), 7D12(44mFSY), and 7D12(44FSK) incubated with or without EGFR receptor. Results for WT-7D12 control are shown in Fig. S2. (C) Structure of nanobody 2Rs15d in complex with HER2 ECD. Residue Y37 of 2Rs15d is shown in proximity to residue Y112 of HER2. (D) Western blot analysis of WT and mutant 2Rs15d crosslinking with HER2 ECD *in vitro*. Two crosslinking bands were detected for 2Rs15d(37mFSY), corresponding to its monomeric and dimeric form.

We further incorporated mFSY into the fragment antigen-binding (Fab) region of an antibody to generate covalent Fabs. Fab consists of one constant and one variable domain of each of the heavy and light chain and is a common small binding fragment of monoclonal antibodies

designated for diagnostic and therapeutic use. Trastuzumab is a well-known HER2-specific antibody for treating breast and stomach cancer. We decided to incorporate mFSY into the Trastuzumab Fab, TrasFab. Guided by the structure of TrasFab-HER2 complex,²⁹ we incorporated mFSY into sites Ser50 and Tyr92 on the light chain of TrasFab, aiming to target Lys593 and Lys569 of HER2, respectively (**Fig. 2.4a**). Through simultaneously expressing the heavy and light chains, we were able to produce and purify the mutant Fab proteins from *E. coli* cells. When incubated with the HER2 ECD, TrasFab(50mFSY) showed detectable crosslinking, while TrasFab(92mFSY) showed more robust crosslinking (**Fig. 2.4b**), showcasing that mFSY-mediated crosslinking was site-dependent. Similar time-dependent strong crosslinking was also seen for the TrasFab(92FSY) mutant. These results represent the first example of a Fab that has been engineered to crosslink its target receptor via latent bioreactive Uaas.

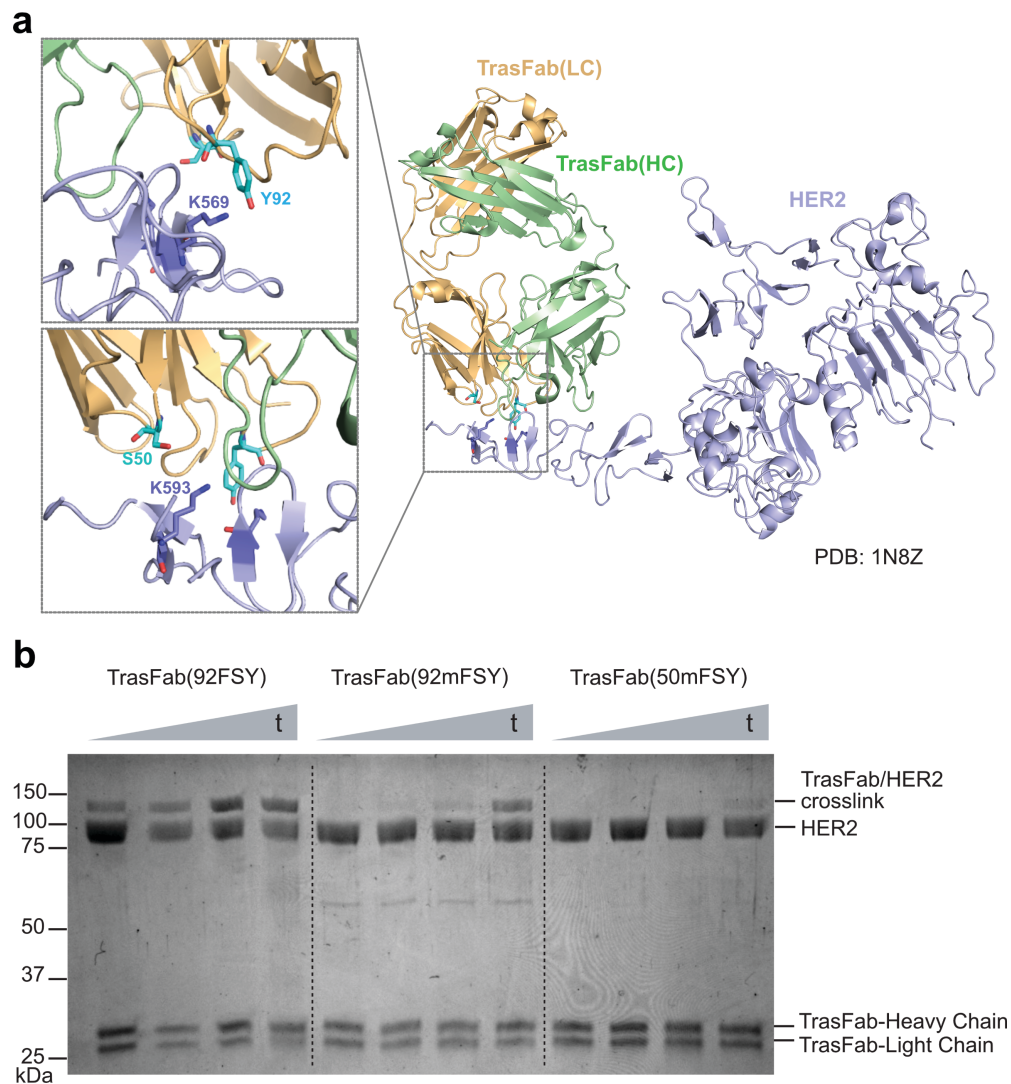


Figure 2.4: Incorporation of mFSY into TrasFab enables first shown instance of Fab-receptor crosslinking with HER2. (A) Structure of Trastuzumab Fab (TrasFab, gold and mint) in complex with HER2 ECD. Residues S50 and Y92 of the TrasFab light chain are shown in proximity to targeted residue K593 and K569 on HER2, respectively. (B) SDS-PAGE analysis of *in vitro* crosslinking between TrasFab mutants and HER2 ECD. t: 0.5, 2, 4, and 24 h.

2.4 Discussion

In summary, we genetically encoded a new latent bioreactive Uaa mFSY into proteins in *E. coli* and mammalian cells. mFSY was efficiently incorporated into various protein binders including an affibody, nanobodies, and most notably the first case of a Fab. These mFSY-engineered proteins crosslinked with their target receptors upon binding through mFSY reacting

with Lys, His, or Tyr residues via proximity-enabled SuFEx reaction. While mFSY generally has comparable crosslinking efficiency with FSY for interchangeable use at some sites, mFSY achieved efficient crosslinking at certain incorporation sites where FSY did not crosslink efficiently. Therefore, mFSY complements FSY in accommodating different target side chain orientations, expanding the proteins covalently targetable by latent bioreactive Uaas. The unique ability of covalent proteins is emerging as recently demonstrated in protein therapeutics^{9,30} and in studying protein-protein interactions.^{19, 31} Possessing the biocompatible multi-targeting fluorosulfate warhead with an expanding reaction orientation, mFSY will be a powerful addition to the arsenal of latent bioreactive Uaas for developing covalent proteins for biological research, synthetic biology, and biotherapeutics.

2.5 Materials and Methods

Reagents and molecular biology

Primers were synthesized and purified by Integrated DNA Technologies (IDT), and plasmids were sequenced by GENEWIZ. All molecular biology reagents were either obtained from New England Biolabs or Vazyme. His-HRP antibody were obtained from ProteinTech Group. pBAD-EGFP, pBAD-dZ_{HER2}, and pBAD-7D12 were used as previously described.^{9,19}

mFSYRS amino acid sequence

DKKPLNTLISATGLWMSRTGTIHKIKHHEVSRSKIYIEMACGDHLVVNNSRSSRTARALR
HHKYRKTCKRCRVSDLEDLNKFLTKANEDQTSVKVKVVSAPTRTKKAMPKSVARAPKP
LENTEAAQAQPSGSKFSPAIPVSTQESVSVPASVSTSISSISTGATASALVKGNTNPITSMS
APVQASAPALTKQTDRLVLLNPKDEISLNSGKPFRELESELLSRRKKDLQQIYAEEREN
YLGKLEREITRFFVDRGFLEIKSPILIPLEYIERMGIDNDTELSKQIFRVDKNFCLRPMLAP
NMYNYLRKLDRALPDPIKTFEIGPCYRKESDGKEHLEEF TMLGFCQMGSCTRENLESII
TDFLNHLGIDFKIVGDSCMVYGD TLDVMHGDLELSSAVVGPIPLDREWIDKPKWIGAGF
GLERLLKVKHDFKNIKRAARSESYYNGISTNL

Bold: mutated residues.

pBAD-dZ_{HER2}-D36/D37TAG

MAVDNKFNKEMRNAYWEIALLPNLNNQQKRAFIRSLY**DD**PSQSANLLAEAKKLNDQA
APKVEVDNKFNKEMRNAYWEIALLPNLNNQQKRAFIRSLY**DD**PSQSANLLAEAKKLND
AQAPKHHHHHHH

Bold: amber codon TAG at 36th/37th position.

pBAD-2Rs15d-Y37TAG

MKYLLPTAAAGLLLLAAQPAMAMGQVQLQESGGGSVQAGGSLKLTCAASGYIFNSCG
MGWYRQSPGRERELVSRISGDGDTWHKESVKGRFTISQDNVKKTLYLQMNSLKPEDTA
VYFCAVCYNLETYWGGGTQVTVSSHHHHHH

Bold: amber codon TAG at 37th position.

pBR322-TrasFab-S50/Y92TAG

Light Chain

MKSLPTAAAGLLLLAAQPAMASDIQMTQSPSSLSASVGDRTITCRASQDVNTAVAW
YQQKPGKAPKLLIYSASFLYSGVPSRFSGRSGTDFTLTISSLQPEDFATYYCQQHYTPP
TFGQGTKVEIKRTVAAPSVFIFPPSDEQLKSGTASVVCLLNNFYPREAKVQWKVDNALQ
SGNSQESVTEQDSKSTYSLSSTLTLSKADYEKHKVYACEVTHQGLSSPVTKSFNRGEC

Heavy Chain

MKKNIAFLASMFVFSIATNAYAEISEVQLVESGGGLVQPGGSLRLSCAASGFNIKDTYI
HWVRQAPGKGLEWVARIYPTNGYTRYADSVKGRFTISADTSKNTAYLQMNSLRAEDT
AVYYCSRWGGDGFYALDYWGQGLVTVSSASTKGPSVFPLAPSSKSTSGGTAALGCLV
KDYFPEPVTVSWNSGALTSGVHTFPAVLQSSGLYSLSSVTVPSSSLGTQTYICNVNHKP
SNTKVDKKVEPKSCDKTHTGGSGSAGGLNDIFEAQKIEWHE

Bold: amber codon TAG at 50th/92nd position of the Light Chain.

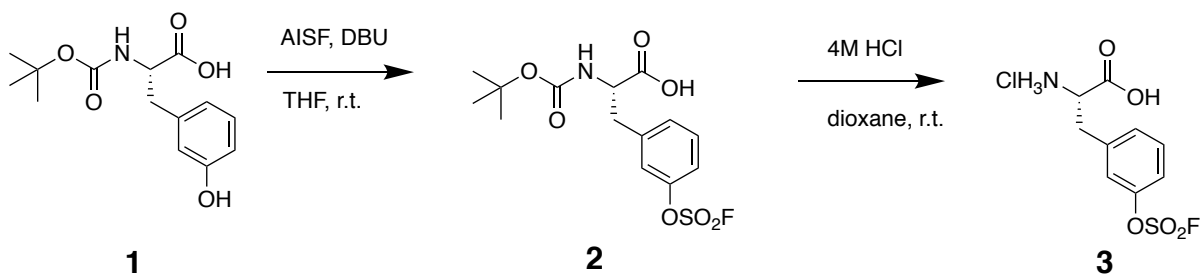
pBAD-7D12-Q116TAG

MKYLELLPTAAAGLLLLAAQPAMAMGQVKLEESGGGSVQTGGSLRLTCAASGRTSRSYGMGWFRQAPGKEREFVSGISWRGDSTGYADSVKGRFTISRDNKNTVDLQMNLSLKPEDTAIYYCAAAAAGSAWYGTLYEYDYWG**Q**GTQVTVSSHHHHHH

Bold: amber codon TAG at 116th position.

Chemical Synthesis of mFSY

Synthesis of aryl fluorosulfates was based on recent methods to synthesize sulfur (IV) fluorides using [4-(acetylamino)phenyl]imidodisulfonyl difluoride (AISF) reagent.²⁰



Synthesis of (S)-2-amino-3-(3-(fluorosulfonyl)oxy)phenyl)propionic acid (3, mFSY). To a 100 mL round-bottom flask were added Boc-(S)-2-Amino-3-(3-hydroxyphenyl)propionic acid (1, 1.15 g, 4.09 mmol) and [4-(acetylamino)phenyl]imidodisulfonyl difluoride (AISF) reagent (1.54 g, 4.90 mmol, 1.2 equiv.). The mixture was dissolved in 25 mL anhydrous tetrahydrofuran and 1,8-diazabicyclo[5.4.0]undec-7-ene (1.37 mL, 9 mmol, 2.2 equiv.) was added dropwise while stirring. The solution was then stirred at r.t. for 30 minutes. The reaction was then diluted with 50 mL ethyl acetate and washed with 1 M HCl (100 mL x 2) and brine (100 mL x 1). The organic

fraction was dried with anhydrous sodium sulfate and concentrated under vacuum. The crude product was then purified by column chromatography using MeOH:CH₂Cl₂ (1:200). The product, (*S*)-2-((*tert*-butoxycarbonyl)amino)-3-(3-((fluorosulfonyl)oxy)phenyl)propanoic acid, was isolated as a white solid (2, 0.774 g, 2.13 mmol, 52%).

S-2-((*tert*-butoxycarbonyl)amino)-3-(3-((fluorosulfonyl)oxy)phenyl)propanoic acid (2, 0.774 g, 2.13 mmol) was added to a scintillation vial and dissolved in 4 M HCl in dioxane (10 mL). The reaction was stirred overnight. The resultant solid was filtered off and washed with cool ether (10 mL x 2) affording the product mFSY-HCl as a white solid (3, 554 mg, 1.85 mmol, 87%).
¹H NMR (400 MHz, D₂O): δ (ppm) 7.62-7.58 (t, J= 16.0 Hz, 1H), 7.50-7.45 (m, J= 19.2 Hz, 3H), 4.36-4.33 (t, J= 13.2, 1H), 3.45-3.29 (m, J= 61.2 Hz, 2H).

¹³C NMR (400 MHz, D₂O): δ (ppm) 171.4, 150.1, 137.3, 131.3, 130.0, 121.8, 120.4, 54.1, 35.3

HR-ESI (+)*m/z*: calculated for C₉H₁₀FNO₅S [M+H]⁺, 264.0264; found 264.0351.

¹H NMR and ¹³C NMR shown in **Figure 2.S4** and **Figure 2.S5** respectively.

Library construction and mFSYRS mutant selection

The pBK-TK3 mutant library of MmPylRS was constructed using the new small-intelligent mutagenesis approach, which uses a single codon for each amino acid and thus allows a greater number of residues to be mutated simultaneously. The following residues of MmPylRS were mutated using the procedures previously described: 302NYT, 305WTG, 306WTG/TAC, 309KYA, 322AYA, 346NDT/VMA/ATG/TGG, 348NDT/VMA/ATG/TGG, 384TTM/TAT, 401VTT, 417NDT/VMA/ATG/TGG.²¹ The selection was performed as previously described.¹⁷

Briefly, pBK-TK3 library was transformed into DH10b-pRep positive selection reporter cells via electroporation. The cells were then plated onto an LB-agar selection plate containing 1 mM

mFSY, 12.5 µg/mL of tetracycline (Tet), 25 µg/mL of kanamycin (Kan), and 75 µg/mL of chloramphenicol (Cm). The selection plate was incubated at 37 °C for 72 h and then stored at 4 °C. Colonies showing green fluorescence were picked and streaked on a fresh LB-agar plate containing either Tet12.5Kan25Cm100 or Tet12.5Kan25Cm100 +1mM mFSY. After 24 h of incubation at 37 °C, 2 clones present mFSY-dependent fluorescence and growth were considered as hits and further characterized. The pBK plasmids encoding PylRS mutants were extracted by miniprep and then separated from reporter plasmids by DNA gel electrophoresis. The purified pBK plasmids were analyzed by Sanger-sequencing.

Incorporation of mFSY into EGFP(182TAG)

pBAD-EGFP(182TAG) was co-transformed with pEVOL-mFSYRS into DH10b and plated on LB agar plate supplemented with 100 µg/mL ampicillin and 34 µg/mL chloramphenicol. A single colony was picked and inoculated into 1 mL 2xYT (5 g/L NaCl, 16 g/L Tryptone, 10 g/L Yeast extract). The cells were left grown at 37 °C, 220 rpm, for 16 h. The cells were then diluted to an OD₆₀₀ of 0.6 in fresh 2XYT supplemented with relevant antibiotics, with or without 1 mM mFSY. The cells were then induced with 0.2% arabinose at either 30 °C for 6 h. The fluorescence intensity was measured with a plate reader (excitation at 485 nm, emission at 528 nm) and normalized to OD at 600 nm.

General incorporation of mFSY into proteins for expression and purification

For the incorporation of mFSY into dZ_{HER2}, 2Rs15d, TrasFab, and 7D12 the procedure of transformation was the same as described above. After transformation, a single colony was picked and left grown at 37 °C, 220 rpm for 16 h. Next morning, the cell culture was diluted 100 times

and then regrown to an OD 0.6-0.8 in 100 mL scale, with good aeration and the relevant antibiotic selection. Then the medium was added with 0.2% arabinose (and 1 mM IPTG for TrasFab) with or without 1 mM mFSY, and the expression were carried out at 18 °C, 220 rpm for 18 hr, 18 °C, or 25 °C. The IMAC chromatography was used for protein purification and the procedure was done as described elsewhere.⁹ TrasFab was purified on the Äkta Pure FPLC protein purification system using an HiTrap® Protein A column. Procedure was described previously.³²

***In vitro* crosslinking of dZ_{HER2}, 2Rs15d, TrasFab, and 7D12 with HER2 and EGFR**

Recombinant extracellular domain (ECD) of HER2 receptor was purchased from Abcam (Cat# ab168896); EGFR-ECD receptor was purchased from Abcam (Cat# ab155726). Purified 1 μM dZ_{HER2}, 2Rs15d, or TrasFab was incubated with 1 μM HER2 ECD in 20 uL 1 X PBS, 7.4 at 37 °C for 16 h. Purified 3 μM 7D12 was incubated with 500 nM EGFR in 20 uL 1 X PBS, 7.4 at 37 °C for 16 h. After incubation, 4x Laemmli Sample Buffer (Bio Rad, Cat# 161-0747) was added into the incubation and heated at 95 °C for 10 min. The samples were separated on SDS-PAGE and either analyzed by Coomassie blue staining or immunoblotted with 1:10000 anti-his monoclonal antibody (Proteintech #HRP66005).

Mass spectrometry

Mass spectrometric measurements were performed as previously described.³³ Briefly for electrospray ionization mass spectrometry, mass spectra of intact proteins were obtained using a QTOF Ultima (Waters) mass spectrometer, operating under positive electrospray ionization (+ESI) mode, connected to an LC-20AD (Shimadzu) liquid chromatography unit. Protein samples were separated from small molecules by reverse phase chromatography on a Waters Xbridge BEH

C4 column (300 Å, 3.5 µm, 2.1 mm x 50 mm), using an acetonitrile gradient from 30-71.4%, with 0.1% formic acid. Each analysis was 25 min under constant flow rate of 0.2 mL/min at RT. Data were acquired from m/z 350 to 2500, at a rate of 1 sec/scan. Alternatively, spectra were acquired by Xevo G2-S QTOF on a Waters ACQUITY UPLC Protein BEH C4 reverse-phase column (300 Å, 1.7 µm, 2.1 mm x 150 mm). An acetonitrile gradient from 5%-95% was used with 0.1% formic acid, over a run time of 5 min and constant flow rate of 0.5 mL/min at RT. Spectrum were acquired from m/z 350 to 2000, at a rate of 1 sec/scan. The spectra were deconvoluted using maximum entropy in MassLynx.

For tandem mass spectrometry, analysis and sequencing of peptides were carried out using a Q Exactive Orbitrap interfaced with Ultimate 3000 LC system. Data acquisition by Q Exactive Orbitrap was as follows: 10 µL of trypsin-digested protein was loaded on an Ace UltraCore super C18 reverse-phase column (300 Å, 2.5 µm, 75 mm × 2.1 mm) via an autosampler. An acetonitrile gradient from 5%-95% was used with 0.1% formic acid, over a run time of 45 min and constant flow rate of 0.2 mL/min at RT. MS data were acquired using a data-dependent top10 method dynamically choosing the most abundant precursor ions from the survey scan for HCD fragmentation using a stepped normalized collision energy of 28, 30 35 eV. Survey scans were acquired at a resolution of 70,000 at m/z 200 on the Q Exactive. Tandem MS data was analyze on MaxQuant.

Flow cytometric analysis of mFSY incorporation into HeLa-GFP(182TAG)

One day before transfection, 4.5×10^4 HeLa-GFP(182TAG) reporter cells were seeded in 9 wells of a Greiner bio-one 12 well-cell culture dish containing 1 mL of DMEM media with 10% FBS and incubated at 37 °C in a CO₂ incubator. Plasmid pMP-mFSYRS (1 µg) was transfected

into target cells using 9 μ L polyethylenimine (PEI) transfection agent. pMP-mFSYRS plasmid was not added to three of the wells (negative control). Six hours post transfection, 1 mM mFSY was added to three wells. The remaining three wells were transfected with pMP-mFSYRS plasmid but did not have mFSY Uaa added. After incubation at 37 °C for 48 h, cells were non-enzymatically detached from the plates using Gibco Cell Dissociation Buffer and collected by centrifugation (500 g, 5 min, r.t.). The cells were resuspended in 300 μ L of FACS buffer (1 \times PBS, 2% FBS, 1 mM EDTA, 0.1% sodium azide, 0.28 μ M DAPI) and analyzed by BD LSRFortessa™ cell analyzer.

Fluorescence confocal microscopy of HeLa-GFP(182mFSY)

One day before transfection, 4.5×10^4 HeLa-GFP(182TAG) cells were seeded in a Greiner bioone CELLview glass bottom dish containing 2 mL of DMEM media with 10% FBS and incubated at 37 °C in a CO2 incubator. Plasmid pMP-mFSYRS (2 μ g) was transfected into the HeLa-GFP(182TAG) cells using 9 μ L polyethylenimine (PEI) transfection agent. Six hours post transfection, 1 mM mFSY was added to the media. A HeLa-GFP(182TAG) cell group that was not transfected with any plasmid was used as a negative control. The cells were incubated at 37 °C for an additional 48 h post transfection and imaged with a Nikon CSU-X1 Spinning Disk microscope.

2.6 Supplemental Figures

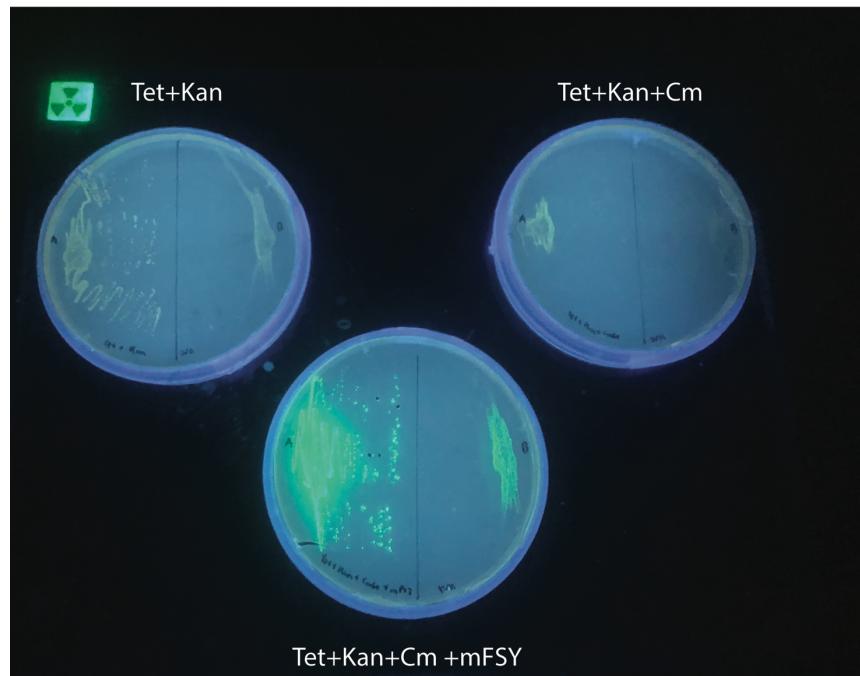


Figure 2.S1: . Selection plates for mFSY-specific synthetase. Addition of mFSY to plates showed robust incorporation of the Uaa into EGFP via the orthogonal tRNAPyl/mFSYRS pair, rendering cells green fluorescent. When mFSY was not added to plates, there was insignificant EGFP fluorescence detected, suggesting negligible misincorporation of native amino acids.

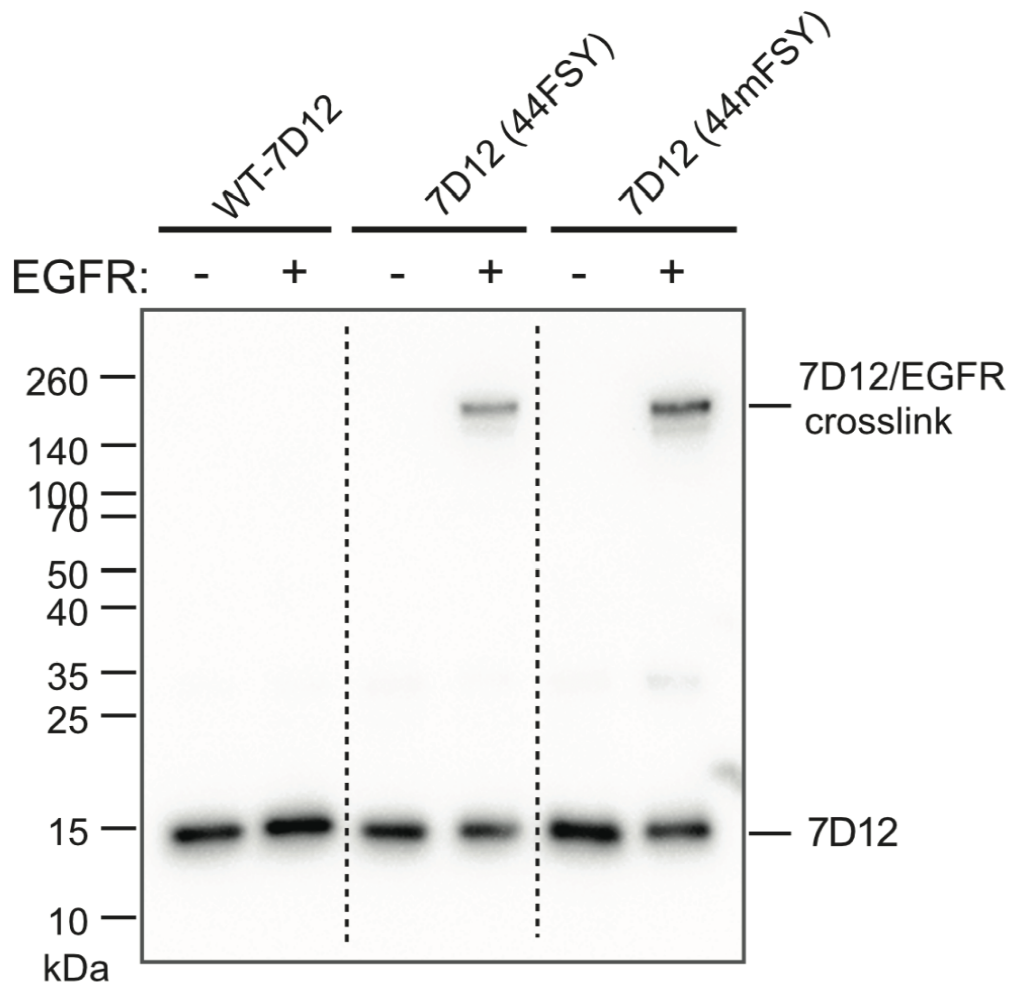


Figure 2.S2: Western blot analysis of WT-7D12, 7D12(44FSY), and 7D12(44mFSY) incubation with the EGFR receptor. WT-7D12 did not crosslink EGFR, while 7D12(44mFSY) crosslinked EGFR in a higher efficiency than 7D12(44FSY) as also observed in Figure 3b.

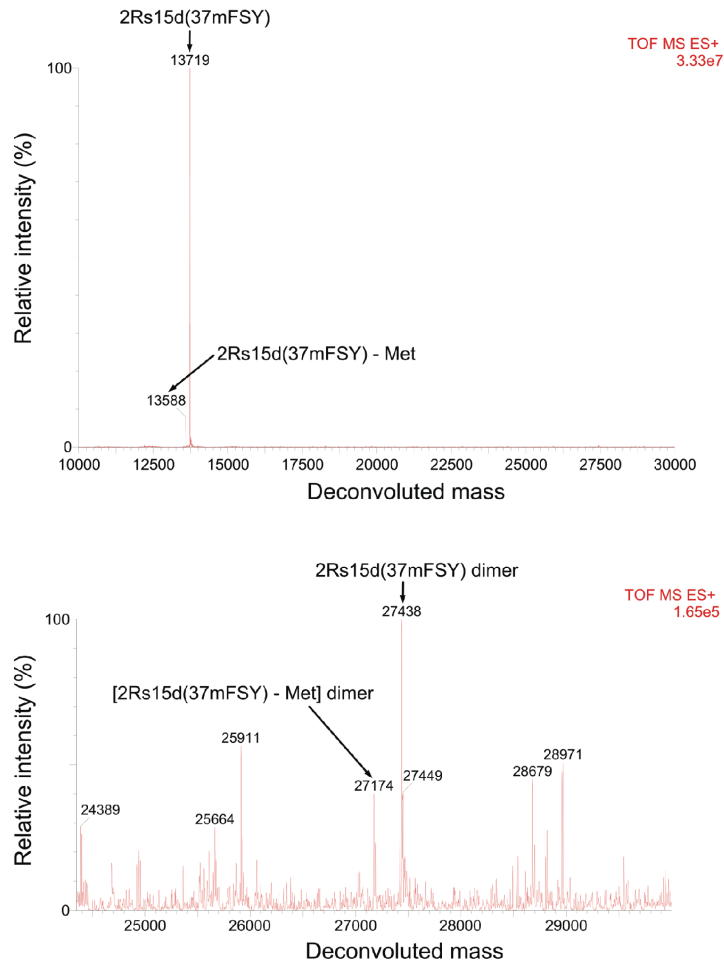


Figure 2.S3: Mass spectra for intact 2Rs15d(37mFSY). Both monomeric and non-cross-linked dimeric 2Rs15d(37mFSY) were detected, together with their –Met (loss of N-terminal Met) species. Monomeric 2Rs15d(37mFSY): expected 13719 Da, observed 13719 Da. Monomeric [2Rs15d(37mFSY) – Met]: expected 13588 Da, observed 13588. Non-cross-linked 2Rs15d(37mFSY) dimer: expected 27438 Da, observed 27438 Da. Non-cross-linked [2Rs15d(37mFSY) – Met] dimer: expected 27176 Da, observed 27174 Da.

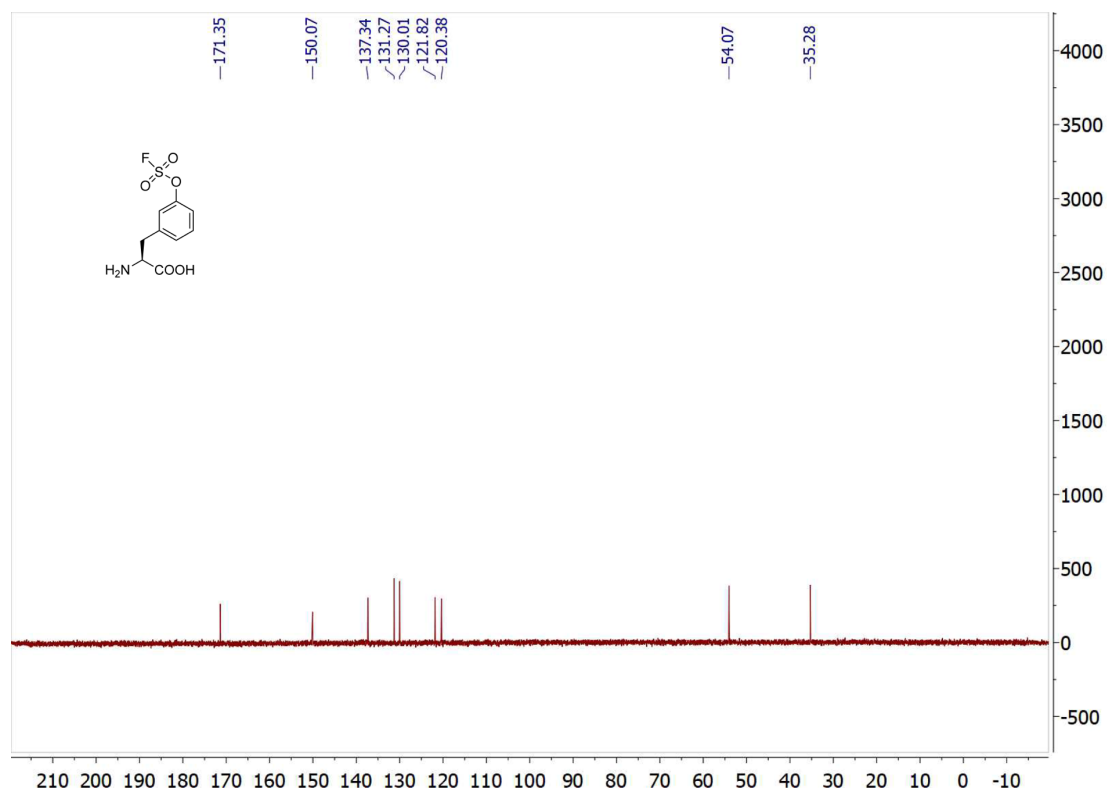
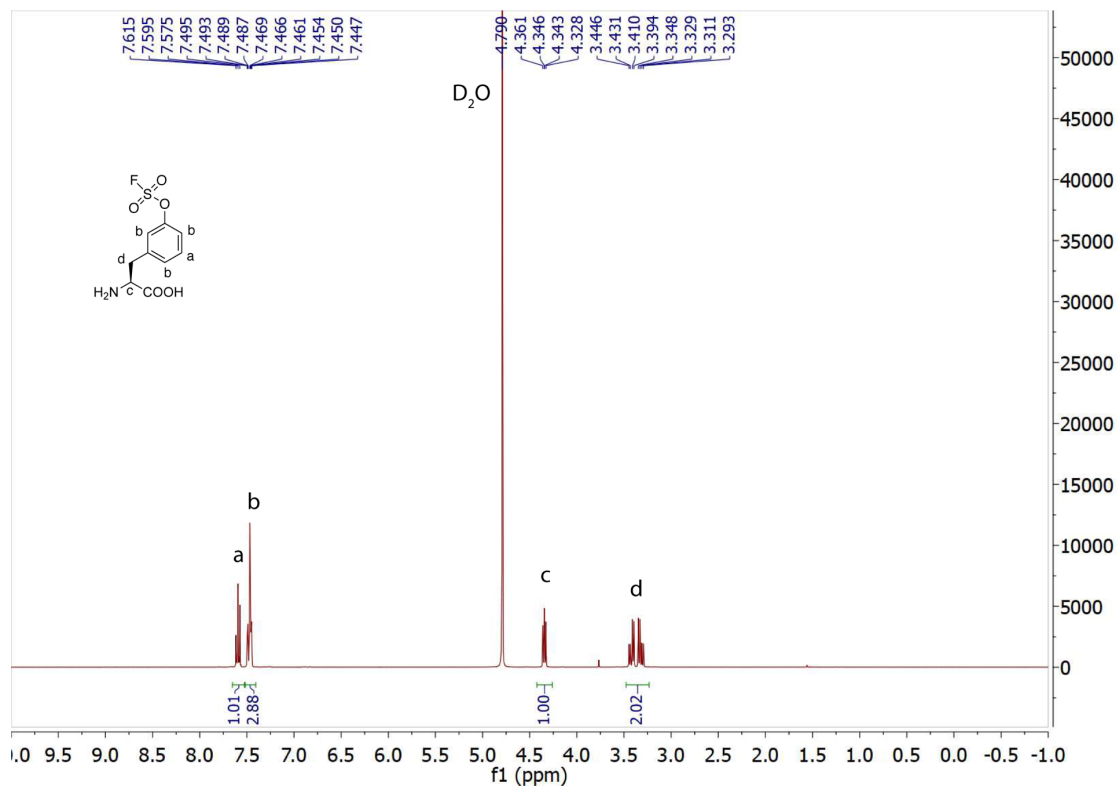


Figure 2.S5: ¹³C NMR for mFSY.

2.7 References

- (1) Cao, L.; Wang, L. New Covalent Bonding Ability for Proteins. *Protein Sci* 2021. <https://doi.org/10.1002/pro.4228>.
- (2) Wang, L.; Brock, A.; Herberich, B.; Schultz, P. G. Expanding the Genetic Code of *Escherichia Coli*. *Science* 2001, 292 (5516), 498–500. <https://doi.org/10.1126/science.1060077>.
- (3) Xiang, Z.; Ren, H.; Hu, Y. S.; Coin, I.; Wei, J.; Cang, H.; Wang, L. Adding an Unnatural Covalent Bond to Proteins through Proximity-Enhanced Bioreactivity. *Nat Methods* 2013, 10 (9), 885–888. <https://doi.org/10.1038/nmeth.2595>.
- (4) Xiang, Z.; Lacey, V. K.; Ren, H.; Xu, J.; Burban, D. J.; Jennings, P. A.; Wang, L. Proximity-Enabled Protein Crosslinking through Genetically Encoding Haloalkane Unnatural Amino Acids. *Angewandte Chemie Int Ed* 2014, 53 (8), 2190–2193. <https://doi.org/10.1002/anie.201308794>.
- (5) Xuan, W.; Shao, S.; Schultz, P. G. Protein Crosslinking by Genetically Encoded Noncanonical Amino Acids with Reactive Aryl Carbamate Side Chains. *Angewandte Chemie Int Ed* 2017, 56 (18), 5096–5100. <https://doi.org/10.1002/anie.201611841>.
- (6) Coin, I.; Katritch, V.; Sun, T.; Xiang, Z.; Siu, F. Y.; Beyermann, M.; Stevens, R. C.; Wang, L. Genetically Encoded Chemical Probes in Cells Reveal the Binding Path of Urocortin-I to CRF Class B GPCR. *Cell* 2013, 155 (6), 1258–1269. <https://doi.org/10.1016/j.cell.2013.11.008>.
- (7) Hoppmann, C.; Maslennikov, I.; Choe, S.; Wang, L. In Situ Formation of an Azo Bridge on Proteins Controllable by Visible Light. *J Am Chem Soc* 2015, 137 (35), 11218–11221. <https://doi.org/10.1021/jacs.5b06234>.
- (8) Yang, B.; Tang, S.; Ma, C.; Li, S.-T.; Shao, G.-C.; Dang, B.; DeGrado, W. F.; Dong, M.-Q.; Wang, P. G.; Ding, S.; Wang, L. Spontaneous and Specific Chemical Cross-Linking in Live Cells

to Capture and Identify Protein Interactions. *Nat Commun* 2017, 8 (1), 2240. <https://doi.org/10.1038/s41467-017-02409-z>.

(9) Li, Q.; Chen, Q.; Klauser, P. C.; Li, M.; Zheng, F.; Wang, N.; Li, X.; Zhang, Q.; Fu, X.; Wang, Q.; Xu, Y.; Wang, L. Developing Covalent Protein Drugs via Proximity-Enabled Reactive Therapeutics. *Cell* 2020, 182 (1), 85-97.e16. <https://doi.org/10.1016/j.cell.2020.05.028>.

(10) Berdan, V. Y.; Klauser, P. C.; Wang, L. Covalent Peptides and Proteins for Therapeutics. *Bioorgan Med Chem* 2021, 29, 115896. <https://doi.org/10.1016/j.bmc.2020.115896>.

(11) Tian, Z.; Wu, L.; Yu, C.; Chen, Y.; Xu, Z.; Bado, I.; Loredó, A.; Wang, L.; Wang, H.; Wu, K.-L.; Zhang, W.; Zhang, X. H.-F.; Xiao, H. Harnessing the Power of Antibodies to Fight Bone Metastasis. *Sci. Adv.* 2021, 7 (26), eabf2051. <https://doi.org/10.1126/sciadv.abf2051>.

(12) Wang, L. Genetically Encoding New Bioreactivity. *New Biotechnol* 2017, 38 (Pt A), 16–25. <https://doi.org/10.1016/j.nbt.2016.10.003>.

(13) Dong, J.; Krasnova, L.; Finn, M. G.; Sharpless, K. B. Sulfur(VI) Fluoride Exchange (SuFEx): Another Good Reaction for Click Chemistry. *Angewandte Chemie Int Ed* 2014, 53 (36), 9430–9448. <https://doi.org/10.1002/anie.201309399>.

(14) Chen, W.; Dong, J.; Plate, L.; Mortenson, D. E.; Brighty, G. J.; Li, S.; Liu, Y.; Galmozzi, A.; Lee, P. S.; Hulce, J. J.; Cravatt, B. F.; Saez, E.; Powers, E. T.; Wilson, I. A.; Sharpless, K. B.; Kelly, J. W. Arylfluorosulfates Inactivate Intracellular Lipid Binding Protein(s) through Chemoselective SuFEx Reaction with a Binding Site Tyr Residue. *J Am Chem Soc* 2016, 138 (23), 7353–7364. <https://doi.org/10.1021/jacs.6b02960>.

(15) Liu, Z.; Li, J.; Li, S.; Li, G.; Sharpless, K. B.; Wu, P. SuFEx Click Chemistry Enabled Late-Stage Drug Functionalization. *J. Am. Chem. Soc.* 2018, 140 (8), 2919–2925. <https://doi.org/10.1021/jacs.7b12788>.

- (16) Narayanan, A.; Jones, L. H. Sulfonyl Fluorides as Privileged Warheads in Chemical Biology. *Chem Sci* 2015, 6 (5), 2650–2659. <https://doi.org/10.1039/c5sc00408j>.
- (17) Wang, N.; Yang, B.; Fu, C.; Zhu, H.; Zheng, F.; Kobayashi, T.; Liu, J.; Li, S.; Ma, C.; Wang, P. G.; Wang, Q.; Wang, L. Genetically Encoding Fluorosulfate-1-Tyrosine To React with Lysine, Histidine, and Tyrosine via SuFEx in Proteins in Vivo. *J Am Chem Soc* 2018, 140 (15), 4995–4999. <https://doi.org/10.1021/jacs.8b01087>.
- (18) Wang, N.; Wang, L. Genetically Encoding Latent Bioreactive Amino Acids and the Development of Covalent Protein Drugs. *Curr Opin Chem Biol* 2022, 66, 102106. <https://doi.org/10.1016/j.cbpa.2021.102106>.
- (19) Liu, J.; Cao, L.; Klauser, P. C.; Cheng, R.; Berdan, V. Y.; Sun, W.; Wang, N.; Ghelichkhani, F.; Yu, B.; Rozovsky, S.; Wang, L. A Genetically Encoded Fluorosulfonyloxybenzoyl-l-lysine for Expansive Covalent Bonding of Proteins via SuFEx Chemistry. *J Am Chem Soc* 2021, 143 (27), 10341–10351. <https://doi.org/10.1021/jacs.1c04259>.
- (20) Zhou, H.; Mukherjee, P.; Liu, R.; Evrard, E.; Wang, D.; Humphrey, J. M.; Butler, T. W.; Hoth, L. R.; Sperry, J. B.; Sakata, S. K.; Helal, C. J.; Ende, C. W. am. Introduction of a Crystalline, Shelf-Stable Reagent for the Synthesis of Sulfur(VI) Fluorides. *Org Lett* 2018, 20 (3), 812–815. <https://doi.org/10.1021/acs.orglett.7b03950>.
- (21) Lacey, V. K.; Louie, G. V.; Noel, J. P.; Wang, L. Expanding the Library and Substrate Diversity of the Pyrrolysyl-tRNA Synthetase to Incorporate Unnatural Amino Acids Containing Conjugated Rings. *Chembiochem* 2013, 14 (16), 2100–2105. <https://doi.org/10.1002/cbic.201300400>.
- (22) Takimoto, J. K.; Dellas, N.; Noel, J. P.; Wang, L. Stereochemical Basis for Engineered Pyrrolysyl-TRNA Synthetase and the Efficient in Vivo Incorporation of Structurally Divergent

Non-Native Amino Acids. *Acs Chem Biol* 2011, 6 (7), 733–743.
<https://doi.org/10.1021/cb200057a>.

(23) Kobayashi, T.; Hoppmann, C.; Yang, B.; Wang, L. Using Protein-Confined Proximity To Determine Chemical Reactivity. *J Am Chem Soc* 2016, 138 (45), 14832–14835.
<https://doi.org/10.1021/jacs.6b08656>.

(24) Wang, W.; Takimoto, J. K.; Louie, G. V.; Baiga, T. J.; Noel, J. P.; Lee, K.-F.; Slesinger, P. A.; Wang, L. Genetically Encoding Unnatural Amino Acids for Cellular and Neuronal Studies. *Nat. Neurosci.* 2007, 10 (8), 1063–1072. <https://doi.org/10.1038/nn1932>.

(25) Eigenbrot, C.; Ultsch, M.; Dubnovitsky, A.; Abrahmsén, L.; Härd, T. Structural Basis for High-Affinity HER2 Receptor Binding by an Engineered Protein. *Proc National Acad Sci* 2010, 107 (34), 15039–15044. <https://doi.org/10.1073/pnas.1005025107>.

(26) Ekerljung, L.; Lennartsson, J.; Gedda, L. The HER2-Binding Affibody Molecule (ZHER2:342)₂ Increases Radiosensitivity in SKBR-3 Cells. *PLoS ONE* 2012, 7 (11), e49579. <https://doi.org/10.1371/journal.pone.0049579>.

(27) Schmitz, K. R.; Bagchi, A.; Roovers, R. C.; van Bergen en Henegouwen, P. M. P.; Ferguson, K. M. Structural Evaluation of EGFR Inhibition Mechanisms for Nanobodies/VHH Domains. *Structure* 2013, 21 (7), 1214–1224. <https://doi.org/10.1016/j.str.2013.05.008>.

(28) D’Huyvetter, M.; Vos, J. D.; Xavier, C.; Pruszynski, M.; Sterckx, Y. G. J.; Massa, S.; Raes, G.; Caveliers, V.; Zalutsky, M. R.; Lahoutte, T.; Devoogdt, N. 131I-Labeled Anti-HER2 Camelid SdAb as a Theranostic Tool in Cancer Treatment. *Clin Cancer Res* 2017, 23 (21), 6616–6628. <https://doi.org/10.1158/1078-0432.ccr-17-0310>.

- (29) Cho, H.-S.; Mason, K.; Ramyar, K. X.; Stanley, A. M.; Gabelli, S. B.; Denney, D. W.; Leahy, D. J. Structure of the Extracellular Region of HER2 Alone and in Complex with the Herceptin Fab. *Nature* 2003, 421 (6924), 756–760. <https://doi.org/10.1038/nature01392>.
- (30) Yu, B.; Li, S.; Tabata, T.; Wang, N.; Cao, L.; Kumar, G. R.; Sun, W.; Liu, J.; Ott, M.; Wang, L. Accelerating PERx Reaction Enables Covalent Nanobodies for Potent Neutralization of SARS-CoV-2 and Variants. *Chem* 2022, 8 (10), 2766–2783. <https://doi.org/10.1016/j.chempr.2022.07.012>.
- (31) Liu, C.; Wu, T.; Shu, X.; Li, S.; Wang, D. R.; Wang, N.; Zhou, R.; Yang, H.; Jiang, H.; Hendriks, I. A.; Gong, P.; Zhang, L.; Nielsen, M. L.; Li, K.; Wang, L.; Yang, B. Identification of Protein Direct Interactome with Genetic Code Expansion and Search Engine OpenUaa. *Adv Biology* 2021, 5 (3), 2000308. <https://doi.org/10.1002/adbi.202000308>.
- (32) Hornsby, M.; Paduch, M.; Miersch, S.; Sääf, A.; Matsuguchi, T.; Lee, B.; Wypisniak, K.; Doak, A.; King, D.; Usatyuk, S.; Perry, K.; Lu, V.; Thomas, W.; Luke, J.; Goodman, J.; Hoey, R. J.; Lai, D.; Griffin, C.; Li, Z.; Vizeacoumar, F. J.; Dong, D.; Campbell, E.; Anderson, S.; Zhong, N.; Gräslund, S.; Koide, S.; Moffat, J.; Sidhu, S.; Kossiakoff, A.; Wells, J. A High Through-Put Platform for Recombinant Antibodies to Folded Proteins*. *Mol Cell Proteom Mcp* 2015, 14 (10), 2833–2847. <https://doi.org/10.1074/mcp.o115.052209>.
- (33) Liu, J.; Chen, Q.; Rozovsky, S. Utilizing Selenocysteine for Expressed Protein Ligation and Bioconjugations. *J Am Chem Soc* 2017, 139 (9), 3430–3437. <https://doi.org/10.1021/jacs.6b10991>.

3. Covalent Proteins as Targeted Radionuclide Therapies Enhance Antitumor Effects

3.1 Abstract

Molecularly targeted radionuclide therapies (TRTs) struggle with balancing efficacy and safety, as current strategies to increase tumor absorption often alter drug pharmacokinetics to prolong circulation and normal tissue irradiation. Here we report the first covalent protein TRT, which, through reacting with the target irreversibly, increases radioactive dose to the tumor without altering the drug's pharmacokinetic profile or normal tissue biodistribution. Through genetic code expansion we engineered a latent bioreactive amino acid into a nanobody, which binds to its target protein and forms a covalent linkage via the proximity-enabled reactivity, crosslinking the target irreversibly *in vitro*, on cancer cells, and on tumors *in vivo*. The radiolabeled covalent nanobody markedly increases radioisotope levels in tumors and extends tumor residence time while maintaining rapid systemic clearance. Furthermore, the covalent nanobody conjugated to the α -emitter actinium-225 inhibits tumor growth more effectively than the non-covalent nanobody without causing tissue toxicity. Shifting the protein-based TRT from noncovalent to covalent mode, this chemical strategy improves tumor responses to TRTs and can be readily scaled to diverse protein radiopharmaceuticals engaging broad tumor targets.

3.2 Introduction

Molecularly targeted radionuclide therapies (TRTs) are a class of systemically administered, isotopically labeled drugs designed to concentrate ionizing radiation to all tumors in the body simultaneously.¹ After localizing to tumors, these drugs exploit cancer's well-known vulnerability to ionizing radiation by producing a continuous source of local radioactive emissions within the tumor to trigger severe and irreparable genetic damage. Since the approval of radioactive iodine for the treatment of well-differentiated thyroid cancer in the 1950s, TRT has found a place in standard of care as a safe alternative to external beam ionizing radiation for patients with targetable cancers including widely metastatic diseases.

Although TRT is a venerable treatment strategy for cancer, only within the past three decades has the nuclear medicine community developed new therapies for other cancer types that recapitulate the success of radioiodine.^{1,2} Indeed, TRT is experiencing a clinical renaissance, with several recent FDA approvals to treat metastatic castration resistant prostate cancer (Pluvicto), neuroendocrine tumors (Lutathera), pheochromocytoma and paraganglioma (Azedra), and osseous metastases (Xofigo). Driving this renaissance has been the prioritization of low molecular weight (MW) TRTs, and particularly small molecule radioligands that rapidly exit the bloodstream to minimize host toxicity yet are still effective antitumor agents by binding highly overexpressed cancer proteins. This transition was motivated by 30 years of largely discouraging prior clinical experiences with various high MW radiopharmaceuticals such as immunoglobulins. Indeed, while the long serum half-life (3-7 days) of immunoglobulins results in high levels of target engagement and tumoral absorbed doses, the prolonged residence in the blood and slow hepatobiliary clearance results in high radiation exposure to radiosensitive normal tissue compartments (e.g., bone marrow) that results in toxicity, thus narrowing or eliminating a therapeutic index.² The evolution

of radiopharmaceuticals targeting prostate specific membrane antigen (PSMA) stands out as an instructive case study on the tension between efficacy and safety. While various radiolabeled forms of the IgG J591, including ^{177}Lu -J591, stalled in clinical trials due to dose limiting toxicities, Pluvicto (^{177}Lu -PSMA 617), a low MW radioligand with weaker affinity for PSMA and lower tumor uptake compared to J591, nevertheless achieved FDA approval for prostate cancer treatment in 2022 due in large part to its better safety profile.³⁻⁵

However, low MW radioligand therapies (RLTs) are rarely curative, and more generally, developing drugs that fit the RLT paradigm is challenging. First, as the drug is rapidly exiting the body, to deliver sufficient dose to tumors, the field is limited to the small minority of highly overexpressed proteins in cancer that can extract sufficient radioligand from circulation. Indeed, prominent RLT drug targets like PSMA, somatostatin receptor type 2, fibroblast activated protein alpha (FAPa), carbonic anhydrase 9, and the bombesin receptor are all highly overexpressed on cancer cells ($>10^5$ receptors per cell). Second, ligand/receptor complexes are intrinsically unstable in biology, and subject to dissociation or degradation after endocytosis, reducing the effective radiation dose. Indeed, longitudinal PET studies in patients have shown that RLTs begin clearing from tumors within 96 hours, and in some extreme cases (e.g., FAPI PET) the radioisotope washes out entirely from the tumor within a few hours.⁶⁻⁹ As leading therapeutic radioisotopes like lutetium-177 (^{177}Lu) and actinium-225 (^{225}Ac) have half-lives that span many days to even weeks, increasing their residence time in the tumor will likely confer more durable antitumor effects. Some investigators have approached this challenge by incorporating hydrophobic binding groups onto the scaffold of RLTs to encourage low affinity interactions with abundant serum proteins like albumin.^{10,11} While animal studies have shown that this strategy increases RLT uptake in tumors and subsequent tumor responses, a prolonged serum half-life increases irradiation to normal tissues

and may incur toxicities. Other investigators have devised antibody pretargeting, wherein they administer a non-radioactive modified antibody followed by a radioligand that binds the antibody through noncovalent interactions or bioorthogonal chemistry.^{12,13} This strategy circumvents the slow pharmacokinetics while delivery a high dose of radiation to the cancer target. However, requiring two separate agents and a delayed delivery of the radioligand increases the complexity of the treatment. The ultimate clinical utility of these strategies remains to be determined.

An ideal radiopharmaceutical would have several characteristics, including high specificity, short blood and normal tissue residence time, and high tumor retention. Rather than trying to increase tumoral uptake of the TRT by manipulating serum half-life, we hypothesized that installing covalent reactivity in the TRT could be a strategy to lengthen the tumoral residence time without significantly altering time in circulation. While covalent reactivity has been installed on low MW radioligands,^{14,15} no covalent protein radiopharmaceutical has been developed for imaging and therapy. Here, we report the development of covalent protein radiopharmaceuticals that leverage proximity-enabled reactivity to bind target irreversibly. We generated a radiolabeled covalent nanobody that bound the human epidermal growth factor receptor 2 (HER2) irreversibly *in vitro* and on cancer cell surfaces (**Fig. 3.1**). Using positron emission tomography (PET), we showed that the covalent nanobody attained highly specific and longer tumor accumulation *in vivo* than the wildtype nanobody. We further demonstrated that the ²²⁵Ac-labeled covalent nanobody more effectively inhibited the growth of HER2-expressing tumors in mice compared to the wildtype nanobody. We showed that not only did the ²²⁵Ac-labeled covalent nanobody inhibited tumor growth at a greater level than the non-covalent counterpart, it also showed no toxicity in key tissues such as the heart, liver, kidneys, or bone marrow. This covalent protein radiopharmaceutical strategy highlights the potential to employ covalent chemistry on proteins *in*

vivo and to shift the protein-based TRT from noncovalent to covalent binding mode for precision medicine.

3.3 Results

We envisioned that a covalent protein radiopharmaceutical would be fast-clearing in circulation but achieve persistent tumor residence through binding the cancer target specifically and irreversibly. However, native proteins and engineered protein binders such as nanobodies and antibodies generally bind to their targets through reversible noncovalent interactions.¹⁶ To break this natural barrier, we recently reported a Proximity-Enabled Reactive Therapeutics (PERx) strategy to generate covalent protein drugs.^{17,18} Through genetic code expansion,¹⁹ a latent bioreactive unnatural amino acid (Uaa) was incorporated into the protein drug, which selectively forms a covalent linkage with a proximal natural residue of the target protein only upon drug-target interaction, resulting in the irreversible binding of the protein drug to its target.^{16,18,20} We have demonstrated that PERx-enabled covalent protein drugs showed drastically higher potency in cancer immunotherapy and in neutralization of SARS-CoV-2 over the noncovalent wildtype proteins.^{18,21} Aside from initial success in increasing drug potency, whether PERx-enabled biocompatible covalent chemistry can advance protein therapeutics via new mechanisms awaits exploration.

Nanobodies have small molecule weight (~15 kDa) for efficient tumor penetrance and rapid clearance from circulation, are generally heat stable and easy to produce in bacteria, can be humanized to minimize potential immunogenicity, and can be readily evolved to bind various targets in high specificity. Our strategy for developing covalent protein radiopharmaceuticals thus started with genetically incorporating a latent bioreactive Uaa into the nanobody followed with

radioisotope labeling. We recently genetically incorporated a latent bioreactive Uaa, fluorosulfate-L-tyrosine (FSY), which is stable in cells and reacts with Lys, His, or Tyr residue on proteins through Sulfur Fluoride Exchange (SuFEx) click chemistry²² only when the two residues are in close proximity.^{23,24} We therefore decided to incorporate FSY into Nb_{HER2},²⁵ a nanobody specific for HER2, to generate a covalent nanobody as the delivery vehicle for radionuclides for PET imaging and TRT (**Fig 3.1b**). HER2 gene amplification and overexpression occurs in a number of different cancers including breast, stomach, ovarian, kidney, prostate, salivary glands, colon, urinary, and lung.²⁶ To image HER2-positive cancer, PET has been the modality of choice for the clinic due to its high spatial resolution and sensitivity.²⁷ Only upon Nb_{HER2} binding to HER2 would FSY selectively react with a target residue of HER2 via proximity-enabled SuFEx reactivity and thus crosslink them irreversibly (**Fig. 3.1b**). The conventional nanobody binds in noncovalent mode and is in dynamic association and dissociation with HER2, which will be cleared from HER2-expressing cells; in contrast, the covalent nanobody would permanently bind to HER2 and thus enhance the specific accumulation of the attached radionuclide to HER2 expressing cells. At non-target sites, covalent nanobody will not generate such covalent crosslink, and thus is quickly cleared as the conventional nanobody to minimize background.

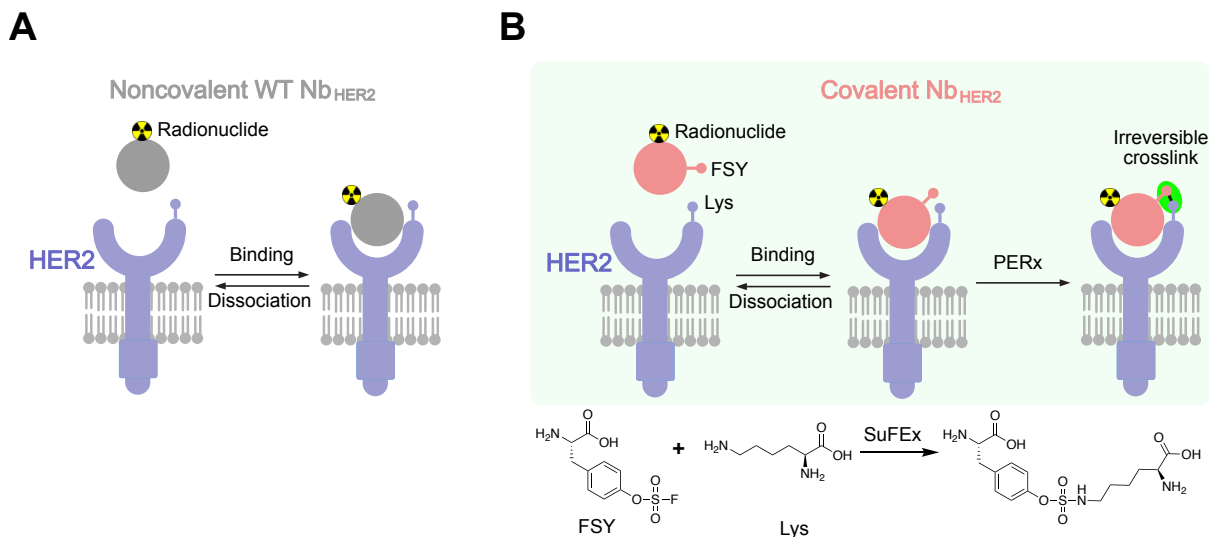


Figure 3.1: Covalent protein radiopharmaceuticals to enhance efficacy and safety for TRT. A schematic comparison of the noncovalent WT Nb_{HER2} (A) and the covalent Nb_{HER2} (B) in targeted delivery of radionuclide to HER2-expressing cancer cells. The noncovalent Nb_{HER2} binds HER2 reversibly allowing dissociation. In contrast, when the covalent Nb_{HER2} binds to HER2, the latent bioreactive Uaa FSY reacts with Lys through proximity-enabled SuFEx reaction, resulting in irreversible crosslinking of Nb_{HER2} with HER2 and persistent tumoral retention of the attached radionuclide.

We first generated a covalent Nb_{HER2} to irreversibly crosslink HER2 *in vitro*. Based on the structure of Nb_{HER2} in complex with HER2 extracellular domain (ECD),^{25,28} we chose Asp54 on Nb_{HER2} as a potential site for FSY incorporation to target Lys150 in proximity on HER2 ECD (**Fig. 3.2a**). The Nb_{HER2}(FSY) mutant protein was produced in *E. coli* through expressing the Nb_{HER2} gene containing a TAG stop codon at site 54 together with the genes for tRNA^{Py1}-FSYRS,²⁴ which incorporates FSY in response to TAG. Western blot analysis of the cell lysate showed that full-length Nb_{HER2} was produced only when 1 mM of FSY was added to the growth media (**Fig. 3.2b**), suggesting FSY incorporation at the TAG site. The Nb_{HER2}(FSY) protein was purified with affinity chromatography in the yield of 0.5 mg/L. To further evaluate the fidelity of FSY incorporation, the purified Nb_{HER2}(FSY) protein was analyzed by electrospray ionization time-of-flight mass spectrometry (**Fig. 3.2c** and **Fig. 3.S1** for WT Nb_{HER2}). A peak was observed at 13767 Da, which

corresponds to intact Nb_{HER2} containing a single FSY residue at position 54 (expected [M+H]⁺ = 13767 Da). A second peak measured at 13635 Da corresponds to Nb_{HER2}(FSY) lacking the initiating Met (expected [M-Met+H]⁺ = 13635 Da), which is expected for proteins expressed in *E. coli* cells. No peaks corresponding to proteins containing any other amino acids at position 54 were observed, confirming high fidelity of FSY incorporation in Nb_{HER2}. To check if FSY incorporation affected Nb_{HER2} binding to HER2, we measured the association of Nb_{HER2} with HER2 using biolayer interferometry (**Fig. 3.S2**). HER2 was incubated with varying concentrations of Nb_{HER2}(WT) or Nb_{HER2}(FSY) for 90 seconds. The association rate constant k_{on} was measured to be $(1.21 \pm 0.01) \times 10^5 \text{ M}^{-1}\text{s}^{-1}$ for Nb_{HER2}(WT) and $(1.15 \pm 0.02) \times 10^5 \text{ M}^{-1}\text{s}^{-1}$ for Nb_{HER2}(FSY), suggesting similar association rate of Nb_{HER2}(WT) and Nb_{HER2}(FSY) with HER2.

To test if Nb_{HER2}(FSY) could covalently crosslink the HER2 ECD, we incubated Nb_{HER2}(WT) or Nb_{HER2}(FSY) with and without HER2 ECD at 37 °C for 4 hours followed with Western blot analysis. A covalent complex was detected only when HER2 ECD was incubated with Nb_{HER2}(FSY) (**Fig. 3.2d**), indicating that the crosslinking was dependent on FSY reactivity as designed. To determine which residue of HER2 was crosslinked by FSY, we trypsin digested the crosslinked Nb_{HER2}(FSY)-HER2 and analyzed the digested sample with tandem mass spectrometry in high resolution. The crosslinked peptide was identified, and a series of b and y ions of the cross-linked peptide unambiguously indicated that FSY54 in Nb_{HER2} reacted with Lys150 in HER2 (**Fig. 3.2e**). No other residues of HER2 were found reacted with FSY, indicating that Nb_{HER2}(FSY) covalently targeted HER2 on Lys150 as predicted from the crystal structure in a highly specific manner. To further evaluate the kinetics of covalent complex formation, Nb_{HER2}(FSY) was incubated with HER2 ECD for different time duration and analyzed with Western blot (**Fig. 3.2f**). Crosslinking was detected as soon as 10 minutes of incubation at 37 °C, and a second-order rate

constant of $34154 \pm 1921 \text{ M}^{-1}\text{min}^{-1}$ was measured (Fig. 3.2g), indicating that Nb_{HER2}(FSY) rapidly and efficiently crosslinked the HER2 ECD *in vitro*.

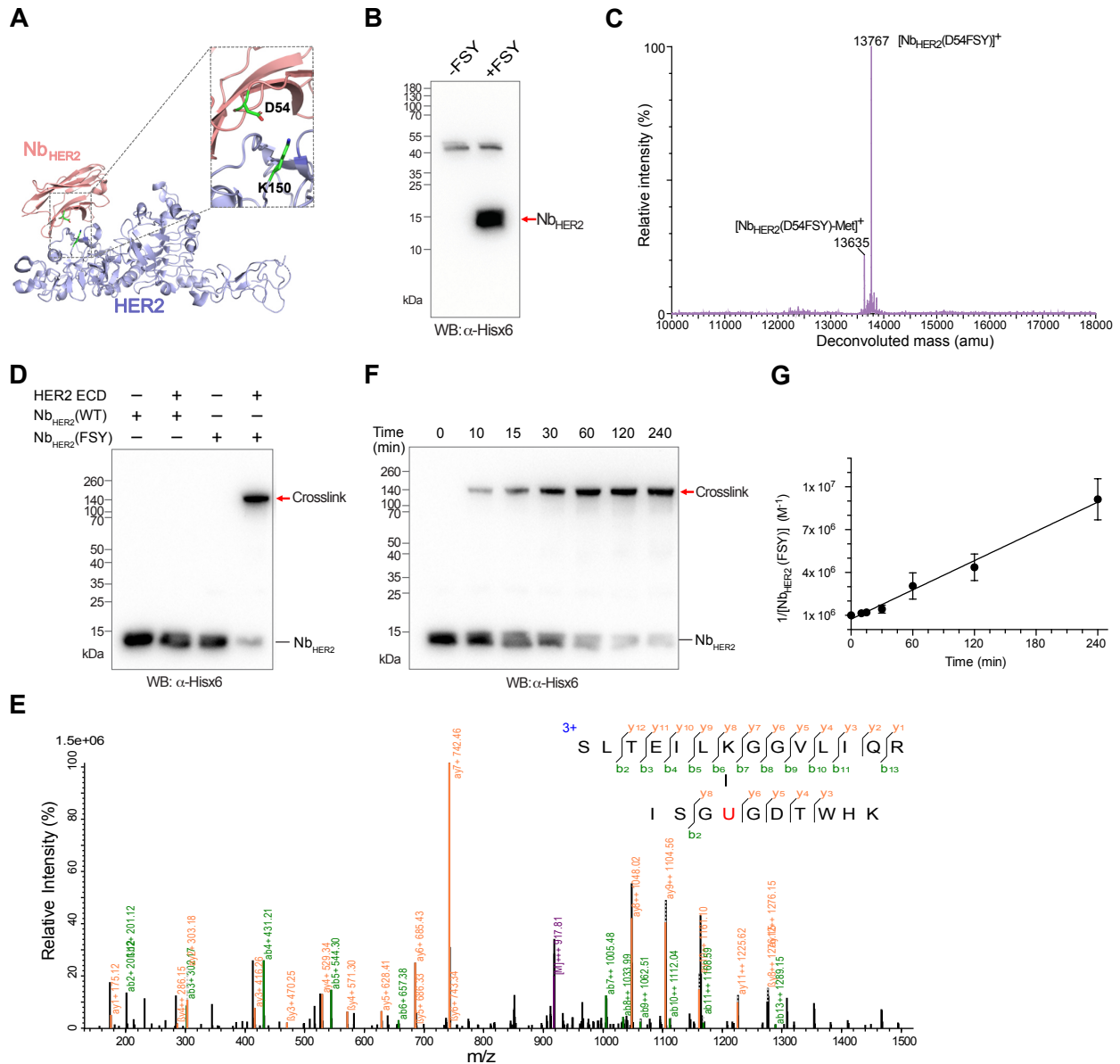


Figure 3.2: Genetically encoding FSY in Nb_{HER2} to covalently crosslink HER2 irreversibly *in vitro*. (A) Crystal structure of Nb_{HER2} bound to HER2 ECD (PDB: 5MY6), showing the FSY incorporation site (D54) and the proximal target residue (K150) in HER2. (B) Western blot analysis of Nb_{HER2}(FSY) production in *E. coli* with and without 1 mM FSY in growth media. A His6x tag was appended at the C-terminus of Nb_{HER2} for detection. (C) Mass spectrum of the intact Nb_{HER2}(FSY) protein confirming FSY incorporation at position 54 in high fidelity. (D) Nb_{HER2}(FSY), but not Nb_{HER2}(WT), crosslinked with HER2 ECD *in vitro*. Indicated proteins were incubated at 37 °C for 4 hours followed with Western blot analysis. (E) Tandem mass spectrum of Nb_{HER2}(FSY) incubation with HER2 ECD confirmed that FSY (represented by U) of Nb_{HER2}(FSY) crosslinked with Lys150 of HER2 as designed. **Figure caption continued on the next page.**

Figure caption continued from previous page. (F) Crosslinking of Nb_{HER2}(FSY) to HER2 ECD occurred efficiently at 10 minutes and increased with time. (G) Kinetics of Nb_{HER2}(FSY) crosslinking with HER2 ECD. Nb_{HER2}(FSY) concentrations in Figure 2G were measured with densitometry and 1/[Nb_{HER2}(FSY)] was plotted against time. Linear regression of the data yielded a second-order rate constant of $34154 \pm 1921 \text{ M}^{-1}\text{min}^{-1}$ (mean \pm s.d.). Error bars represent s.d., n = 3 independent experiments.

We next tested if Nb_{HER2}(FSY) could covalently crosslink full-length native HER2 receptor on the cell surface of NCI-N87, a HER2-positive gastric cancer cell line. We treated NCI-N87 cells with different concentrations of Nb_{HER2}(FSY) and compared to PBS and Nb_{HER2}(WT). Cells were then lysed and analyzed with Western blot (**Fig. 3.3a**). PBS or Nb_{HER2}(WT) treated cells did not show any crosslinking of HER2, whereas Nb_{HER2}(FSY) treated cells all exhibited a covalent complex of HER2 with Nb_{HER2}(FSY). In addition, to determine if cell surface crosslinking was HER2-dependent, we treated additional cell lines with varying expression level of HER2. NCI-N87 and SK-OV-3 (ovarian cancer) both have high HER2 expression while MDA-MB-453 and MDA-MB-468 (breast cancer) both have undetectable HER2 expression. Covalent HER2 crosslinking by Nb_{HER2}(FSY) was detected on NCI-N87 and SK-OV-3 cells but not on MDA-MB-453 and MDA-MB-468 cells (**Fig. 3.3b**). Moreover, except with HER2, no other crosslinking bands were detected for Nb_{HER2} in all four tested cell lines, suggesting that Nb_{HER2}(FSY) was highly selective in crosslinking the HER2 receptor on cell surface.

We further tested whether Nb_{HER2}(FSY) could crosslink HER2 on tumor *in vivo*. Nb_{HER2}(WT) or Nb_{HER2}(FSY) was delivered via intravenous tail vein injection into mouse xenografted with HER2-expressing NCI-N87 tumor. The tumor was dissected 6 hours post-injection, homogenized and immunoblotted to detect crosslinking. Nb_{HER2}(WT) did not yield any crosslinking with HER2, whereas Nb_{HER2}(FSY) showed apparent crosslinking with HER2 (**Fig. 3.3c**). Taken together, the *in vitro*, on-cell and on-tumor crosslinking assay indicate that Nb_{HER2}(FSY) was able to bind to the HER2 receptor selectively, efficiently, and irreversibly.

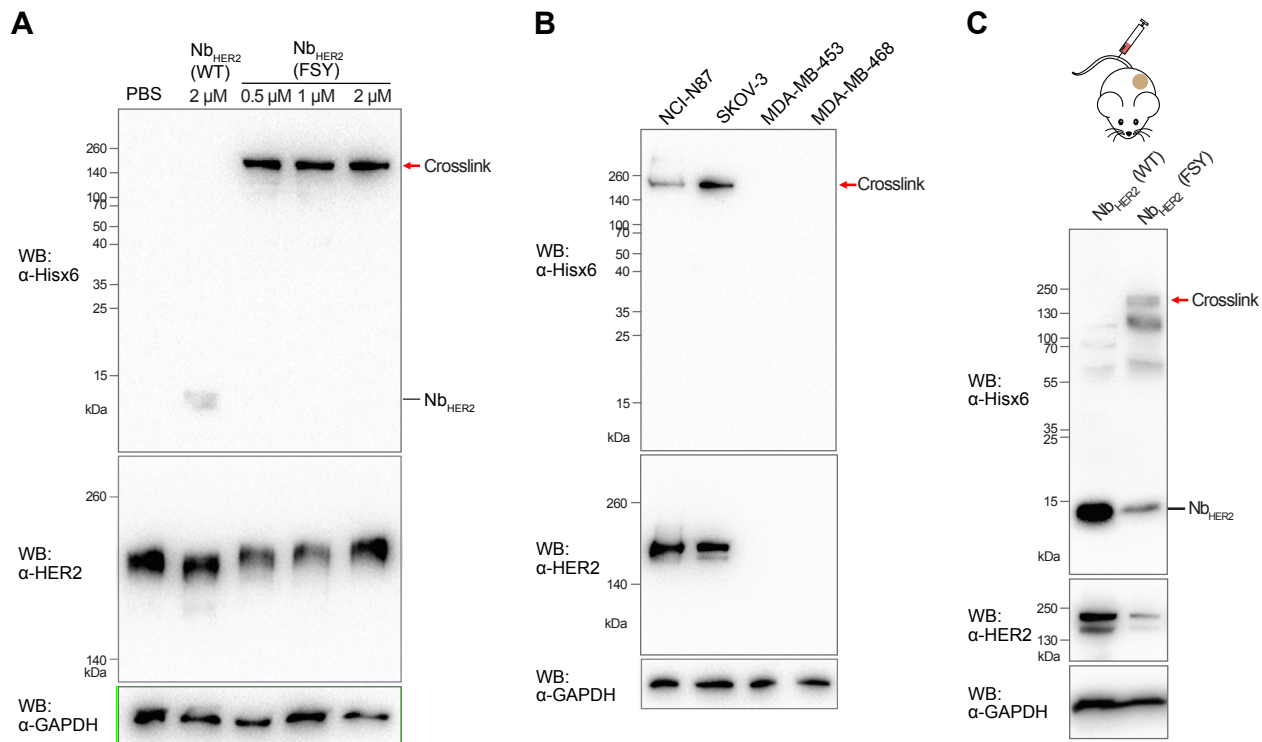


Figure 3.3: Nb_{HER2}(FSY) covalently crosslinked native HER2 on cancer cells and on tumor *in vivo*. (A) Nb_{HER2}(FSY) covalently crosslinked HER2 on NCI-N87 cell surface. Nb_{HER2} proteins were incubated with NCI-N87 cells for 3 hours followed with Western blot analysis. (B) Crosslinking of Nb_{HER2}(FSY) with cancer cells were HER2 specific. Crosslinking occurred only on NCI-N87 and SK-OV-3 cells, which have detectable HER2 expression. (C) Nb_{HER2}(FSY) covalently crosslinked HER2 on NCI-N87 tumor *in vivo*. Nb_{HER2}(FSY) or Nb_{HER2}(WT) was injected into mice xenografted with HER2-expressing NCI-N87 tumor. After 6 hours post-injection, the tumor was excised and homogenized, followed with Western blot analysis.

To assess if Nb_{HER2}(FSY) could enhance tumor accumulation and target-to-background ratio, we radiolabeled Nb_{HER2}(WT) and Nb_{HER2}(FSY) and monitored the resultant radiopharmaceuticals in xenografted mice through microPET/CT imaging. Nb_{HER2}(WT) and Nb_{HER2}(FSY) were labelled with iodine-124 (¹²⁴I) using [¹²⁴I]NaI and the established iodination reagent IODO-GEN (**Fig. 3.4a**).²⁹ ¹²⁴I is a positron emitter with a long half-life ($t_{1/2} \sim 4.2$ days) suitable for PET and pharmacokinetic studies.³⁰ The radiochemical purity was 99.9% for ¹²⁴I-Nb_{HER2}(WT) and 95.2% for ¹²⁴I-Nb_{HER2}(FSY) (**Fig. 3.S3**). We also similarly labeled Nb_{HER2}(FSY) with cold NaI and showed that iodine labeling did not impair the ability of Nb_{HER2}(FSY) to covalently crosslink HER2 (**Fig. 3.4b**). Next, male nude mice bearing subcutaneous NCI-N87 tumor were injected with

$^{124}\text{I-Nb}_{\text{HER2}}(\text{WT})$ or $^{124}\text{I-Nb}_{\text{HER2}}(\text{FSY})$ intravenously. Both $^{124}\text{I-Nb}_{\text{HER2}}(\text{WT})$ and $^{124}\text{I-Nb}_{\text{HER2}}(\text{FSY})$ were co-injected with L-lysine to avoid peak catabolism in the kidneys for renal protection.^{31,32} To evaluate pharmacokinetics, blood clearance of $^{124}\text{I-Nb}_{\text{HER2}}(\text{WT})$ and $^{124}\text{I-Nb}_{\text{HER2}}(\text{FSY})$ was monitored using a dynamic PET acquisition for 90 min post-injection on a dedicated small animal microPET/CT. Both were cleared from blood circulation rapidly (**Fig. 3.S4**). The $t_{1/2}$ for fast phase was measured 5.76 s for $^{124}\text{I-Nb}_{\text{HER2}}(\text{WT})$ and 3.35 s for $^{124}\text{I-Nb}_{\text{HER2}}(\text{FSY})$, suggesting that FSY incorporation did not prolong the desired rapid clearance of the radio-labeled nanobody.

The mice were subsequently imaged with microPET/CT. The radiotracer uptake in liver, kidney, thyroid, and skeletal muscle were qualitatively similar for $^{124}\text{I-Nb}_{\text{HER2}}(\text{WT})$ and $^{124}\text{I-Nb}_{\text{HER2}}(\text{FSY})$ (**Fig. 3.S5**), indicating that FSY incorporation did not significantly alter the biodistribution of the radiolabeled nanobody in normal organs lacking HER2. In contrast, a marked difference was detected on the tumor. From 3 to 10 hours post-injection, the on-tumor activity showed similar levels between $^{124}\text{I-Nb}_{\text{HER2}}(\text{WT})$ and $^{124}\text{I-Nb}_{\text{HER2}}(\text{FSY})$ in the PET images (**Fig. 3.4c**). However, a dramatic difference was observed from 24 to 72 hours post-injection. At 24 hours post injection, $^{124}\text{I-Nb}_{\text{HER2}}(\text{WT})$ was no longer detectable in tumor, whereas $^{124}\text{I-Nb}_{\text{HER2}}(\text{FSY})$ was clearly detectable in tumor from 24 – 72 hours post injection. Quantification of tumoral uptake using region of interest analysis revealed that $^{124}\text{I-Nb}_{\text{HER2}}(\text{FSY})$ had ~4.5, 5, and 4-fold of activity over $^{124}\text{I-Nb}_{\text{HER2}}(\text{WT})$ at 24, 48, and 72 h post-injection, respectively (**Fig. 3.4d**). The total radiation, quantified by area under the curve (AUC), was 78 ± 4 for $^{124}\text{I-Nb}_{\text{HER2}}(\text{FSY})$ and 43 ± 4 for $^{124}\text{I-Nb}_{\text{HER2}}(\text{WT})$, showing 81.4% more radiation accumulation to tumor by $^{124}\text{I-Nb}_{\text{HER2}}(\text{FSY})$. Three-dimensional maximum intensity projections of the PET/CT data showed that, from 24 to 72 hours post-injection, mice injected with $^{124}\text{I-Nb}_{\text{HER2}}(\text{FSY})$ had the tumor distinctly visible and virtually no retention in normal tissues with the exception of the thyroid (**Fig.**

3.4e). The thyroid was visible due to scavenging of free ^{124}I anion that is known released by catabolism *in vivo*.³³ Extended retention of ^{124}I -Nb_{HER2}(FSY) at the tumor site thus would result in the observed higher level of thyroid uptake than ^{124}I -Nb_{HER2}(WT). Collectively, these data show that the covalent nanobody dramatically improved tumoral retention of the labeled radionuclide without changing the pharmacokinetic profile.

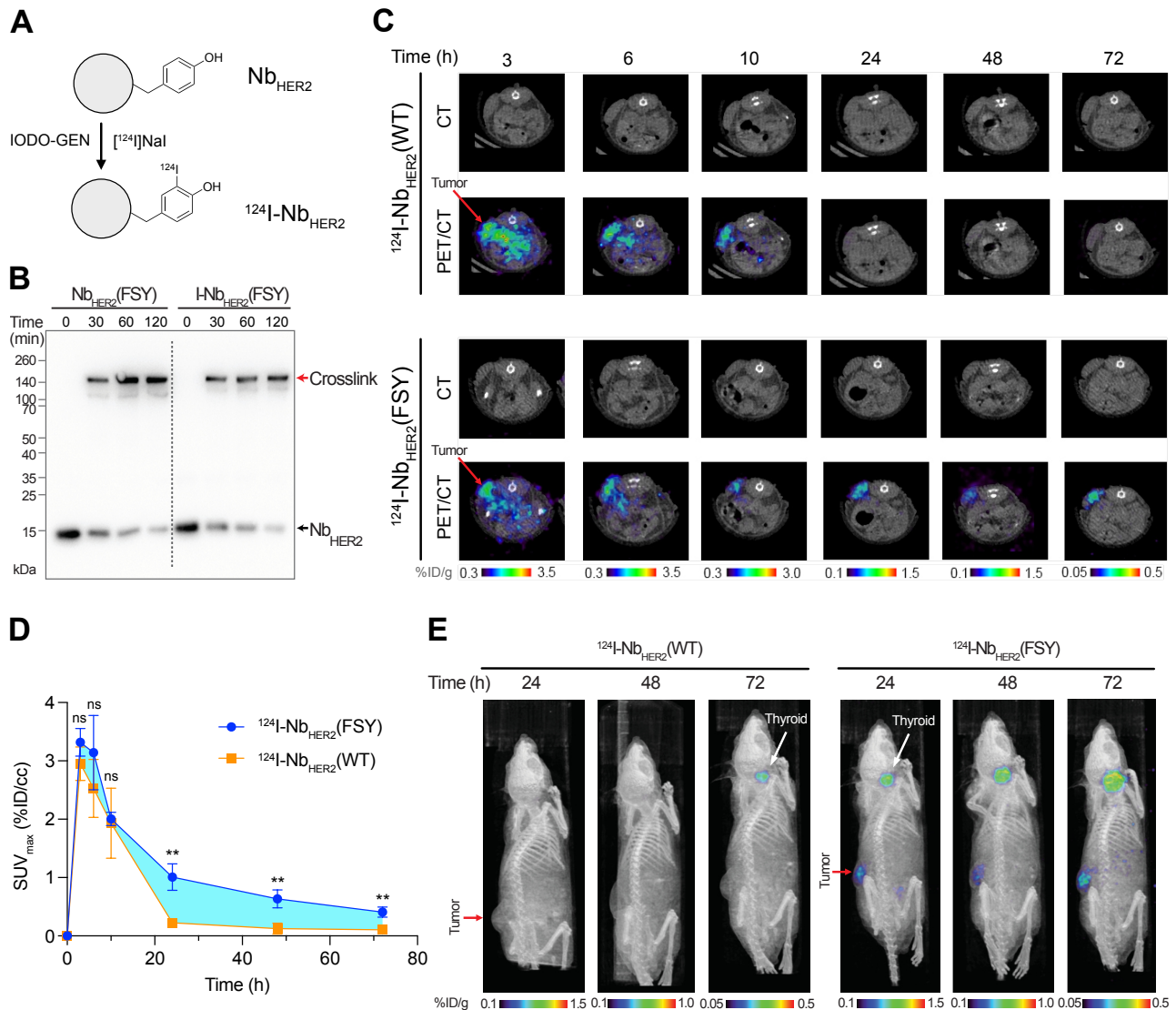


Figure 3.4: Radiolabeled covalent nanobody ^{124}I -Nb_{HER2}(FSY) prolonged tumor retention, increased tumor accumulation, and exhibited low background in mice. (A) Schematic procedures to radiolabel WT and covalent Nb_{HER2} with ^{124}I by IODO-GEN. Tyrosine is usually labeled at the ortho position with mono- or di-iodination. **Figure caption continued on the next page.**

Figure caption continued from previous page. (B) Iodine labeling did not impair Nb_{HER2}(FSY) crosslinking with HER2. The cold NaI labeled product I-Nb_{HER2}(FSY) or the unlabeled Nb_{HER2}(FSY) was incubated with HER2 ECD for crosslinking, followed with Western blot analysis. (C) The covalent ¹²⁴I-Nb_{HER2}(FSY) enabled specific and sustained tumor accumulation of ¹²⁴I. Tumors were clearly detectable 24-72 hours post-injection for ¹²⁴I-Nb_{HER2}(FSY) but not ¹²⁴I-Nb_{HER2}(WT). Representative decay-corrected PET images of mice xenografted with HER2-expressing NCI-N87 tumor and injected with either ¹²⁴I-Nb_{HER2}(WT) or ¹²⁴I-Nb_{HER2}(FSY) are shown. The transverse images of mice were taken at 3-72 hours post-injection. Color bars indicate percent injected dose per gram (%ID/g). (D) The covalent ¹²⁴I-Nb_{HER2}(FSY) significantly enhanced tumor accumulation of ¹²⁴I than ¹²⁴I-Nb_{HER2}(WT). The standardized uptake value (SUV) of ¹²⁴I in tumor was quantified in percent injected dose per cm³ (%ID/cc) and plotted with post-injection time. The increase in tumor uptake by ¹²⁴I-Nb_{HER2}(FSY) over ¹²⁴I-Nb_{HER2}(WT) is highlighted in cyan. Error bars represent s.d.; n = 3 mice for ¹²⁴I-Nb_{HER2}(WT) injection; n = 4 mice for ¹²⁴I-Nb_{HER2}(FSY) injection; ns, not significant; ** p < 0.01; Student's t-test for statistical analysis. (E) The covalent ¹²⁴I-Nb_{HER2}(FSY) enabled clear imaging of tumor distinct from the background. 3D PET image reconstruction of mice 24-72 hours post-injection of ¹²⁴I-Nb_{HER2}(WT) or ¹²⁴I-Nb_{HER2}(FSY) are shown. Color bars indicate %ID/g. n = 3 mice for ¹²⁴I-Nb_{HER2}(WT) injection; n = 4 mice for ¹²⁴I-Nb_{HER2}(FSY) injection.

We next asked if the increase in tumoral retention of the covalent nanobody compared to the WT nanobody was sufficiently large to impact antitumor effects. To address this question, we prepared Nb_{HER2}(WT) and Nb_{HER2}(FSY) labeled with ²²⁵Ac, an emerging radioisotope that produces alpha emissions. We chose ²²⁵Ac as α -emitters are more effective antitumor agents due to their higher linear energy transfer properties compared to α -emitters like ¹⁷⁷Lu,³⁴ and the tumoral uptake levels of the nanobody would likely necessitate a potent payload. Moreover, ²²⁵Ac TRTs are under clinical investigation, and the early data suggest the radioisotope is well tolerated *in vivo*.^{35,36}

To prepare for the TRTs, Nb_{HER2}(WT) and Nb_{HER2}(FSY) were conjugated with Macropa-PEG₄-TFP ester (**Fig. 3.5a**). Macropa was chosen as the chelator as recent data have shown that it chelates ²²⁵Ac efficiently.^{37,38} Mass spectrometric analysis of the conjugated samples confirmed that both Nb_{HER2}(WT) and Nb_{HER2}(FSY) were successfully conjugated with Macropa-PEG₄, showing two peaks of approximately equal intensity corresponding to the unlabeled and singly

labeled nanobody, respectively (**Fig 3.5b**). To ensure that the conjugation of Macropa-PEG₄ did not affect nanobody's covalent crosslinking ability, we incubated Macropa-PEG₄-Nb_{HER2}(WT) or Macropa-PEG₄-Nb_{HER2}(FSY) with and without the HER2 ECD at 37 °C for up to 2 hours and analyzed the samples via Western blot (**Fig. 3.5c**). The Macropa-PEG₄-Nb_{HER2}(FSY) could still effectively crosslink HER2, suggesting that the Macropa-PEG₄ label had not negatively impacted the covalency of our nanobody. Macropa-PEG₄-Nb_{HER2}(WT) and Macropa-PEG₄-Nb_{HER2}(FSY) were then radiolabeled with ²²⁵Ac yielding ²²⁵Ac-Nb_{HER2}(WT) and ²²⁵Ac-Nb_{HER2}(FSY), respectively. The radiochemical purity was >95% for ²²⁵Ac-Nb_{HER2}(WT) and ²²⁵Ac-Nb_{HER2}(FSY) (**Fig. 3.S6**).

To evaluate TRT efficacy *in vivo*, we xenografted HER2-expressing NCI-N87 tumors subcutaneously in male athymic nu/nu mice and treated them twice with either ²²⁵Ac-Nb_{HER2}(WT), ²²⁵Ac-Nb_{HER2}(FSY), or saline via tail vein injection on day 0 and day 7 (**Fig. 3.5d**). The mice received doses of ~0.8 μCi at the same molar activity (0.67 μCi/pmol). Tumor growth was measured over 23 days via calipers and the mice were euthanized on day 26. When compared with the saline control, while injection with ²²⁵Ac-Nb_{HER2}(WT) showed no tumor growth inhibition, injection with the covalent nanobody ²²⁵Ac-Nb_{HER2}(FSY) slowed down tumor growth significantly (**Fig. 3.5e**). Endpoint analysis also showed that the tumor weight was significantly reduced when mice were treated with ²²⁵Ac-Nb_{HER2}(FSY) but not with ²²⁵Ac-Nb_{HER2}(WT) (**Fig. 3.5f**). The body weight changes serve as a sensitive indicator of general health status. The weight of the mice in either of the three groups did not change significantly after treatment (**Fig. 3.5g**), indicating no systemic toxicity. To further demonstrate that the radiolabeled nanobodies did not cause significant toxicity to organs, the liver, kidney, heart and bone marrow were treated with hematoxylin and eosin stains and examined by an independent pathologist for signs of

abnormalities. Most ^{225}Ac radiation-induced toxicity occurs at either the liver, kidney, or bone marrow. HER2-targeting drugs often cause cardiotoxicity,³⁹ and therefore the heart was analyzed as well. No abnormalities were detected in any tissue samples from the groups treated with either $^{225}\text{Ac-Nb}_{\text{HER2}}(\text{FSY})$ or $^{225}\text{Ac-Nb}_{\text{HER2}}(\text{WT})$ (**Fig. 3.5h**), suggesting no toxicity and systematic clearance of the radiolabeled nanobodies after treatment.

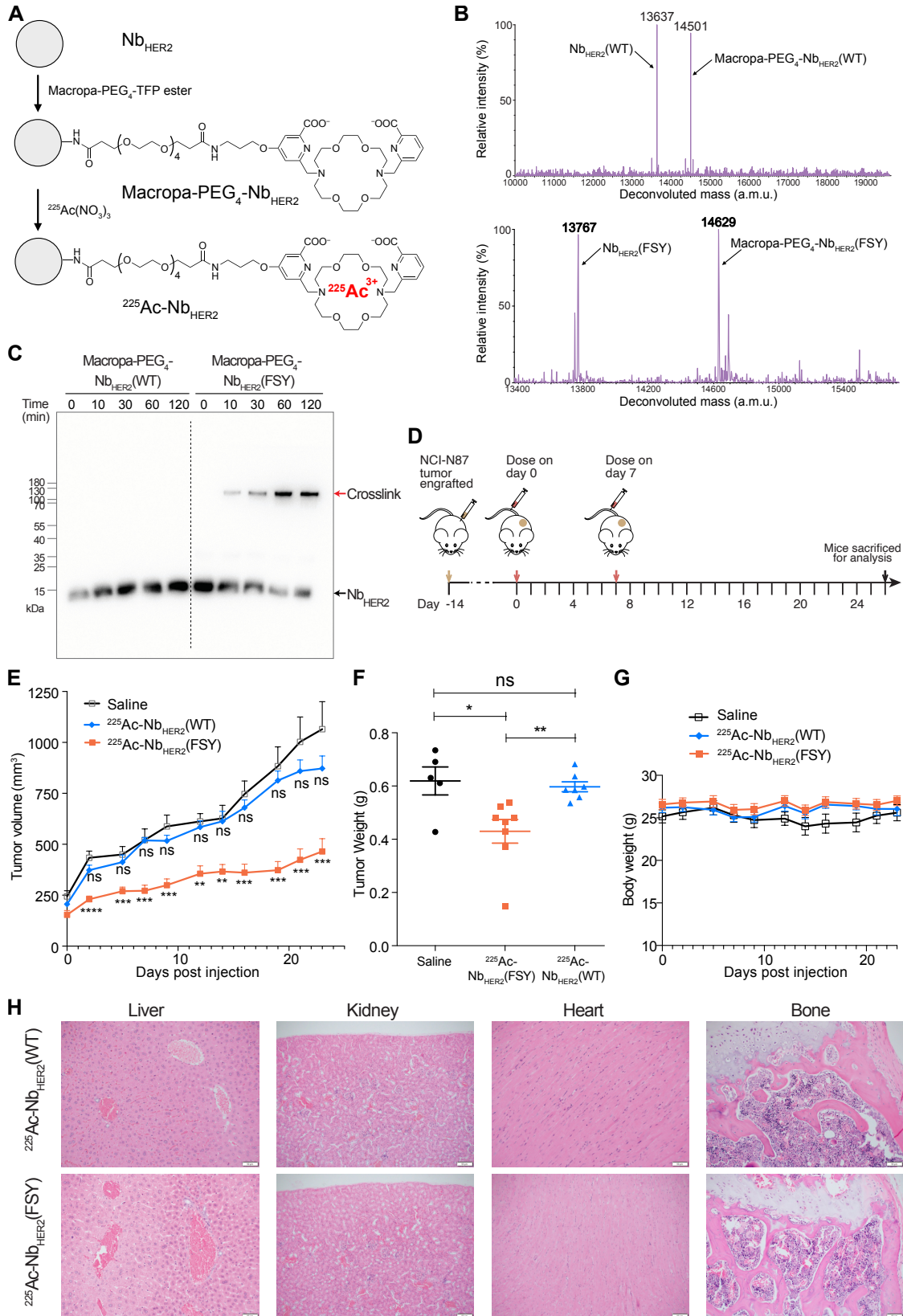


Figure 3.5: α -Emitter labeled covalent $^{225}\text{Ac-NbHER2(FSY)}$ inhibited tumor growth in mice without tissue toxicity. (A) Schematic procedures to radiolabel WT and covalent Nb_{HER2} with ^{225}Ac . (B) Mass spectrometric analyses confirming successful conjugation of Macropa-PEG4 on Nb_{HER2}(WT) (top panel) and Nb_{HER2}(FSY) (bottom panel). (C) Western blot analysis confirming that Macropa-PEG4 labeling did not impair Nb_{HER2}(FSY) crosslinking with HER2. Crosslinking of Macropa-PEG4-Nb_{HER2}(FSY) to HER2 ECD occurred efficiently after 10 minutes incubation and increased with time, while no crosslinking was detected with Macropa-PEG4-Nb_{HER2}(WT). (D) Experiment scheme for TRT of NCI-N87 tumor in mice. (E) Growth curves of engrafted NCI-N87 tumors indicate that $^{225}\text{Ac-NbHER2(FSY)}$ inhibited tumor growth while $^{225}\text{Ac-NbHER2(WT)}$ did not. (F) Weight comparison of dissected tumors showing tumor weight reduction by $^{225}\text{Ac-NbHER2(FSY)}$ treatment. (G) Mice body weight remained stable over the course of the therapy study. For panels E-G, error bars represent SEM; n = 8 mice for $^{225}\text{Ac-NbHER2(FSY)}$ treatment group; n = 7 mice for $^{225}\text{Ac-NbHER2(WT)}$ treatment group; n = 5 mice for vehicle saline control. ns, not significant; *p < 0.05; ** p < 0.01; *** p < 0.001; **** p < 0.0001; Student's t-test for statistical analysis. (H) Representative microscopic images of hematoxylin and eosin stained liver, kidneys, heart, and bone marrow for both $^{225}\text{Ac-NbHER2(WT)}$ and $^{225}\text{Ac-NbHER2(FSY)}$ treatment groups. No abnormalities were detected in the tissues. Scale bar, 50 μm .

3.4 Discussion

As we now understand TRT is a viable option to treat common and heterogeneous solid tumor types like metastatic castration resistant prostate cancer, there is an urgent need to develop new strategies to maximize their antitumor activity. This is an unusual challenge, as many of the approaches used to attenuate the toxicity of other cancer therapeutics are likely not relevant to TRT. For example, prodrug masking, one of the most venerable approaches for restricting drug activity to tumors, is likely not possible for TRT given the continuous decay of the isotopic payload. It's also not evident whether common drug delivery strategies used to expand the therapeutic window for chemotherapies (e.g., liposome encapsulation) have any relevance to TRT, as the TRT mass dose is often so low that the ligand's bioactivity rarely factors into its pharmacological profile. The mode of administration is also expected to be limited to intravenous, intraarterial, or intratumoral routes, as rapid delivery to the tumor is essential to limit host toxicity. Thus, and quite tragically, the field has been stuck in a safety/efficacy dilemma wherein increasing tumor absorption of the TRT is best achieved by lengthening its serum half-life, which by necessity

further increases radiation to normal tissue compartments.

Herein, we present the first chemical strategy to increase tumor absorption of a protein-based radiopharmaceutical without impacting its other pharmacokinetic properties. By genetically engineering the latent bioreactive Uaa FSY into the nanobody Nb_{HER2}, we generated a covalent nanobody that specifically and irreversibly targeted HER2 via the PERx mechanism *in vitro*, on cancer cells, and on tumor *in vivo*. With radioisotope ¹²⁴I labeling, the covalent nanobody enhanced radionuclide accumulation and showed prolonged residence in HER2-expressing tumors while still maintaining fast clearance from circulation in mice, which enabled exceptional contrast for tumor detection and low background activity in other tissues for molecular imaging in mice. When we labeled the same covalent nanobody with the potent α -emitter ²²⁵Ac, the resultant covalent ²²⁵Ac-Nb_{HER2}(FSY) had a much higher antitumor efficacy targeting HER2-expressing tumors than the ²²⁵Ac-Nb_{HER2}(WT) counterpart while having no detectable toxicity in normal tissues.

Leveraging fast-clearing proteins to bind target covalently, our method thus can enable a new class of radiopharmaceuticals for TRT to simultaneously achieve efficacy and safety. Existing protein radiopharmaceuticals bind their targets only through noncovalent interactions; our covalent protein radiopharmaceutical changes this paradigm and exploits the therapeutic benefits of covalency. The covalent binding is realized through proximity-enabled reactivity of the latent bioreactive Uaa, which safeguards the reaction to be highly specific between the covalent protein and its target.¹⁸ Indeed, off-target crosslinking is not detected *in vivo* in mice or in human serum.¹⁸ In this study, similar systemic clearance of radiolabeled Nb_{HER2}(FSY) as Nb_{HER2}(WT) and no tissue abnormalities both suggest no off-target covalent binding. The proximity-enabled reaction mechanism of our covalent protein radiopharmaceutical thus uniquely allows it to react and durably reside at the tumor site only, which is critical for the improved efficacy and safety. Indeed,

a recent TRT study dosed 2.29 μCi of ^{225}Ac -labeled noncovalent WT Nb_{HER2} in mice, which results in substantial inflammatory lesions in kidney.⁴⁰ Our covalent Nb_{HER2}(FSY) permitted a drastic lower dose of 0.8 μCi for tumor inhibition and did not cause tissue toxicities.

Our method can readily expand the repertoire of radiopharmaceuticals that work in the unique covalent mechanism to target a broad range of cancer specific proteins with various expression levels. Radiopharmaceuticals approved for radionuclide therapy in oncology have used small-molecule, peptide or antibody as the delivery vehicle with caveats either in efficacy or safety.¹ Through irreversible covalent binding, our method will enable the broad use of proteins with MW below the renal filtration threshold as the delivery vehicle. Aside from nanobody demonstrated herein, these proteins can be affibody,¹⁸ single-chain variable fragment (ScFv), Fab,⁴¹ DARPins, *de novo* designed mini-binders, and so on, which can be readily developed with well-defined binding and selectivity against various antigens. Our method requires the incorporation of only a single latent bioreactive amino acid, and genetic incorporation of latent bioreactive Uaas into proteins can be carried out in both prokaryotic and eukaryotic cells,^{42,43} permitting the ready conversion of all these proteins into covalent proteins. In addition, through chemically synthesizing the PERx-capable functional group into peptides, we expect that the PERx principle can be similarly applied to generate peptide-based covalent radiopharmaceuticals.⁴⁴ Moreover, covalent protein binders are able to crosslink both high and low-abundance targets efficiently.^{45,46} Unlike current low MW radioligands that are limited to highly overexpressed receptors, the covalent protein radiopharmaceuticals can be suitable for targets with various expression levels. Irreversible binding will also make covalent radiopharmaceuticals suitable for targets that do not internalize. Lastly, beyond cancer, the improved efficacy and safety of covalent protein radiopharmaceuticals will expand the scope of TRT to non-cancerous diseases such as heart,

gastrointestinal, endocrine and neurological diseases. For the generalization of this covalent protein radiopharmaceutical strategy, the crosslinking kinetics and specificity are both critical. The reaction must be fast enough to crosslink sufficient targets before the drug clears the blood, and meanwhile must be target specific to avoid off-target crosslinking. The crosslinking kinetics can be affected by radiopharmaceutical and target concentration, their association and dissociation rate, as well as the reactivity between the Uaa and target residue. Therefore, selection of protein binder with appropriate binding kinetics, development of new latent bioreactive Uaas with enhanced proximity-enabled reactivity, and optimization of Uaa incorporation sites may facilitate the generation of effective covalent protein radiopharmaceuticals for various targets.²¹ In addition, pharmacokinetics differs between mice and humans, and our current study was performed in mice and did not address potential HER2 on-target toxicity, which both warrant further investigation for clinical translation.

In summary, covalent protein radiopharmaceuticals enabled highly specific, extended retention of radionuclide in tumors while sparing normal tissues, thus enhancing the efficacy and safety of TRT. Shifting the protein-based TRT from noncovalent to covalent binding mode, covalent protein radiopharmaceuticals have the potential to expand TRT across diverse targets and disease areas for precision medicine.

3.5 Materials and Methods

Reagents

Primers were synthesized and purified by Integrated DNA Technologies (IDT), and plasmids were sequenced by GENEWIZ. All molecular biology reagents were either obtained from New England Biolabs or Vazyme. His-HRP and GAPDH-HRP antibodies were obtained from ProteinTech Group. HER2/ErbB2 antibody was obtained from Cell Signaling Technology.

Nb_{HER2} amino acid sequence

MKYLLPTAAAGLLLLAAQPAMAMGQVQLQESGGGSVQAGGSLKLTCAASGYIFNSCGMG
WYRQSPGRERELVSRISGDGDTWHKESVKGRFTISQDNVKKTLYLQMNSLKPEDTAVY
FCAVCYNLETYWGQGTQVTVSSHHHHHHH

pelB leader sequence is highlighted in *italics*.

Residue D54 in **bold** was the site where FSY was incorporated.

Protein expression and purification

Plasmids pBad-Nb_{HER2} (WT) was transformed into SHuffle T7 Express electrocompetent *E. coli* cells. pBad-Nb_{HER2} (D54TAG) and pEvol-FSYRS was co-transformed DH10b electrocompetent *E. coli* cells. For expression, transformed bacteria was culture in 2xYT at 37 °C with either 100 µg/mL ampicillin only (for Nb_{HER2} (WT)) or 100 µg/mL ampicillin and 34 µg/mL chloramphenicol (for Nb_{HER2} (D54TAG)). The culture was induced with 0.2% arabinose once OD₆₀₀ reached 0.6-0.8. For Nb_{HER2} (D54TAG), 1 mM FSY was added right before induction. The expression was induced for 16-20 h at 18 °C, and the bacterial pellets were collected by centrifugation at 8000 g for 15 min. The bacterial pellets were resuspended in lysis buffer (25 mM

sodium phosphate, 500 mM NaCl, 20 mM imidazole, 1 mg/mL lysozyme, 0.1 mg/mL DNase, and protease inhibitor; pH 7.5). The IMAC chromatography was used for protein purification and the procedure was described previously.⁴⁷

Mass spectrometry

Mass spectrometric measurements were performed as previously described.^{47,48} Mass spectra of intact proteins were obtained through electrospray ionization mass spectrometry, operating in positive electrospray ionization mode (ESI+), using a Xeno G25 Q-ToF mass spectrometer. The mass spectrometer was connected to an LC-20AD (Shimadzu) liquid chromatography unit. Using reverse phase chromatography, the protein sample was separate from small molecules using a Waters Xbridge BEH C4 column (300 Å, 3.5 µm, 2.1 mm x 50 mm). An acetonitrile gradient (30-71.4%) with 0.1% formic acid was used with a 0.2 mL/min constant flow rate at RT. Data was obtained at a rate of 1 sec/scan between 10000 to 18000 m/z. MassLynx mass spectrometry software was used to deconvolute the spectra. Nb_{HER2} mass was calculated with the pelB leader sequence removed and the formation of two disulfide bonds.

For tandem mass spectrometry, the peptides were analyzed and sequence using a Q Exactive Orbitrap interfaced with Ultimate 3000 LC system. To prepare the peptide, 5 µg of Nb_{HER2} (FSY) was incubated with 12.5 µg of HER2 ECD for 16 h at 37 °C. The crosslinking reaction was then subsequently digested with trypsin. The trypsin digested crosslink peptide was then injected into an Ace UltraCore super C18 reverse-phase column (300 Å, 2.5 µm, 75 mm x 2.1 mm). An acetonitrile gradient (5-95%) with 0.1% formic acid was used with a 0.2 mL/min constant flow rate at RT. Stepped collision energy HCD was used to fragmentize the crosslinked peptide with a normalized collision energy of 28, 30, 35 eV. Survey scans were acquired at a resolution of 70,000

at m/z 200 on the Q Exactive. Cross-linked peptides were searched with pLink 2 and OpenUaa search engine.^{49, 50}

Crosslinking of Nb_{HER2} with HER2 ECD *in vitro*

Recombinant extracellular domain (ECD) of HER2 receptor was purchased from Abcam (Cat# ab168896). Purified 1 μ M Nb_{HER2} (WT) or Nb_{HER2} (FSY) was incubated with 1 μ M HER2 in 10 μ L 1 X PBS, pH 7.4 for 4 h or indicated time points at 37 °C. After incubation, 4x Laemmli sample buffer (Bio Rad, Cat# 161-0747) with 2-mercaptoethanol was added into the incubation and heated at 95 °C for 10 min. The samples were separated on SDS-PAGE and either analyzed by Coomassie blue staining or Western blot. For Western blotting, the PVDF membrane was blocked with 5% milk for 1 h at RT while rocking. The membrane was then treated with 1:10000 anti-his monoclonal antibody (Proteintech #HRP66005) in 5% milk at RT while rocking. The membrane was then washed three times with PBST before imaging.

Biolayer interferometry (BLI) measurement

The association kinetics between human HER2 and Nb_{HER2} was measured with BLI using the Octet Red384 system (ForteBio). Biotinylated human HER2 protein (HE2-H82E2, Acro Biosystems) was first loaded to streptavidin (SA) sensor (ForteBio #18-5019) by incubating the SA sensor in 100 nM biotinylated human HER2 in the Kinetic Buffer (0.005 % (v/v) Tween 20 and 0.1 % BSA in PBS, pH = 7.4) at 25 °C. The sensor was equilibrated (baseline step) in the Kinetic Buffer for 120 s, after which the sensor was incubated with varying concentrations (12.5, 25, 50, 100, and 200 nM) of Nb_{HER2}(WT) or Nb_{HER2}(FSY) (association step) for 90 s, followed

with dissociation step in the Kinetic Buffer for 400 s. Data was fitted for a 1:1 stoichiometry and kinetic rate constant was calculated using the built in software.

Crosslinking of Nb_{HER2} with HER2 on cells

NCI-N87 cells (2×10^5) was seeded in 12-well plates and cultured with RPMI 1640 + 10% FBS. After 16 h, 1 μ M Nb_{HER2} (WT) or Nb_{HER2} (FSY) was added into culture for a final 0.5 mL volume. After 3 h incubation, the cells were washed twice with 1X PBS and dissociated with enzyme free dissociation buffer. The cells were collected and lysed with 100 μ L Pierce RIPA buffer with protease inhibitor cocktail for 1 h on ice. The cell lysates were analyzed with Western blots using antibodies specific for Hisx6 (Proteintech #HRP66005, 1:10000 dilution), HER2 (Cell signaling #2165S 1:1000 dilution), or GAPDH (Proteintech #HRP60004, 1:10000 dilution). The Western blots detecting HER2 required a secondary anti-Rabbit incubation (scbiotech #sc-2357, 1:5000 dilution). The Western blot condition is described above.

Crosslinking of Nb_{HER2} with HER2 on tumor *in vivo*

NCI-N87 cells (5.0×10^6) were resuspended in 200 μ L PBS and subcutaneously injected into the left flank in mice (age 6-8 weeks, male, 25.0 ± 3.0 g). After 21 days, 50 μ g of either Nb_{HER2} (WT) or Nb_{HER2} (FSY) and 30 mg L-lysine was intravenously injected into each mouse. The mice were sacrificed at 6 h post-injection and the NCI-N87 tumor was excised from the mice. The tumors were added 500 μ L of RIPA and 1x protease inhibitor and was homogenized and lysed. The cell lysates were analyzed with Western blot as described above.

¹²⁴I Radiolabeling of Nb_{HER2}

Nb_{HER2} (WT) or Nb_{HER2} (FSY) was labeled with ¹²⁴I by using the direct iodination strategy. In a Pierce iodination tube, 3.0 mCi of Na¹²⁴I was added and the pH was adjusted to 7 with 100 μL HEPES (1 M). Three mg of Nb_{HER2} (WT) or Nb_{HER2} (FSY) were added to the iodination tube and the reaction was carried out for 20 min at room temperature with frequent shaking. To check the radiolabeling efficiency, instant thin layer chromatography (iTLC) was performed using Whatman filter paper and 20 mM citric acid as mobile phase. The radiolabeled proteins were purified using G25 columns and PBS.

Preparation of Macropa-PEG₄-Nb_{HER2} and ²²⁵Ac radiolabeling

Macropa-PEG₄-TFP ester was synthesized using a previously reported method.³⁷ 110 nmol of Macropa-PEG₄-TFP ester was incubated with 7 nmol of either Nb_{HER2} (WT) or Nb_{HER2} (FSY) in 0.1 M Carbonate-Bicarbonate buffer pH 9.0 at 37 °C for 2 h. Then, Macropa-PEG₄-Nb_{HER2} (WT) or Macropa-PEG₄-Nb_{HER2} (FSY) was purified with a PD-10 desalting column using PBS, pH 7.4 as an eluent. For radiolabeling, actinium-225 (10 μCi) was incubated with either 15 pmol Macropa-PEG₄-Nb_{HER2} (WT) or 15 pmol Macropa-PEG₄-Nb_{HER2} (FSY) in 20 μL 2M NH₄OAc pH 5.8 buffer and 5 μL of L-Ascorbic Acid (150 mg/mL). The reaction proceeded for 30 min at 37 °C while shaking. The radiolabeling efficiency was measured using iTLC using iTLC-SG using 10 mM EDTA, pH=5.5 as a mobile phase and the radiolabeling yields were > ~95%. The radioimmunoconjugates ²²⁵Ac-Nb_{HER2}(WT) and ²²⁵Ac-Nb_{HER2}(FSY) were injected into mice without further purification.

Mice

All mouse protocols were approved by institutional animal care and use program and were carried out in compliance with the guidelines published by the Association for Assessment and Accreditation of Laboratory Animal Care (AAALAC). Mice were randomly assigned to experimental groups. Male mice 6-8 weeks, Nu/J (stain# 002019, The Jackson Laboratory) were used in all *in vivo* studies.

***In vivo* ^{124}I -Nb_{HER2}(WT) and ^{124}I -Nb_{HER2}(FSY) PET imaging studies**

PET imaging with ^{124}I labeled Nb_{HER2} (WT) or Nb_{HER2} (FSY) were done in NCI-N87 tumor bearing nude mice (age 6-8 weeks, male, 25.0 ± 3.0 g). NCI-N87 tumors were xenografted in mice by injecting 5.0×10^6 NCI-N87 cells subcutaneously in left flank. The mice were injected intravenously with 0.25 mg of cold NaI to suppress thyroid uptake. The kidney uptake was suppressed by co-injection of 30 mg of L-lysine per mice. Mice were injected with 50.0 ± 5.0 μCi ^{124}I labeled nanobodies (n = 4 for Nb_{HER2} (FSY), n = 3 for Nb_{HER2} (WT)) for the dynamic PET imaging and 80.0 – 100.0 μCi for the static PET imaging intravenously. PET dynamic images were acquired for 90 min with CT for 5 min. Static PET/CT images (n = 4 for Nb_{HER2} (FSY), n = 3 for Nb_{HER2} (WT)) were acquired at different time points post injections (3 h, 6 h, 10 h, 24 h, 48 h, 72 h). PET data were acquired on Siemens Inveon microPET/CT. The PET data was reconstructed and analyzed with AMIDE software.

***In vivo* ^{225}Ac -Nb_{HER2}(WT) and ^{225}Ac -Nb_{HER2}(FSY) therapy studies**

NCI-N87 tumors were xenografted in mice as described above. Once the xenografted-tumor reached 100-300 mm³ (Day 0), the mice were injected with 0.8 ± 0.2 μCi ^{225}Ac labeled nanobodies

(n = 8 for Nb_{HER2} (FSY), n = 7 for Nb_{HER2} (WT)) or Saline (n=5). The mice were also co-injected with 30 mg of L-lysine per mice. On Day 7, the mice were co-injected again with $0.8 \pm 0.2 \mu\text{Ci}$ ²²⁵Ac labeled nanobodies or saline and 30 mg of L-lysine per mice. The tumor growth was with a digital caliper in two dimensions, and tumor volume was calculated using the formula: tumor volume = length x width²/2. At day 26, the mice were sacrificed for analysis. The liver, kidney, heart, and bone were dissected and processed for hematoxylin and eosin (H&E) staining and analysis. The microscopic images of the H&E slides were analyzed by a trained pathologist (E.C.) and no abnormalities were observed with the tissues.

Quantification and statistical analysis

All quantitative data and statistical analysis were analyzed by Student's t test using Prism 6.0 (GraphPad software). All the P values were calculated using GraphPad PRISM 6.0 with the following significance: n.s. p > 0.05; * p < 0.05; ** p < 0.01; *** p < 0.001; **** p < 0.0001. Statistical details for each experiment can be found in the figures and the legends.

3.6 Supplemental Figures

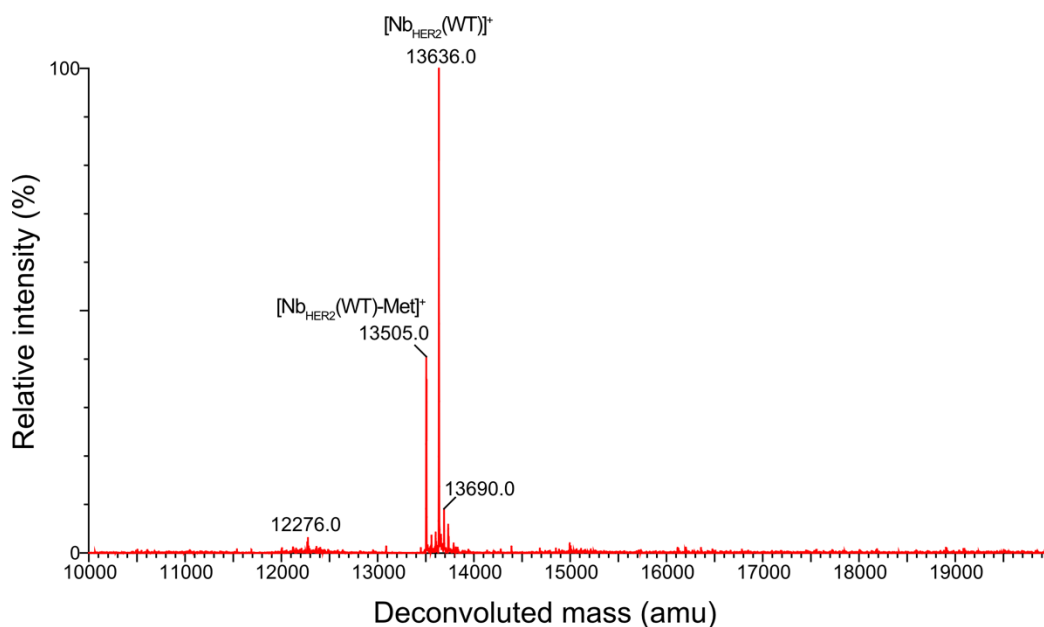


Figure 3.S1: Mass Spectrum of Nb_{HER2}(WT). Electrospray ionization time-of-flight mass spectrum of intact Nb_{HER2}(WT). Expected mass 13636 Da; observed 13636 Da. The -Met peak was also detected, which indicates loss of N-terminal Met residue and is expected for proteins expressed in *E. coli* cells.

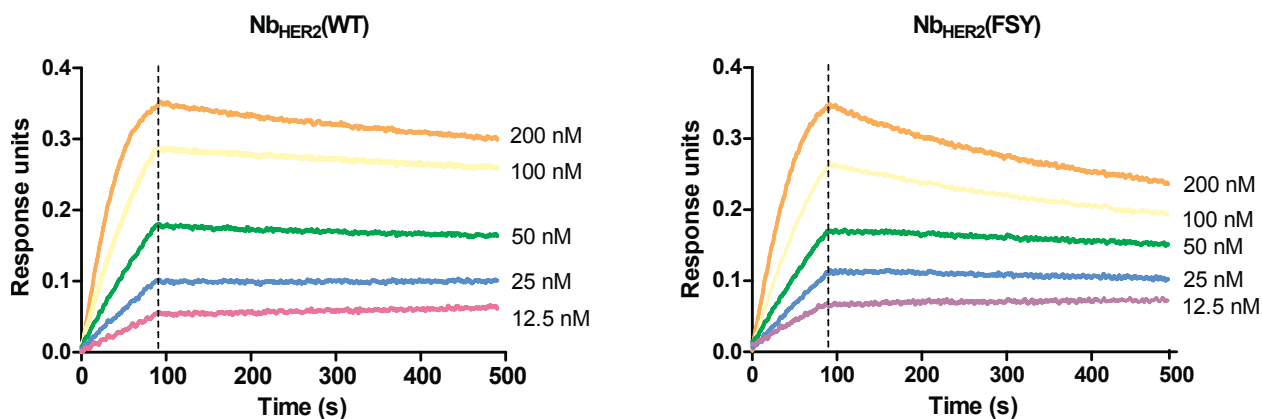


Figure 3.S2: Biolayer interferometry of HER2 and Nb_{HER2}(WT) or Nb_{HER2}(FSY). Biotinylated human HER2 was loaded onto the streptavidin sensor and then incubated with varying concentrations of Nb_{HER2}(WT) or Nb_{HER2}(FSY) for 90 seconds followed with dissociation for 400 seconds.

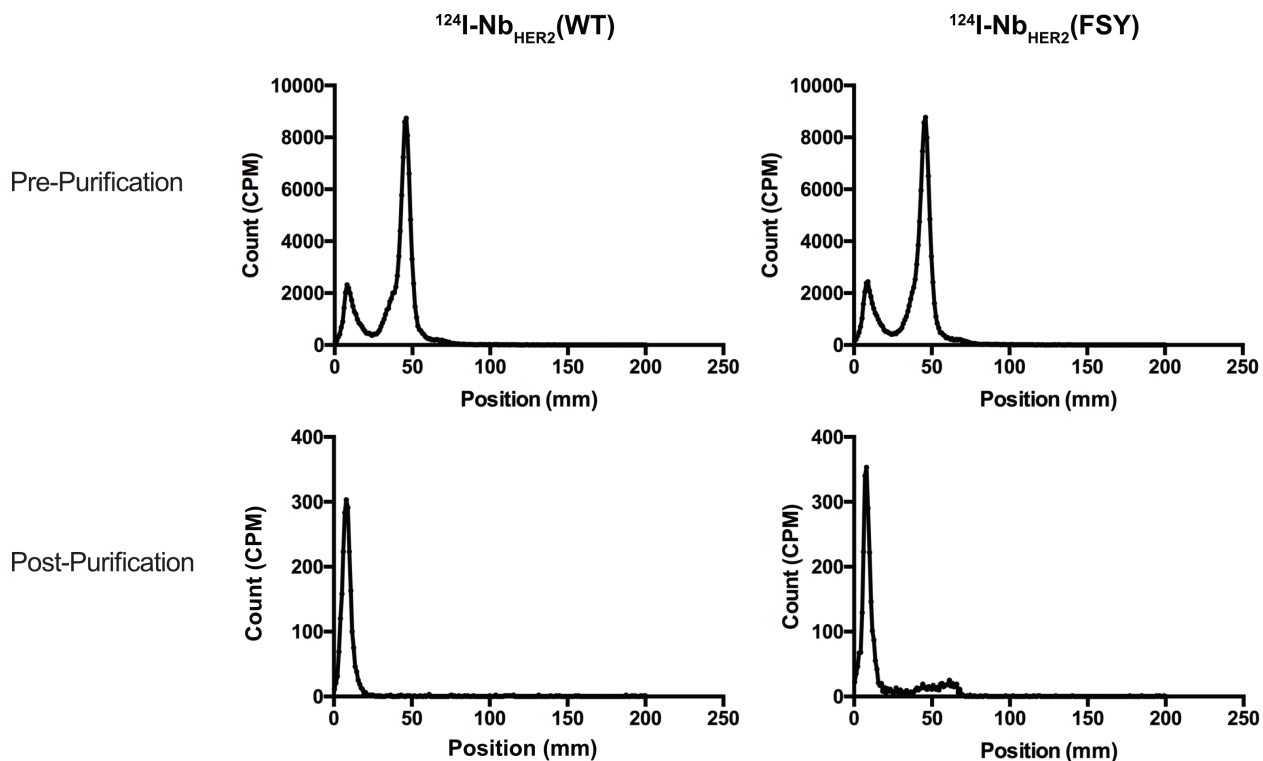


Figure 3.S3: Radiochemical yield and purity of $^{124}\text{I-Nb}_{\text{HER2}}$ (WT) and $^{124}\text{I-Nb}_{\text{HER2}}$ (FSY). Radiolabeling efficiency for $^{124}\text{I-Nb}_{\text{HER2}}$ (WT) and $^{124}\text{I-Nb}_{\text{HER2}}$ (FSY) measured through iTLC. The calculated radiochemical yield was 24.5% for $^{124}\text{I-Nb}_{\text{HER2}}$ (WT) and 23.5% for $^{124}\text{I-Nb}_{\text{HER2}}$ (FSY). The calculated post-purification radiochemical purity was 99.9% for $^{124}\text{I-Nb}_{\text{HER2}}$ (WT) and 95.2% for $^{124}\text{I-Nb}_{\text{HER2}}$ (FSY).

Blood pool time activity curves

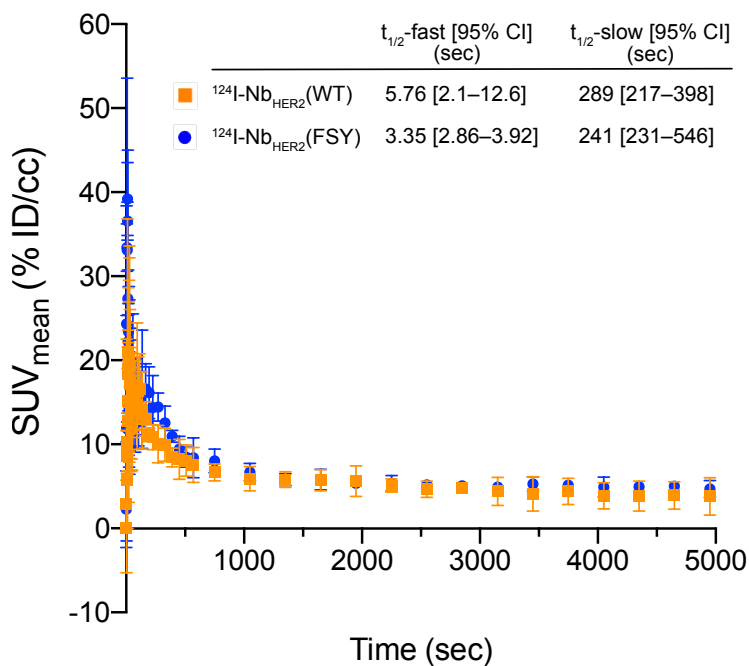


Figure 3.S4: $^{124}\text{I-Nb}_{\text{HER2}}$ (WT) and $^{124}\text{I-Nb}_{\text{HER2}}$ (FSY) both were cleared from blood rapidly. Dynamic PET acquisition was used to measure the standardized uptake value (SUV) in blood in percent injected dose per cm^3 (% ID/cc) at indicated time points. The data were fitted with two phase exponential decay to yield the $t_{1/2}$ values. Error bars represent 95% CI; $n = 3$ mice.

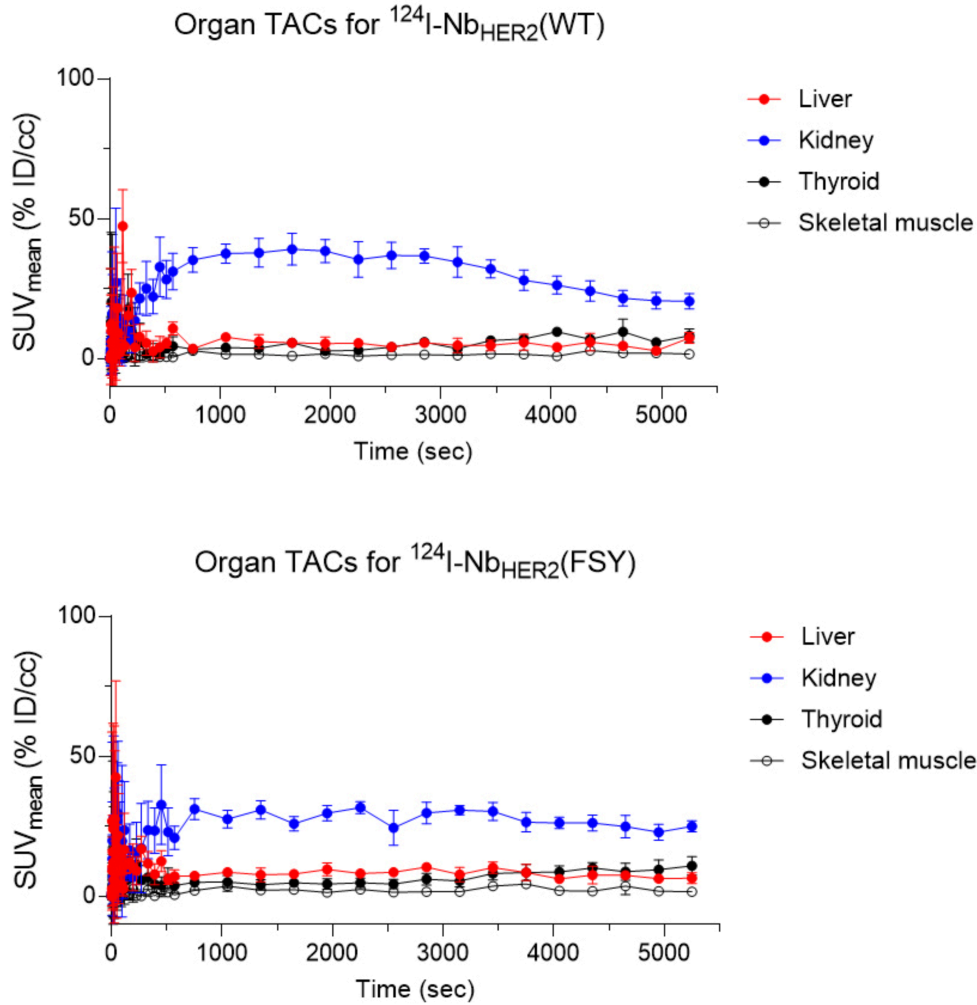


Figure 3.S5: $^{124}\text{I-Nb}_{\text{HER2}}(\text{WT})$ and $^{124}\text{I-Nb}_{\text{HER2}}(\text{FSY})$ showed similar biodistribution in normal organs. Standardized uptake value (SUV) in percent injected dose per cm^3 (% ID/cc) was plotted with time to yield the time activity curve (TAC) in indicated organs. Error bars represent s.d.; $n = 3$ mice for $^{124}\text{I-Nb}_{\text{HER2}}(\text{WT})$ injection; $n = 4$ mice for $^{124}\text{I-Nb}_{\text{HER2}}(\text{FSY})$ injection.

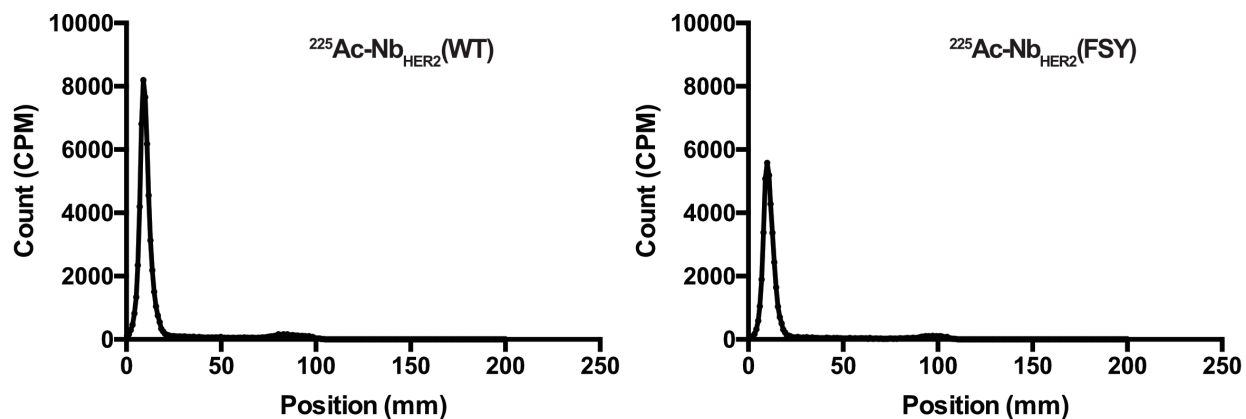


Figure 3.S6: Radiochemical yield of $^{225}\text{Ac-Nb}_{\text{HER2}}(\text{WT})$ and $^{225}\text{Ac-Nb}_{\text{HER2}}(\text{FSY})$. Radiolabeling efficiency for $^{225}\text{Ac-Nb}_{\text{HER2}}(\text{WT})$ and $^{225}\text{Ac-Nb}_{\text{HER2}}(\text{FSY})$ measured through iTLC. The calculated radiochemical yield was 96.6% for $^{225}\text{Ac-Nb}_{\text{HER2}}(\text{WT})$ and 95.5% for $^{225}\text{Ac-Nb}_{\text{HER2}}(\text{FSY})$.

Primer	Oligonucleotide Sequence (5'→3')
Nb _{HER2} -54TAG-For	TCGTATCTCCGGCTAGGGCGACACGTGGCATAAAGA
Nb _{HER2} -54TAG-Rev	CCTAGCCGGAGATACGAGAAACCAGCTCGCGC

Figure 3.T1: Primers used for cloning Nb_{HER2}(D54TAG)

Time (Sec)	¹²⁴ I-Nb _{HER2} (WT)			¹²⁴ I-Nb _{HER2} (FSY)		
	Mean	%CV	n	Mean	%CV	n
0.0	0.000	0.000	3	0.000	0.000	3
1.0	2.873	39.809	3	2.273	81.006	3
3.0	5.791	40.821	3	11.922	45.349	3
5.0	8.633	64.796	3	24.338	23.252	3
7.0	9.079	11.151	3	33.405	3.384	3
9.0	10.302	13.451	3	33.105	24.861	3
11.0	12.786	19.769	3	39.200	4.458	3
13.0	18.398	40.322	3	36.570	2.479	3
15.0	15.121	17.214	3	27.334	26.049	3
17.0	18.467	11.206	3	22.210	15.471	3
19.0	18.945	20.587	3	23.417	5.760	3
21.0	21.018	2.105	3	19.693	11.706	3
23.0	15.043	31.929	3	18.727	21.577	3
25.0	19.299	21.352	3	14.158	19.489	3
27.0	20.209	26.688	3	15.468	6.286	3
29.0	20.038	24.442	3	16.823	24.845	3
32.5	17.167	20.796	3	15.108	10.015	3
37.5	14.845	7.211	3	18.160	12.574	3
42.5	14.144	20.985	3	17.407	11.565	3
47.5	11.993	12.520	3	15.046	6.898	3
52.5	13.925	20.116	3	14.842	5.571	3
57.5	14.976	11.220	3	17.534	18.316	3
65.0	14.689	9.445	3	16.528	7.026	3
75.0	15.824	10.572	3	14.723	15.565	3
85.0	14.692	7.968	3	15.665	11.620	3
95.0	16.917	17.906	3	16.121	7.816	3
105.0	16.416	9.846	3	14.200	12.561	3
115.0	16.608	10.107	3	15.408	8.527	3
135.0	14.019	13.281	3	16.551	17.095	3
165.0	13.020	6.328	3	16.571	7.342	3
195.0	11.143	2.927	3	16.144	7.633	3
225.0	10.826	5.637	3	14.381	10.723	3
270.0	10.028	8.974	3	14.438	4.609	3
330.0	9.955	7.951	3	12.543	6.453	3
390.0	8.439	5.362	3	10.963	2.613	3
450.0	8.209	11.667	3	9.431	6.445	3
510.0	8.047	9.336	3	8.470	5.733	3
570.0	7.550	11.109	3	8.389	11.446	3
750.0	6.671	6.013	3	8.025	7.158	3
1050.0	5.930	9.837	3	6.680	6.330	3
1350.0	5.788	6.635	3	5.802	4.882	3
1650.0	5.729	8.825	3	5.787	8.566	3
1950.0	5.625	13.164	3	5.359	4.329	3
2250.0	5.111	6.317	3	5.365	7.036	3

2550.0	4.660	8.224	3	5.163	4.561	3
2850.0	4.766	4.851	3	5.074	5.178	3
3150.0	4.382	15.335	3	4.912	3.419	3
3450.0	4.092	20.182	3	5.280	6.493	3
3750.0	4.410	14.264	3	5.124	1.424	3
4050.0	3.869	16.361	3	4.910	9.841	3
4350.0	3.856	18.892	3	4.954	2.017	3
4650.0	3.911	16.928	3	5.040	1.697	3
4950.0	3.801	23.464	3	4.693	8.517	3

Figure 3.T2: Values in Figure 3.S4.

3.7 References

- (1) Bodei, L.; Herrmann, K.; Schöder, H.; Scott, A. M.; Lewis, J. S. Radiotheranostics in Oncology: Current Challenges and Emerging Opportunities. *Nat. Rev. Clin. Oncol.* 2022, 19 (8), 534–550. <https://doi.org/10.1038/s41571-022-00652-y>.
- (2) Sgouros, G.; Bodei, L.; McDevitt, M. R.; Nedrow, J. R. Radiopharmaceutical Therapy in Cancer: Clinical Advances and Challenges. *Nat Rev Drug Discov* 2020, 19 (9), 589–608. <https://doi.org/10.1038/s41573-020-0073-9>.
- (3) Hofman, M. S.; Emmett, L.; Sandhu, S.; Iravani, A.; Joshua, A. M.; Goh, J. C.; Pattison, D. A.; Tan, T. H.; Kirkwood, I. D.; Ng, S.; Francis, R. J.; Gedye, C.; Rutherford, N. K.; Weickhardt, A.; Scott, A. M.; Lee, S.-T.; Kwan, E. M.; Azad, A. A.; Ramdave, S.; Redfern, A. D.; Macdonald, W.; Guminski, A.; Hsiao, E.; Chua, W.; Lin, P.; Zhang, A. Y.; McJannett, M. M.; Stockler, M. R.; Violet, J. A.; Williams, S. G.; Martin, A. J.; Davis, I. D.; Group, T. T. I. and the A. and N. Z. U. and P. C. T.; Azad, A. A.; Chua, W.; Davis, I. D.; Dhiantravan, N.; Emmett, L.; Ford, K.; Hofman, M. S.; Francis, R. J.; Gedye, C.; Goh, J. C.; Guminski, A.; Hsiao, E.; Iravani, A.; Joshua, A. M.; Kirkwood, I. D.; Langford, A.; Lawrence, N.; Lee, S.-T.; Lin, P.; Martin, A. J.; McDonald, W.; McJannett, M. M.; Ng, S.; Pattison, D. A.; Ramdave, S.; Rana, N.; Redfern, A. D.; Rutherford, N. K.; Sandhu, S.; Scott, A. M.; Stockler, M. R.; Subramaniam, S.; Tan, T. H.; Violet, J. A.; Weickhardt, A.; Williams, S. G.; Yip, S.; Zhang, A. Y. [177Lu]Lu-PSMA-617 versus Cabazitaxel in Patients with Metastatic Castration-Resistant Prostate Cancer (TheraP): A Randomised, Open-Label, Phase 2 Trial. *Lancet* 2021, 397 (10276), 797–804. [https://doi.org/10.1016/s0140-6736\(21\)00237-3](https://doi.org/10.1016/s0140-6736(21)00237-3).

- (4) Tagawa, S. T.; Milowsky, M. I.; Morris, M.; Vallabhajosula, S.; Christos, P.; Akhtar, N. H.; Osborne, J.; Goldsmith, S. J.; Larson, S.; Taskar, N. P.; Scher, H. I.; Bander, N. H.; Nanus, D. M. Phase II Study of Lutetium-177–Labeled Anti-Prostate-Specific Membrane Antigen Monoclonal Antibody J591 for Metastatic Castration-Resistant Prostate Cancer. *Clin. Cancer Res.* 2013, 19 (18), 5182–5191. <https://doi.org/10.1158/1078-0432.ccr-13-0231>.
- (5) Sartor, O.; Bono, J. de; Chi, K. N.; Fizazi, K.; Herrmann, K.; Rahbar, K.; Tagawa, S. T.; Nordquist, L. T.; Vaishampayan, N.; El-Haddad, G.; Park, C. H.; Beer, T. M.; Armour, A.; Pérez-Contreras, W. J.; DeSilvio, M.; Kpamegan, E.; Gericke, G.; Messmann, R. A.; Morris, M. J.; Krause, B. J.; Investigators, V. Lutetium-177–PSMA-617 for Metastatic Castration-Resistant Prostate Cancer. *N. Engl. J. Med.* 2021, 385 (12), 1091–1103. <https://doi.org/10.1056/nejmoa2107322>.
- (6) Giesel, F.; Adeberg, S.; Syed, M.; Lindner, T.; Jimenez, L. D.; Mavriopoulou, E.; Staudinger, F.; Tonndorf-Martini, E.; Regnery, S.; Rieken, S.; ElShafie, R.; Röhrich, M.; Flechsig, P.; Kluge, A.; Altmann, A.; Debus, J.; Haberkorn, U. A.; Kratochwil, C. FAPI-74 PET/CT Using Either 18F-AlF or Cold-Kit 68Ga-Labeling: Biodistribution, Radiation Dosimetry and Tumor Delineation in Lung Cancer Patients. *J. Nucl. Med.* 2020, 62 (2), jnumed.120.245084. <https://doi.org/10.2967/jnumed.120.245084>.
- (7) Zang, J.; Fan, X.; Wang, H.; Liu, Q.; Wang, J.; Li, H.; Li, F.; Jacobson, O.; Niu, G.; Zhu, Z.; Chen, X. First-in-Human Study of 177Lu-EB-PSMA-617 in Patients with Metastatic Castration-Resistant Prostate Cancer. *Eur. J. Nucl. Med. Mol. Imaging* 2019, 46 (1), 148–158. <https://doi.org/10.1007/s00259-018-4096-y>.

- (8) Meyer, C.; Dahlbom, M.; Lindner, T.; Vauclin, S.; Mona, C.; Slavik, R.; Czernin, J.; Haberkorn, U.; Calais, J. Radiation Dosimetry and Biodistribution of ^{68}Ga -FAPI-46 PET Imaging in Cancer Patients. *J. Nucl. Med.* 2020, 61 (8), 1171–1177. <https://doi.org/10.2967/jnumed.119.236786>.
- (9) Loktev, A.; Lindner, T.; Mier, W.; Debus, J.; Altmann, A.; Jäger, D.; Giesel, F.; Kratochwil, C.; Barthe, P.; Roumestand, C.; Haberkorn, U. A Tumor-Imaging Method Targeting Cancer-Associated Fibroblasts. *J. Nucl. Med.* 2018, 59 (9), 1423–1429. <https://doi.org/10.2967/jnumed.118.210435>.
- (10) Kelly, J. M.; Amor-Coarasa, A.; Ponnala, S.; Nikolopoulou, A.; Williams, C.; DiMagno, S. G.; Babich, J. W. Albumin-Binding PSMA Ligands: Implications for Expanding the Therapeutic Window. *J. Nucl. Med.* 2019, 60 (5), 656–663. <https://doi.org/10.2967/jnumed.118.221150>.
- (11) Zhang, J.; Wang, H.; Jacobson, O.; Cheng, Y.; Niu, G.; Li, F.; Bai, C.; Zhu, Z.; Chen, X. Safety, Pharmacokinetics, and Dosimetry of a Long-Acting Radiolabeled Somatostatin Analog ^{177}Lu -DOTA-EB-TATE in Patients with Advanced Metastatic Neuroendocrine Tumors. *J. Nucl. Med.* 2018, 59 (11), 1699–1705. <https://doi.org/10.2967/jnumed.118.209841>.
- (12) Zeglis, B. M.; Sevak, K. K.; Reiner, T.; Mohindra, P.; Carlin, S. D.; Zanzonico, P.; Weissleder, R.; Lewis, J. S. A Pretargeted PET Imaging Strategy Based on Bioorthogonal Diels–Alder Click Chemistry. *J. Nucl. Med.* 2013, 54 (8), 1389–1396. <https://doi.org/10.2967/jnumed.112.115840>.
- (13) Rondon, A.; Degoul, F. Antibody Pretargeting Based on Bioorthogonal Click Chemistry for Cancer Imaging and Targeted Radionuclide Therapy. *Bioconjugate Chem.* 2020, 31 (2), 159–173. <https://doi.org/10.1021/acs.bioconjchem.9b00761>.

- (14) Chang, J. W.; Bhuiyan, M.; Tsai, H.; Zhang, H. J.; Li, G.; Fathi, S.; McCutcheon, D. C.; Leoni, L.; Freifelder, R.; Chen, C.; Moellering, R. E. In Vivo Imaging of the Tumor-Associated Enzyme NCEH1 with a Covalent PET Probe. *Angewandte Chemie Int Ed* 2020, 59 (35), 15161–15165. <https://doi.org/10.1002/anie.202004762>.
- (15) Nedrow-Byers, J. R.; Jabbes, M.; Jewett, C.; Ganguly, T.; He, H.; Liu, T.; Benny, P.; Bryan, J. N.; Berkman, C. E. A Phosphoramidate-based Prostate-specific Membrane Antigen-targeted SPECT Agent. *Prostate* 2012, 72 (8), 904–912. <https://doi.org/10.1002/pros.21493>.
- (16) Xiang, Z.; Ren, H.; Hu, Y. S.; Coin, I.; Wei, J.; Cang, H.; Wang, L. Adding an Unnatural Covalent Bond to Proteins through Proximity-Enhanced Bioreactivity. *Nat Methods* 2013, 10 (9), 885–888. <https://doi.org/10.1038/nmeth.2595>.
- (17) Cao, L.; Wang, L. New Covalent Bonding Ability for Proteins. *Protein Sci* 2021. <https://doi.org/10.1002/pro.4228>.
- (18) Li, Q.; Chen, Q.; Klauser, P. C.; Li, M.; Zheng, F.; Wang, N.; Li, X.; Zhang, Q.; Fu, X.; Wang, Q.; Xu, Y.; Wang, L. Developing Covalent Protein Drugs via Proximity-Enabled Reactive Therapeutics. *Cell* 2020, 182 (1), 85-97.e16. <https://doi.org/10.1016/j.cell.2020.05.028>.
- (19) Wang, L.; Brock, A.; Herberich, B.; Schultz, P. G. Expanding the Genetic Code of Escherichia Coli. *Science* 2001, 292 (5516), 498–500. <https://doi.org/10.1126/science.1060077>.
- (20) Wang, L. Genetically Encoding New Bioreactivity. *New Biotechnol* 2017, 38 (Pt A), 16–25. <https://doi.org/10.1016/j.nbt.2016.10.003>.
- (21) Yu, B.; Li, S.; Tabata, T.; Wang, N.; Cao, L.; Kumar, G. R.; Sun, W.; Liu, J.; Ott, M.; Wang, L. Accelerating PERx Reaction Enables Covalent Nanobodies for Potent Neutralization of SARS-CoV-2 and Variants. *Chem* 2022, 8 (10), 2766–2783. <https://doi.org/10.1016/j.chempr.2022.07.012>.

- (22) Dong, J.; Krasnova, L.; Finn, M. G.; Sharpless, K. B. Sulfur(VI) Fluoride Exchange (SuFEx): Another Good Reaction for Click Chemistry. *Angewandte Chemie Int Ed* 2014, 53 (36), 9430–9448. <https://doi.org/10.1002/anie.201309399>.
- (23) Liu, J.; Cao, L.; Klauser, P. C.; Cheng, R.; Berdan, V. Y.; Sun, W.; Wang, N.; Ghelichkhani, F.; Yu, B.; Rozovsky, S.; Wang, L. A Genetically Encoded Fluorosulfonyloxybenzoyl-L-lysine for Expansive Covalent Bonding of Proteins via SuFEx Chemistry. *J Am Chem Soc* 2021, 143 (27), 10341–10351. <https://doi.org/10.1021/jacs.1c04259>.
- (24) Wang, N.; Yang, B.; Fu, C.; Zhu, H.; Zheng, F.; Kobayashi, T.; Liu, J.; Li, S.; Ma, C.; Wang, P. G.; Wang, Q.; Wang, L. Genetically Encoding Fluorosulfate-1-Tyrosine To React with Lysine, Histidine, and Tyrosine via SuFEx in Proteins in Vivo. *J Am Chem Soc* 2018, 140 (15), 4995–4999. <https://doi.org/10.1021/jacs.8b01087>.
- (25) Vaneycken, I.; Devoogdt, N.; Gassen, N. V.; Vincke, C.; Xavier, C.; Wernery, U.; Muyldermans, S.; Lahoutte, T.; Caveliers, V. Preclinical Screening of Anti-HER2 Nanobodies for Molecular Imaging of Breast Cancer. *Faseb J* 2011, 25 (7), 2433–2446. <https://doi.org/10.1096/fj.10-180331>.
- (26) Oh, D.-Y.; Bang, Y.-J. HER2-Targeted Therapies — a Role beyond Breast Cancer. *Nat Rev Clin Oncol* 2020, 17 (1), 33–48. <https://doi.org/10.1038/s41571-019-0268-3>.
- (27) Tamura, K.; Kurihara, H.; Yonemori, K.; Tsuda, H.; Suzuki, J.; Kono, Y.; Honda, N.; Kodaira, M.; Yamamoto, H.; Yunokawa, M.; Shimizu, C.; Hasegawa, K.; Kanayama, Y.; Nozaki, S.; Kinoshita, T.; Wada, Y.; Tazawa, S.; Takahashi, K.; Watanabe, Y.; Fujiwara, Y. ⁶⁴Cu-DOTA-Trastuzumab PET Imaging in Patients with HER2-Positive Breast Cancer. *J Nucl Med* 2013, 54 (11), 1869–1875. <https://doi.org/10.2967/jnumed.112.118612>.

- (28) D'Huyvetter, M.; Vos, J. D.; Xavier, C.; Pruszynski, M.; Sterckx, Y. G. J.; Massa, S.; Raes, G.; Caveliers, V.; Zalutsky, M. R.; Lahoutte, T.; Devoogdt, N. 131I-Labeled Anti-HER2 Camelid SdAb as a Theranostic Tool in Cancer Treatment. *Clin Cancer Res* 2017, 23 (21), 6616–6628. <https://doi.org/10.1158/1078-0432.ccr-17-0310>.
- (29) Salacinski, P. R. P.; McLean, C.; Sykes, J. E. C.; Clement-Jones, V. V.; Lowry, P. J. Iodination of Proteins, Glycoproteins, and Peptides Using a Solid-Phase Oxidizing Agent, 1,3,4,6-Tetrachloro-3 α ,6 α -Diphenyl Glycoluril (Iodogen). *Anal. Biochem.* 1981, 117 (1), 136–146. [https://doi.org/10.1016/0003-2697\(81\)90703-x](https://doi.org/10.1016/0003-2697(81)90703-x).
- (30) Belov, V. V.; Bonab, A. A.; Fischman, A. J.; Heartlein, M.; Calias, P.; Papisov, M. I. Iodine-124 as a Label for Pharmacological PET Imaging. *Mol Pharmaceut* 2011, 8 (3), 736–747. <https://doi.org/10.1021/mp100358f>.
- (31) Kobayashi, H.; Yoo, T. M.; Kim, I. S.; Kim, M. K.; Le, N.; Webber, K. O.; Pastan, I.; Paik, C. H.; Eckelman, W. C.; Carrasquillo, J. A. L-Lysine Effectively Blocks Renal Uptake of 125I- or 99mTc-Labeled Anti-Tac Disulfide-Stabilized Fv Fragment. *Cancer Res* 1996, 56 (16), 3788–3795.
- (32) Chan, H. S.; Konijnenberg, M. W.; Daniels, T.; Nysus, M.; Makvandi, M.; Blois, E. de; Breeman, W. A.; Atcher, R. W.; Jong, M. de; Norenberg, J. P. Improved Safety and Efficacy of 213Bi-DOTATATE-Targeted Alpha Therapy of Somatostatin Receptor-Expressing Neuroendocrine Tumors in Mice Pre-Treated with l-Lysine. *EJNMMI Res.* 2016, 6 (1), 83. <https://doi.org/10.1186/s13550-016-0240-5>.

- (33) Robinson, M. K.; Doss, M.; Shaller, C.; Narayanan, D.; Marks, J. D.; Adler, L. P.; Trotter, D. E. G.; Adams, G. P. Quantitative Immuno-Positron Emission Tomography Imaging of HER2-Positive Tumor Xenografts with an Iodine-124 Labeled Anti-HER2 Diabody. *Cancer Res.* 2005, 65 (4), 1471–1478. <https://doi.org/10.1158/0008-5472.can-04-2008>.
- (34) King, A. P.; Lin, F. I.; Escorcia, F. E. Why Bother with Alpha Particles? *Eur. J. Nucl. Med. Mol. Imaging* 2021, 49 (1), 7–17. <https://doi.org/10.1007/s00259-021-05431-y>.
- (35) Kratochwil, C.; Bruchertseifer, F.; Rathke, H.; Bronzel, M.; Apostolidis, C.; Weichert, W.; Haberkorn, U.; Giesel, F. L.; Morgenstern, A. Targeted α -Therapy of Metastatic Castration-Resistant Prostate Cancer with ^{225}Ac -PSMA-617: Dosimetry Estimate and Empiric Dose Finding. *J. Nucl. Med.* 2017, 58 (10), 1624–1631. <https://doi.org/10.2967/jnumed.117.191395>.
- (36) Ac-225-DOTATOC - an empiric dose finding for alpha particle emitter based radionuclide therapy of neuroendocrine tumors | Journal of Nuclear Medicine. https://jnm.snmjournals.org/content/56/supplement_3/1232 (accessed 2023-08-09).
- (37) Bobba, K. N.; Bidkar, A. P.; Meher, N.; Fong, C.; Wadhwa, A.; Dhrona, S.; Sorlin, A.; Bidlingmaier, S.; Shuere, B.; He, J.; Wilson, D. M.; Liu, B.; Seo, Y.; VanBrocklin, H. F.; Flavell, R. R. Evaluation of $^{134}\text{Ce}/^{134}\text{La}$ as a PET Imaging Theranostic Pair for ^{225}Ac α -Radiotherapeutics. *J. Nucl. Med.* 2023, 64 (7), 265355. <https://doi.org/10.2967/jnumed.122.265355>.
- (38) Thiele, N. A.; Brown, V.; Kelly, J. M.; Amor-Coarasa, A.; Jermilova, U.; MacMillan, S. N.; Nikolopoulou, A.; Ponnala, S.; Ramogida, C. F.; Robertson, A. K. H.; Rodríguez-Rodríguez, C.; Schaffer, P.; Williams, C.; Babich, J. W.; Radchenko, V.; Wilson, J. J. An Eighteen-Membered Macrocyclic Ligand for Actinium-225 Targeted Alpha Therapy. *Angew. Chem. Int. Ed.* 2017, 56 (46), 14712–14717. <https://doi.org/10.1002/anie.201709532>.

- (39) Mohan, N.; Jiang, J.; Dokmanovic, M.; Wu, W. J. Trastuzumab-Mediated Cardiotoxicity: Current Understanding, Challenges, and Frontiers. *Antib. Ther.* 2018, 1 (1), 13–17. <https://doi.org/10.1093/abt/tby003>.
- (40) Rodak, M.; Dekempeneer, Y.; Wojewódzka, M.; Caveliers, V.; Covens, P.; Miller, B. W.; Sevenois, M. B.; Bruchertseifer, F.; Morgenstern, A.; Lahoutte, T.; D’Huyvetter, M.; Pruszynski, M. Preclinical Evaluation of ²²⁵Ac-Labeled Single-Domain Antibody for the Treatment of HER2pos Cancer. *Mol. Cancer Ther.* 2022, 21 (12), 1835–1845. <https://doi.org/10.1158/1535-7163.mct-21-1021>.
- (41) Klauser, P. C.; Berdan, V. Y.; Cao, L.; Wang, L. Encoding Latent SuFEx Reactive Meta-Fluorosulfate Tyrosine to Expand Covalent Bonding of Proteins. *Chem Commun* 2022, 58 (48), 6861–6864. <https://doi.org/10.1039/d2cc01902g>.
- (42) Wang, N.; Wang, L. Genetically Encoding Latent Bioreactive Amino Acids and the Development of Covalent Protein Drugs. *Curr Opin Chem Biol* 2022, 66, 102106. <https://doi.org/10.1016/j.cbpa.2021.102106>.
- (43) Wang, L. Engineering the Genetic Code in Cells and Animals: Biological Considerations and Impacts. *Accounts Chem Res* 2017, 50 (11), 2767–2775. <https://doi.org/10.1021/acs.accounts.7b00376>.
- (44) Hoppmann, C.; Wang, L. Proximity-Enabled Bioreactivity to Generate Covalent Peptide Inhibitors of P53–Mdm4. *Chem Commun* 2016, 52 (29), 5140–5143. <https://doi.org/10.1039/c6cc01226d>.
- (45) Sun, W.; Wang, N.; Liu, H.; Yu, B.; Jin, L.; Ren, X.; Shen, Y.; Wang, L. Genetically Encoded Chemical Crosslinking of RNA in Vivo. *Nat. Chem.* 2023, 15 (1), 21–32. <https://doi.org/10.1038/s41557-022-01038-4>.

- (46) Singh, J.; Petter, R. C.; Baillie, T. A.; Whitty, A. The Resurgence of Covalent Drugs. *Nat. Rev. Drug Discov.* 2011, 10 (4), 307–317. <https://doi.org/10.1038/nrd3410>.
- (47) Liu, J.; Li, S.; Aslam, N. A.; Zheng, F.; Yang, B.; Cheng, R.; Wang, N.; Rozovsky, S.; Wang, P. G.; Wang, Q.; Wang, L. Genetically Encoding Photocaged Quinone Methide to Multitarget Protein Residues Covalently in Vivo. *J Am Chem Soc* 2019, 141 (24), 9458–9462. <https://doi.org/10.1021/jacs.9b01738>.
- (48) Liu, J.; Zheng, F.; Cheng, R.; Li, S.; Rozovsky, S.; Wang, Q.; Wang, L. Site-Specific Incorporation of Selenocysteine Using an Expanded Genetic Code and Palladium-Mediated Chemical Deprotection. *J Am Chem Soc* 2018, 140 (28), 8807–8816. <https://doi.org/10.1021/jacs.8b04603>.
- (49) Chen, Z.-L.; Meng, J.-M.; Cao, Y.; Yin, J.-L.; Fang, R.-Q.; Fan, S.-B.; Liu, C.; Zeng, W.-F.; Ding, Y.-H.; Tan, D.; Wu, L.; Zhou, W.-J.; Chi, H.; Sun, R.-X.; Dong, M.-Q.; He, S.-M. A High-Speed Search Engine PLink 2 with Systematic Evaluation for Proteome-Scale Identification of Cross-Linked Peptides. *Nat Commun* 2019, 10 (1), 3404. <https://doi.org/10.1038/s41467-019-11337-z>.
- (50) Liu, C.; Wu, T.; Shu, X.; Li, S.; Wang, D. R.; Wang, N.; Zhou, R.; Yang, H.; Jiang, H.; Hendriks, I. A.; Gong, P.; Zhang, L.; Nielsen, M. L.; Li, K.; Wang, L.; Yang, B. Identification of Protein Direct Interactome with Genetic Code Expansion and Search Engine OpenUaa. *Adv Biology* 2021, 5 (3), 2000308. <https://doi.org/10.1002/adbi.202000308>.

4. Engineered Covalent Neuregulin Ligand Modulates HER4 Signaling

4.1 Abstract

Neuregulins are a diverse family of growth factors that bind and activate the human epidermal growth factor receptor (HER) family. Neuregulin plays a pivotal role in activating the HER3 and HER4 signaling axis leading to downstream pathways such as PI3K/AKT and MAPK which influence cell proliferation, survival, and differentiation. Dysregulation of these receptors leading to aberrant signaling has been observed in a variety of cancers; this underscores the importance of neuregulin as a therapeutic target. Here, we develop a covalent neuregulin capable of specifically crosslinking with HER4 via a proximity-enabled reactive therapeutic (PERx) mechanism that alters the signaling axis of the receptor. The covalent neuregulin shows remarkable specificity, only crosslinking HER4 when the receptor is in the HER2/HER4 heterodimer complex. Furthermore, the covalent neuregulin downregulates downstream signaling and inhibits cell proliferation in primary cardiomyocytes, which are dependent on HER4 signaling. Our results demonstrate a new strategy for manipulating growth factor ligands through PERx and modulating them for new therapeutic opportunities.

4.2 Introduction

Human epidermal growth factor receptors (HER) are essential regulators of cell growth, differentiation, and survival.^{1,2} The HER family is comprised of EGFR, HER2, HER3, and HER4; these receptors are activated via ligand binding and subsequent homo- and heterodimerization

leading to activation of downstream signaling pathways.³ These ligands have emerged as crucial regulators in cellular signaling pathways and play an essential role in modulating diverse cellular responses.⁴ Neuregulin (NRG) ligands initiate the activation of HER receptors by binding to the extracellular domain of HER3 and HER4 receptors.⁵ NRG/HER signaling dysfunction is associated with many cancers including breast, lung, stomach, pancreas, kidney, bladder, ovary, prostate, colon, and brain.^{6,7} In fact, cancer therapies rely on blocking NRG binding to HER receptors in order to decrease downstream signaling and tumor growth.⁸ Furthermore, NRGs play a central role in neural development, acting as key regulators of neuronal migration, axon guidance, and synapse formation.⁹ In cardiac physiology, NRGs ensure proper cardiac architecture and efficient pumping function.¹⁰ Indeed, recombinant NRGs have even been tested in clinical trial as a therapy for heart failure for their cytoprotective mechanisms in cardiomyocytes.¹¹

While most NRG ligands exhibit a high degree of specificity in their interactions, NRG1 β promiscuously binds both HER3 and HER4 homodimers and HER2/HER3 and HER2/HER4 heterodimers with high affinity (< 6 nM).¹² However, activating HER3 and HER4 can promote a wide range of different physiological functions based on the tissue specificity of both receptors. For instance, NRG1 β /HER2/HER4 signaling has widely been reported to promote myocardial regeneration in the heart¹³, whereas NRG1 β /HER2/HER3 signaling drives mammary tumorigenesis in breast cancer.¹⁴ Indeed, the inhibitory antibody against HER2, trastuzumab (Herceptin), is effective in targeting HER2-positive breast cancer, but due to the lack of heterodimer specificity, has been shown to have cardiotoxicity.¹⁵ Due to the complexity of these interactions, new approaches are needed to develop more targeted therapies with functional selectivity for personalized medicine. One approach to develop bias signaling or functional selectivity is to engineer the ligand itself to alter the signaling outcomes. Previously, investigators

have engineered bivalent NRG1 β ligands that could bias signaling in HER3-expressing cancer cells by driving HER3 homodimer formation over HER2/HER3 heterodimer.¹⁶ By altering the signaling response, the bivalent NRG was able to inhibit proliferation and increase apoptosis, demonstrating the potential of engineering HER ligands for therapy.

Bivalent NRG1 β allows for the bias binding of a homodimer over a heterodimer receptor complex. An alternative approach is necessary to bias NRG1 β binding to one of the heterodimer complexes over the other. We hypothesized that by engineering covalent reactivity into NRG1 β , we could improve the selectivity of the ligand so that NRG1 β could only crosslink with one heterodimer over another. In this study, we develop a covalent targeting NRG1 β that leverages proximity-enabled reactivity that binds the HER4 target irreversibly. Remarkably, the covalent NRG1 β only crosslinks the HER2/HER4 heterodimer over the HER2/HER3 heterodimer or the HER3 and HER4 homodimers. We further demonstrate that the covalent mechanism antagonizes the HER2/HER4 heterodimer complex, inhibiting signaling and cardiomyocyte cell proliferation. The covalent ligand strategy highlights a novel therapeutic modality in developing functional selectivity in growth factor ligands.

4.3 Results

Engineering a Covalent Mechanism in NRG1 β via Proximity-Enabled Reactivity

We previously demonstrated that latent bioreactive unnatural amino acids (Uaas) can be genetically incorporated into proteins and improve the therapeutic efficacy of the protein drug.^{17,18,19} However, a covalent mechanism can not only improve the potency but also the selectivity of the binder due to the two-step mechanism of binding followed by covalent bond

formation.²⁰ We envisioned that by installing a bioreactive Uaa into NRG1 β , we could improve its selectivity by targeting HER2/HER4 over HER2/HER3 (**Fig. 4.1**). Furthermore, previous studies have shown that altered binding kinetics in HER ligands demonstrate biased agonism and functional selectivity,⁴ therefore we hypothesized that with a covalent mechanism we would get a different signaling outcome and cell fate.

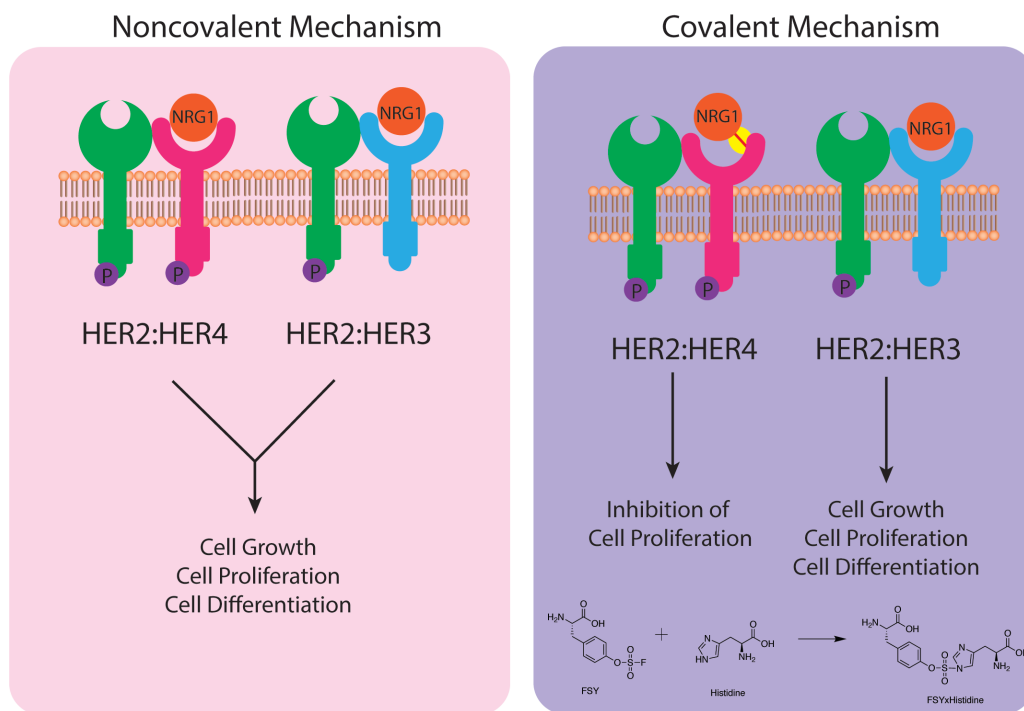


Figure 4.1: Selectively targeting HER2/HER4 heterodimer by installing a covalent mechanism in neuregulin. A schematic comparison between noncovalent WT neuregulin and covalent neuregulin. WT neuregulin binds and activated both HER2/HER3 and HER2/HER3 while in contrast, covalent neuregulin selectively crosslinks HER2/HER4 and alters signaling responses.

To develop a covalent NRG1 β , we genetically encoded fluorosulfate-L-tyrosine (FSY) which remains inert in proteins inside cells and reacts with tyrosine, lysine, and histidine when in proximity via sulfur-fluoride exchange (SuFEx).²¹ To test if FSY-incorporated NRG1 β could selectively crosslink one heterodimer over another, we incorporated FSY into various sites in NRG1 β along the NRG1 β /HER4 interface. Due to the low expression levels of HER heterodimers,

we incubated NRG1 β mutants with Expi293 cells lysate transfected with either HER2/HER3 or HER2/HER4 and identified the crosslink band via western blot analysis. In this small mutant screen (14 sites), we identified one suitable site (H178FSY) in which a crosslinking band was identified only when the ligand was incubated with HER2/HER4 and not when incubated with HER2/HER3 (**Fig. 4.S1**). To evaluate the kinetics of crosslinking, NRG1 β (WT) or NRG1 β (H178FSY) was incubated with NIH/3T3 transfected with HER2/HER4 for different time points and analyzed with western blot analysis (**Fig. 4.2a**). Untransfected NIH/3T3 cell line has an undetectable expression of HER2, HER3, or HER4 receptors and therefore is compatible to crosslinking and signaling detection.²² Crosslinking was identified within 1h of incubation and increased over 6h. After 24h, the receptors have mostly degraded likely due to receptor activated internalization.

To understand how NRG1 β could be crosslinking HER4 and not HER3, we looked into the NRG1 β bound structure of both HER4 (**Fig. 4.2b**)²³ and HER3 (**Fig. 4.2c**)²⁴. In the NRG1 β -HER4 structure, NRG1 β (H178FSY) has the potential to crosslink either Y98 or K100 on HER4. Compared to the NRG1 β -HER3 structure, while the tyrosine is conserved between HER3 and HER4 (labeled Y123 on HER3), K100 is not. To confirm that whether Y98 or K100 is required for crosslinking, we incubated NRG1 β (H178FSY) with either HER2/HER4 (WT), HER2/HER4(Y98F), or HER2/HER4(K100R) (**Fig. 4.2d**). While a covalent complex formed with HER2/HER4 (WT), no covalent complex was identified with either mutations suggesting that both Y98 and K100 is required for crosslinking.

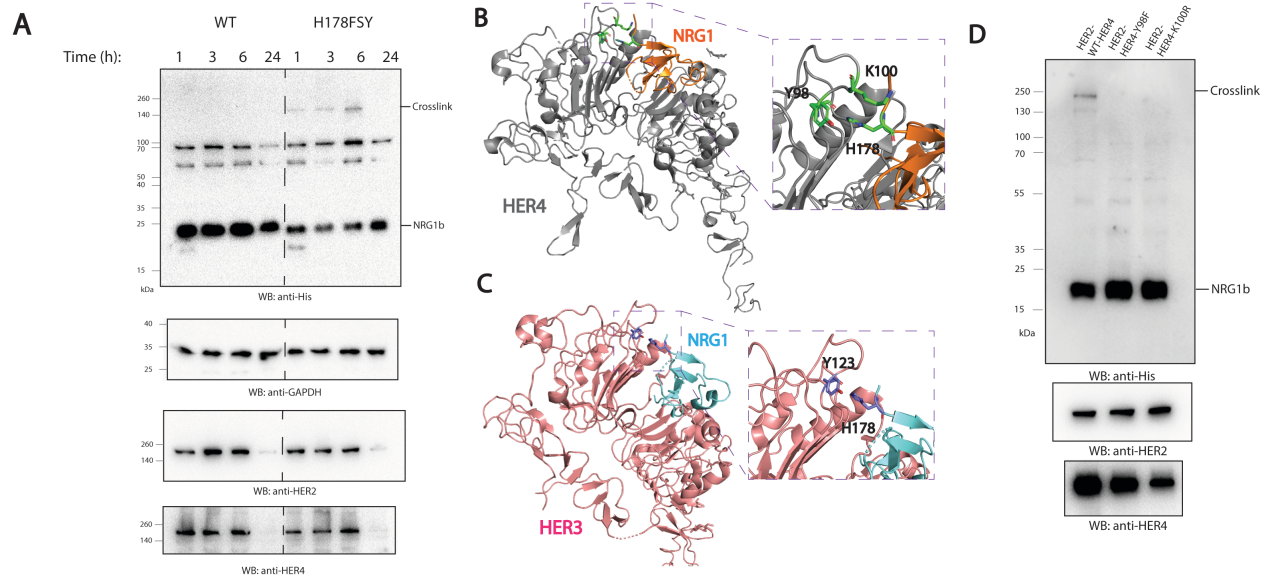


Figure 4.2: Developing NRG1 β (H178FSY) to covalently crosslink HER2/HER4. (A) Western blot analysis of NIH/3T3 cell line expressing full-length HER2 and HER4 treated with either 0.25 μ M NRG1 β (WT) or 0.25 μ M NRG1 β (H178FSY). A His6x tag was appended at the C-terminus of NRG1 β for detection. (B) Crystal structure of NRG1 β bound to HER4 (PDB: 3U7U) showing the FSY incorporation site (H178) and proximal target residues (K100 and Y98). (C) Crystal structure of NRG1 β bound to HER3 (PDB: 7MN5) with FSY incorporation site (H178) and proximal residue (Y123). (D) Crosslinking of NRG1 β (H178FSY) with NIH/3T3 cell line expressing with HER2/HER4(WT), HER2/HER4(Y98F), or HER2/HER4(K100R). Crosslinking was only detected with HER2/HER4(WT).

NRG1 β (178FSY) specifically crosslinks the HER2/HER4 heterodimer species

We next tested the selectivity of NRG1 β (H178FSY) for various combination of HER3 and HER4 homo- and heterodimers. We incubated NRG1 β (WT), NRG1 β (H178FSY), or negative control PBS with NIH/3T3 cells transfected with just HER3, HER2/HER3, HER4, or HER2/HER4 (**Fig. 4.3**). As expected, no crosslinking band was detected for NRG1 β (WT) or PBS control with any of the cells expressing HER receptors. For NRG1 β (H178FSY), crosslinking band was not detected with cells expressing HER3 or HER2/HER3, however surprisingly no crosslinking band was identified with NRG1 β (H178FSY) incubated with cells expressing HER4 alone. As expected a covalent complex was identified with NRG1 β (H178FSY) incubated with cells expressing

HER2/HER4. NRG1 β has a 60-fold lower affinity for the HER4 homodimer over the HER2/HER4 heterodimer therefore the lack of crosslinking to the HER4 homodimer could be explain by the difference in binding affinity.

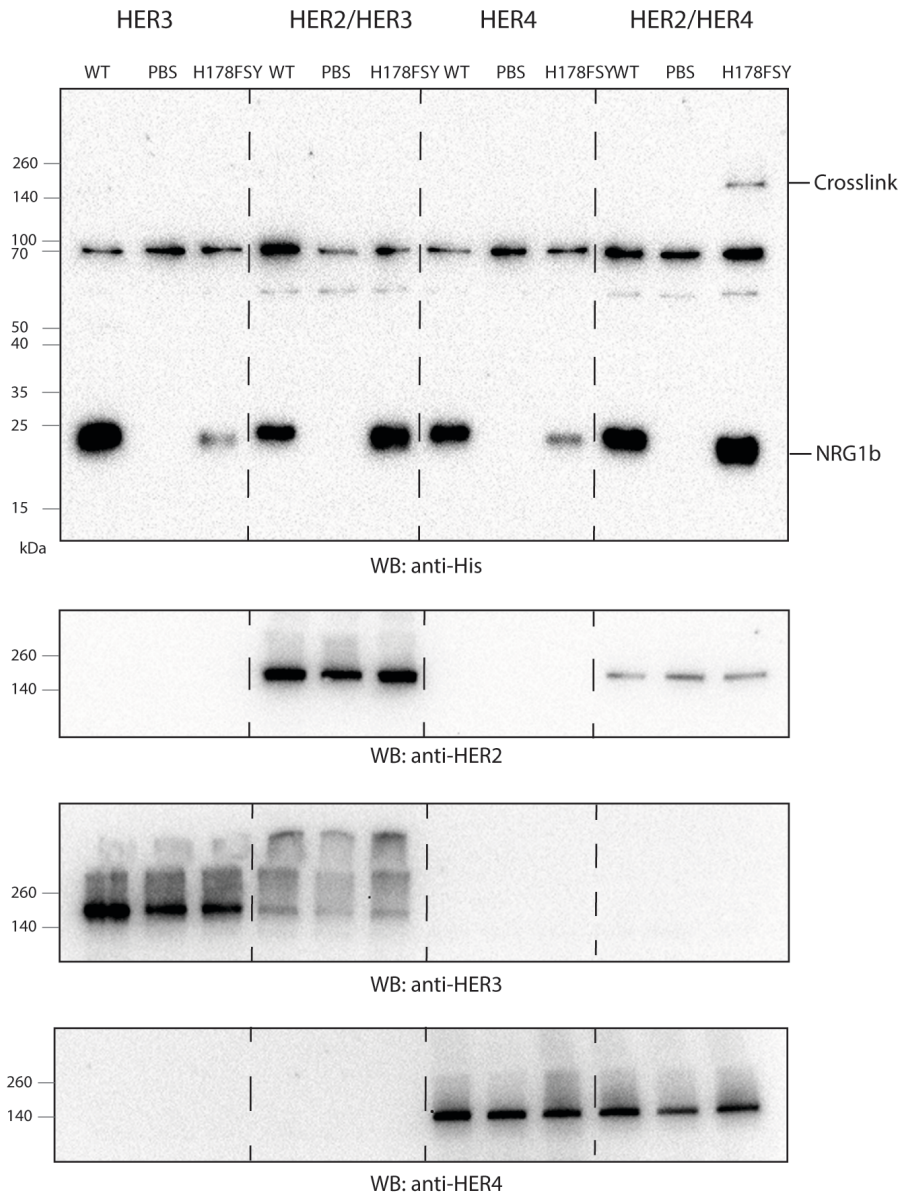


Figure 4.3: Characterizing receptor selectivity of NRG1 β (H178FSY). Western blot analysis of NIH/3T3 cell line expressing either full-length HER3, HER2/HER3, HER4, or HER2/HER4 when treated with either 0.25 μ M NRG1 β (WT), PBS, or 0.25 μ M NRG1 β (H178FSY) over 4h. Crosslinking was only detected when cells expressing HER2/HER4 was treated with 0.25 μ M NRG1 β (H178FSY).

NRG1 β (H178FSY) inhibits HER2:HER4 signaling

We next asked if the NRG1 β (H178FSY) can change the HER receptor and downstream signaling outcomes based on the altered binding kinetics of a covalent mechanism. We compared the ability of NRG1 β (WT) and NRG1 β (H178FSY) to stimulate culture NIH/3T3 cells stably expressing HER2 (V956R)/HER4(I712Q). The V956R and I712Q mutations in HER2 and HER4 forces the receptor activation through the heterodimer rather than the homodimer as observed through other HER receptor family.^{25,26} To analyze the signaling kinetics of the HER activation, we quenched and lysed the stimulated cells after several different time points and used western blot analysis to look at phosphorylation at HER4, HER2, and ERK (**Fig. 4.4a**). With the NRG1 β (WT) treated cells phosphorylation of HER2 and HER4 was observed after 2 min to stimulation and after 10 min for ERK (**Fig. 4.4b, 4.4c, and 4.4d**). Remarkably, NRG1 β (H178FSY) had far less phosphorylation in HER4, HER2, or ERK and phosphor-HER4 and phosphor-HER2 was only slightly stimulated compared to NRG1 β (WT) treated cells. This result suggests that NRG1 β (H178FSY) covalent mechanism had changed the signaling kinetics of the HER2/HER4 receptors.

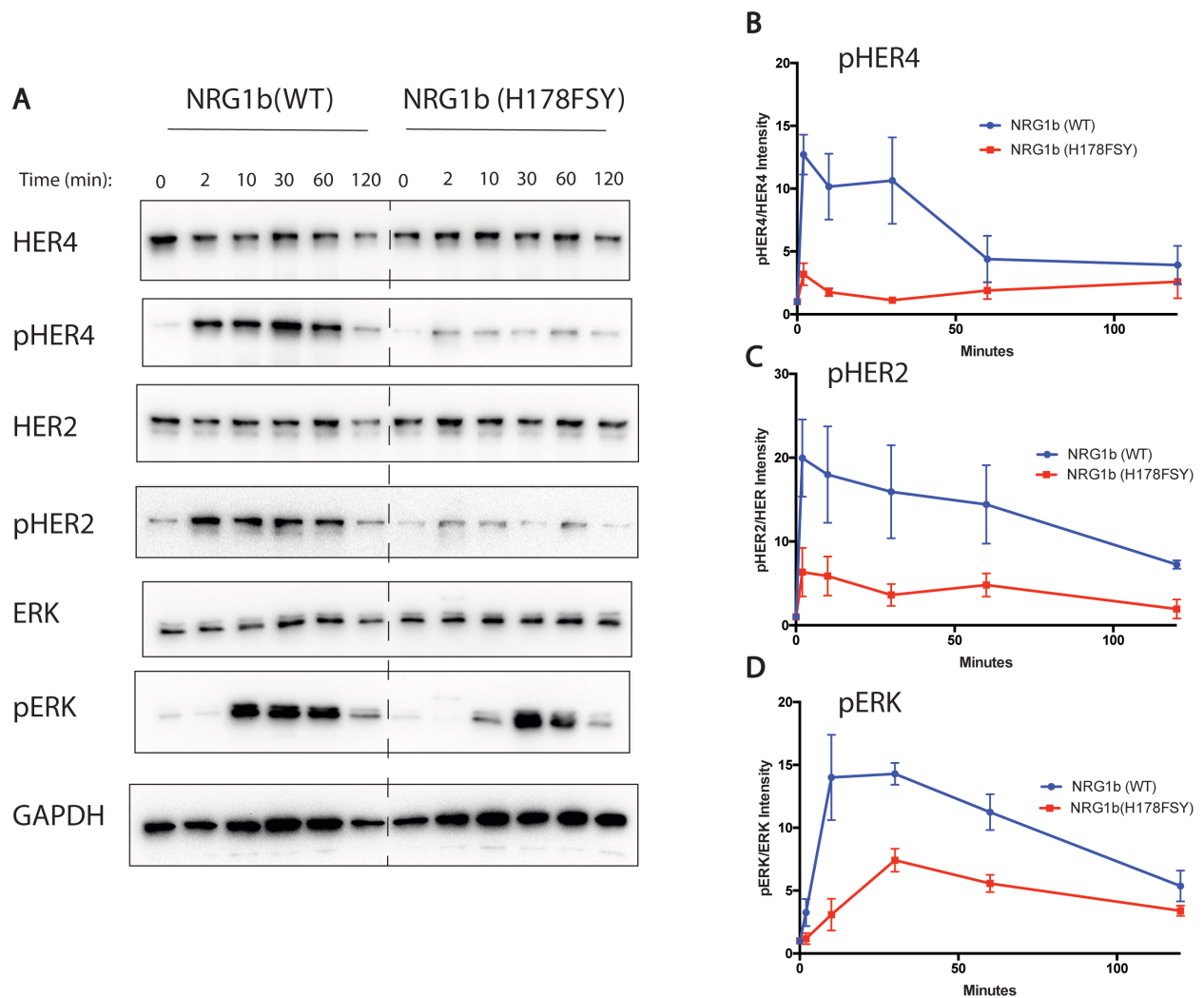


Figure 4.4: NRG1 β (H178FSY) inhibits HER2/HER4 signaling. (A) NIH/3T3 cell line expressing HER2(V956R)/HER4(I712Q) was stimulated with either 100 nM NRG1 β (WT) or 100 nM NRG1 β (H178FSY) and quenched at time points between 0-120min. Western blot analysis was done to detect phosphorylation of HER4, HER2, and ERK showing NRG1 β (H178FSY) had far less activation compared to NRG1 β (WT). The phosphorylation kinetics was measured with densitometry and (B) $\frac{pHER4/HER4}{pHER4(t=0)/HER4(t=0)}$, (C) $\frac{pHER2/HER2}{pHER2(t=0)/HER2(t=0)}$, (D) $\frac{pERK/ERK}{pERK(t=0)/ERK(t=0)}$, was plotted against time. Error bars represent s.e.m., n=3 independent experiments.

To further test whether NRG1 β (H178FSY) could indeed antagonize the HER2/HER4 receptor, we hypothesized that pretreating the NIH/3T3 cells stably expressing HER2(V956R)/HER4(I712Q) with NRG1 β (H178FSY) could prevent the receptors from activating even with NRG1 β (WT) stimulation. We pretreated the cells with either PBS or NRG1 β

(H178FSY) for 10 min and start the stimulation with NRG1 β (WT) and observed the phosphorylation after several different timepoints (**Fig. 4.5a**). While the PBS treated cells had normal activation response, the NRG1 β (H178FSY)-pretreated cells were not able to activate as similar lack of phosphorylation was observed in HER4, HER2 and ERK (**Fig. 4.5b, 4.5c, and 4.5d**). Taken together, not only can NRG1 β (H178FSY) treated cells not activate the receptor, the covalent mechanism makes NRG1 β (H178FSY) an antagonist towards cells expressing HER2/HER4.

NRG1 β (H178FSY) inhibits cell proliferation in primary cardiomyocytes

The binding of NRG1 β onto HER4 plays an important role in cardiomyocyte proliferation. Specifically, the ternary complex of NRG1 β , HER2, and HER4 has been previously shown to affect the ability of primary rat cardiomyocytes to promote DNA synthesis.¹³ To evaluate how NRG1 β (H178FSY) could promote different cellular responses, we treated primary rat cardiomyocytes with either NRG1 β (WT), NRG1 β (H178FSY), or 0.1% BSA and performed an EdU assay which quantifies cell proliferation via DNA synthesis (**Fig. 4.5e**). While NRG1 β (WT) induced significantly more DNA synthesis compared to the 0.1% BSA control NRG1 β (H178FSY) did not significantly induce synthesis. This result is consistent with the observation that NRG1 β (H178FSY) does not promote signaling and antagonizes the HER2/HER4 receptor complex.

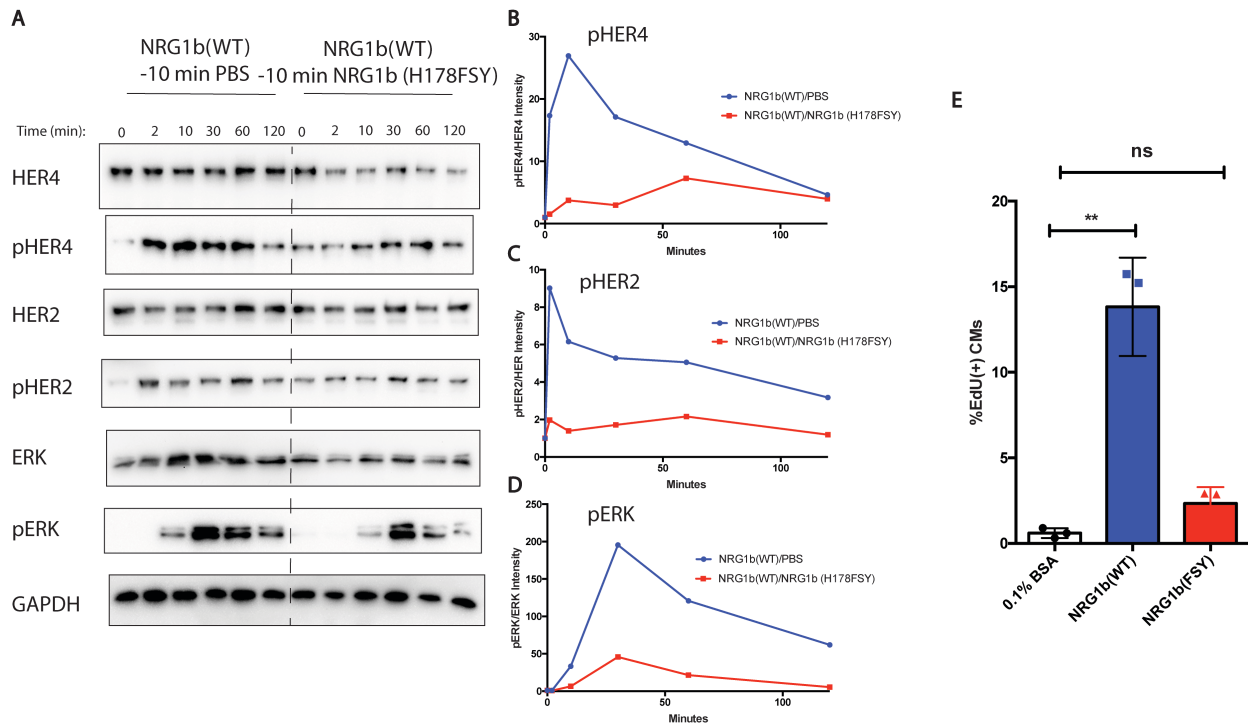


Figure 4.5: NRG1 β (H178FSY) blocks HER2/HER4 activation and inhibits cardiomyocyte cell proliferation. (A) Stimulation of NIH/3T3 cell line expressing HER2(V956R)/HER4(I712Q) using 100 nM NRG1 β (WT) that was first pretreated with either PBS or 100 nM NRG1 β (H178FSY). Western blot analysis shows lower signaling over the time course. The phosphorylation kinetics was measured with densitometry and (B) $\frac{pHER4/HER4}{pHER4(t=0)/HER4(t=0)}$, (C) $\frac{pHER2/HER2}{pHER2(t=0)/HER2(t=0)}$, (D) $\frac{pERK/ERK}{pERK(t=0)/ERK(t=0)}$, was plotted against time. (E) Primary rat cardiomyocyte (P0) treated with either 0.1%BSA, NRG1 β (WT), or NRG1 β (H178FSY). DNA synthesis was measured via an EdU assay showing NRG1 β (H178FSY) had far less cell proliferation.

4.4 Discussion

Our study demonstrates the capability of utilizing a PERx strategy to selectively target a specific protein complex and alter its signaling kinetics and cellular outcome through a covalent binding mechanism. Through genetic code expansion, we incorporated bioreactive Uaa FSY into NRG1 β and identified a mutant, NRG1 β (H178FSY), that could selectively crosslink the HER2/HER4 heterodimer complex over HER3 or HER4 homodimer and the HER2/HER3

heterodimer. The covalent mechanism of NRG1 β (H178FSY) was able to inhibit HER2/HER4 signaling and block NRG1 β (WT) from activating the HER2/HER4 receptor complex as well as downstream signaling. Finally, NRG1 β (H178FSY) was able to inhibit cardiomyocyte proliferation which requires HER4 signaling.

Compared to conventional noncovalent protein binders, proteins with a covalent mechanism not only increase the potency and drug-target resident time, but also allow binders to selectively crosslink one complex over another. Indeed, this selectivity has been taken advantage of when designing small molecule drugs that can form covalent bonds only with specific oncogenic mutations making the therapy more specific to that oncoprotein.²⁷ Recently, studies have shown that genetically incorporating FSY into interleukin-2 (IL-2) can selectively promote Treg activation by selectively crosslinking the CD25 receptor over the CD122 and CD132.²⁸ Here, we demonstrate that NRG1 β (H178FSY) can only crosslink the HER2/HER4 heterodimer complex potentially due to the lack of proximal lysine available in the HER2/HER3 heterodimer. The covalent targeting mechanism takes advantage of subtle differences in residue interactions to drive either mutant or protein complex selectivity.

In terms of efficacy, it seems counterintuitive at first that developing a covalent agonist, which can stay on the target longer than a noncovalent counterpart, could antagonize the receptor rather than make a better agonist. However, previous studies in EGFR have shown that altered binding kinetics can drive different signaling responses.⁴ In one case, EREG or EPGN ligands which bind EGFR at lower affinities have shown sustained signaling compared to the high affinity ligand EGF. This change in binding kinetics also changes the cellular responses as EREG and EPGN drive cell differentiation whereas EGF leads to enhanced cell proliferation. Our results further confirm that changing affinity on a ligand can drive different and novel signaling and cellular responses. While

the mechanisms of exactly how ligands with a covalent mechanism could promote distinct cellular signaling remain unclear, manipulating these ligands for different cellular response could have interesting implications for therapy.

4.5 Material and Methods

Reagents:

Primers were synthesized and purified by Integrated DNA Technologies (IDT), and plasmids were sequenced by GENEWIZ. All molecular biology reagents were either obtained from New England Biolabs or Vazyme. His-HRP (Proteintech #HRP66005) and GAPDH-HRP (Proteintech #HRP60004) antibodies were obtained from ProteinTech Group. HER4 (Cat. # 4795), pHER4 (Cat. # 4757), HER2 (Cat. # 2165), pHER2 (Cat. # 2247), HER3 (Cat. #12708) ERK (Cat. # 4696), pERK (Cat. # 4370) antibody was obtained from Cell Signaling Technology.

NRG1 β amino acid sequence:

*MSDKIIHLTDDSFDTDVLKADGAILVDFWAEWCGPCKMIAPILDEIADEYQGKLTVAKLNIDQ
NPGTAPKYGIRGIPTLLLFKNGEVAATKVGALS \mathbf{K} GQLKEFLDANLAGSGSGLEVLFQGPSHL
VKCAEKEKTFCVNGGECFMVKDLSNPSRYLCKCPNEFTGDRCQNYVMASFYKHLGIEG
SGSGSDYKDDDDKAAALEHHHHHHH*

Thyroxine A sequence highlighted in *italics*

Residue H178 in **bold** was the site where FSY was incorporated.

NRG1 β expression and purification:

A thyroxine A (TrxA) was fused to the EGF-like domain of NRG1 β (residues 177-236, NRG1 isoform 6) with a C-terminal Flag and 6x His tags. Plasmid p32a-TrxA-NRG1 β (WT) was transformed into SHuffle T7 Express electrocompetent *E. coli* cells. P32a- TrxA-NRG1 β (H178TAG) and pEvol-FSYRS was co-transformed SHuffle T7 electrocompetent. Transformed bacteria was culture in Terrific broth at 37 °C with either 100 μ g/mL ampicillin only (for NRG1 β (WT)) or 100 μ g /mL ampicillin and 34 μ g /mL chloramphenicol (for NRG1 β (H178TAG)). For

NRG1 β (WT), the culture was induced with 1 mM IPTG and for NRG1 β (H178TAG), the culture was induced with 0.2% arabinose and 1 mM IPTG once OD₆₀₀ reached 0.9. For NRG1 β (H178TAG), 1.5 mM FSY was added right before induction. The expression was induced for 24 h at 25 °C, and the bacterial pellets were collected by centrifugation at 8000 g for 15 min.

The bacterial pellets were resuspended in lysis buffer (25 mM sodium phosphate, 500 mM NaCl, 1 mg/mL lysozyme, 0.1 mg/mL DNase, and protease inhibitor; pH 7.5). The resuspended pellets were sonicated until thoroughly lysed. The lysate was clarified through ultracentrifugation and incubated with Flag beads for 1h at 4 °C while rotating. After incubation, the beads were centrifuged, and the supernatant was removed. The Flag beads were then washed with cold PBS (pH 7.4) before incubating with Flag peptide elution (500 ug/mL) for 1h at 4 °C. After elution, the Flag beads were filtered out and the elution was buffer exchanged to PBS (pH 7.4) via 10K concentrator

Small Mutant Screen to Identify Crosslinking Site:

The expression of HER receptors in Expi293 cells was described previously. Shortly, HER2 and HER3 or HER2 and HER4 constructs were transfected into 60 mL of Expi293 mammalian cell suspension following standard expression protocol (Life Technologies). The cells were collected, flash froze and stored at -80. The cells were then defrosted and resuspended with lysis buffer (50 mM Tris-HCl pH 7.4, 150 mM NaCl, 1 mM NaVO₃, 1 mM NaF, 1 mM EDTA, protease inhibitors, DNase I, and 1% n-dodecyl- β -D-maltoside (DDM) (Inalco)) and lysed for 2 h while rotating at 4 °C. The lysate was then clarified through ultracentrifugation.

The NRG1 β mutants were expression was described above; the lysate was clarified through ultracentrifugation and a 0.44 μ M filter and incubated with Flag beads for 1 h. The Flag beads

were then washed and incubated with HER2/HER3 or HER2/HER4 lysate overnight while rotating at 4 °C. After incubation beads were centrifuged and supernatant was removed. The beads were washed with TBS with 0.5 mM DDM and eluted with Flag peptide elution (500 ug/mL) for 1h at 4 °C. 4x Laemmli sample buffer (Bio Rad, Cat# 161-0747) with 2-mercaptoethanol was added to the elution and heated at 95 °C for 10 min. The samples were separated on SDS-PAGE and analyzed by Western blot. For Western blotting, the PVDF membrane was blocked with 5% milk for 1 h at RT while rocking. The membrane was then treated with 1:10000 anti-his monoclonal antibody (Proteintech #HRP66005) in 5% milk at RT while rocking. The membrane was then washed three times with TBST before imaging.

Crosslinking of NRG1 β on NIH3t3 cells expression HER receptors

Cloning of full length HER receptors in pCDNA4 expression vector was previously described. 0.15 million NIH/3T3 cells were seeded into each well of a 6-well plate and transfected with 3 μ g total DNA (1.5 μ g per receptor plasmid or 1.5 μ g + 1.5 μ g empty vector for single receptor controls) using Lipofectamine p300 transfection kit. After 48h, the cells were treated with either PBS, 0.25 μ M NRG1 β (WT), or 0.25 μ M NRG1 β (H178TAG). After 5 h incubation, the cells were washed twice with 1X PBS and dissociated with enzyme free dissociation buffer (Gibco). The cells were collected and lysed with 100 uL Pierce RIPA buffer with protease inhibitor cocktail for 1 h on ice. The cell lysates were analyzed with western blots using antibodies specific for Hisx6 (Proteintech #HRP66005, 1:10000 dilution), HER2 (Cell signaling #2165S 1:1000 dilution), HER3 (Cell signaling #12708 1:500 dilution), HER4 (Cell signaling #4795 1:1000 dilution) or GAPDH (Proteintech #HRP60004, 1:10000 dilution).

NRG1 β -stimulated signaling assay

Stable cell lines were made via stable transfection of HER2(V956R)/HER4(I712Q) using lentiviral infection of NIH/3T3 cell line. These NIH/3T3 cells expressing HER2(V956R)/HER4(I712Q) were stimulated with either 100 nM NRG1 β (WT) or 100 nM NRG1 β (H178TAG) at 37 °C. For pretreatment, cells were incubated with either PBS or 100 nM NRG1 β (H178TAG). To quench the stimulation, the cells were cooled on ice and washed with cold PBS 2 times and lysed with 400 μ L RIPA buffer (Complete protease inhibitor, 1 mM sodium orthovanadate, 1 mM sodium fluoride in PBS). The lysate was collected and analyzed with western blot with antibodies specific for HER2 (Cell signaling #2165S, 1:1000 dilution), pHER2 (Cell signaling #2247, 1:500 dilution), HER4 (Cell signaling #4795, 1:1000 dilution), pHER4 (Cell signaling #4757, 1:1000 dilution), ERK (Cell signaling #4696, 1:1000 dilution), pERK (Cell signaling #4370, 1:1000 dilution), or GAPDH (Proteintech #HRP60004, 1:10000 dilution).

NRG1 β -stimulated cardiomyocyte assay

P0 primary cardiomyocytes were isolated from male rats and cultured in serum-containing media for 48h. The begin the stimulation, the media was exchanged with serum-free media with wither 0.1% BSA, 50 nM NRG1 β (WT), or 50 nM NRG1 β (H178TAG). For the detection of DNA synthesis, 20 μ M 5'-Ethyneyl-2'-deoxyuridine (EdU) was also added and the cells incubated for 4 days. To visualize EdU-incorporated cardiomyocytes the cells were stained with Cardiac Troponin T (Thermo Scientific; Cat No #MS295P1), PCM1 (Proteintech; Cat No #19856-1-AP), as well as DAPI. CMs were counted as EdU+ if positive for all signals–EdU overlapping with PCM1 and DAPI, within the nuclear pocket of a cTnT+ cell body (to avoid counting potential EdU+

fibroblasts). Total number of EdU+ CMs counted was normalized to the total number of CMs (PCM1+;cTnT+; DAPI+) in a given well.

4.6 Supplemental Figures

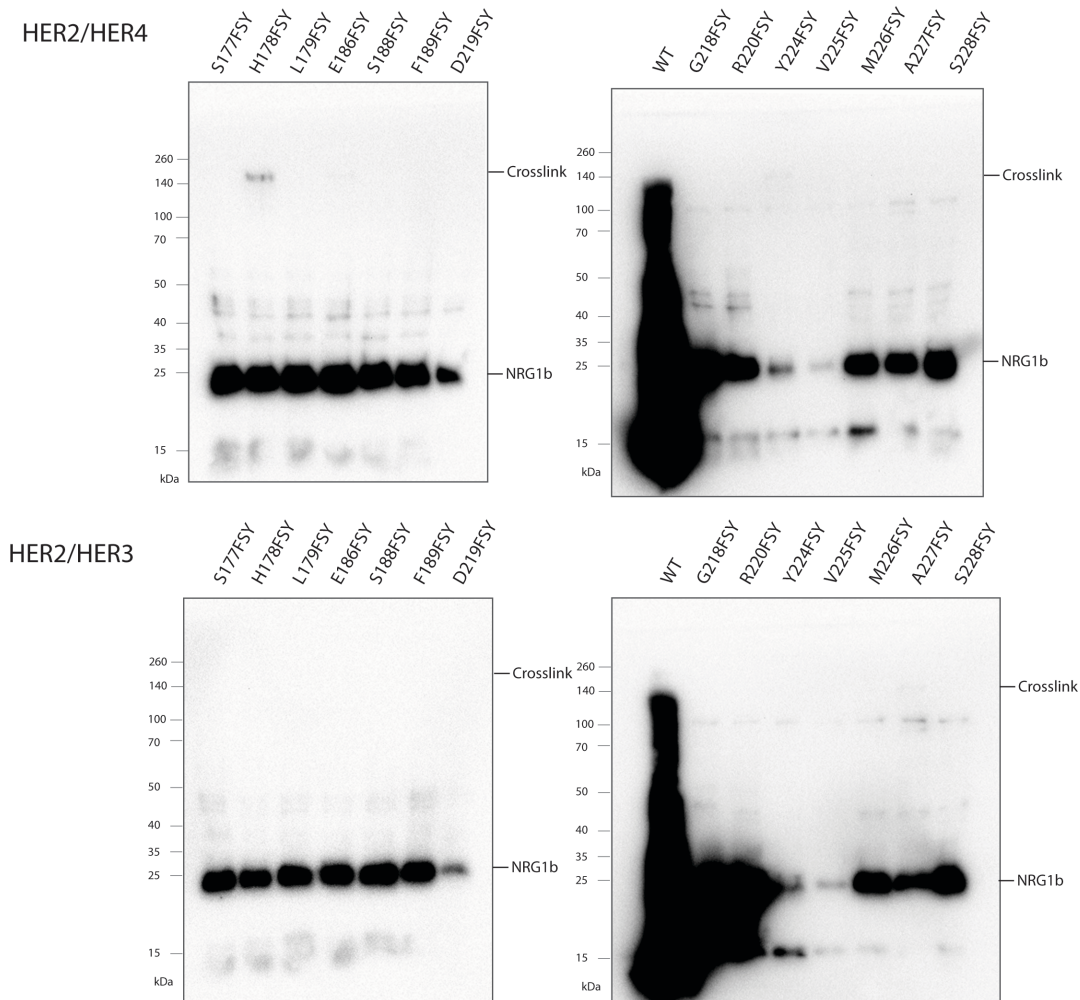


Figure 4.S1: Small mutant screen reveals NRG1 β (H178FSY) crosslinks HER2/HER4 but not HER2/HER3. Western blot analysis was of NIH/3T3 cells expressing either HER2/HER4 or HER2/HER3 treated with various NRG1 β FSY-mutants. Only NRG1 β (H178FSY) was identified to crosslink HER2/HER4.

4.7 References

- (1) Wieduwilt, M. J.; Moasser, M. M. The Epidermal Growth Factor Receptor Family: Biology Driving Targeted Therapeutics. *Cell Mol Life Sci* 2008, *65* (10), 1566–1584. <https://doi.org/10.1007/s00018-008-7440-8>.
- (2) Yarden, Y.; Sliwkowski, M. X. Untangling the ErbB Signalling Network. *Nat Rev Mol Cell Bio* 2001, *2* (2), 127–137. <https://doi.org/10.1038/35052073>.
- (3) Sergina, N. V.; Moasser, M. M. The HER Family and Cancer: Emerging Molecular Mechanisms and Therapeutic Targets. *Trends Mol Med* 2007, *13* (12), 527–534. <https://doi.org/10.1016/j.molmed.2007.10.002>.
- (4) Freed, D. M.; Bessman, N. J.; Kiyatkin, A.; Salazar-Cavazos, E.; Byrne, P. O.; Moore, J. O.; Valley, C. C.; Ferguson, K. M.; Leahy, D. J.; Lidke, D. S.; Lemmon, M. A. EGFR Ligands Differentially Stabilize Receptor Dimers to Specify Signaling Kinetics. *Cell* 2017, *171* (3), 683–695.e18. <https://doi.org/10.1016/j.cell.2017.09.017>.
- (5) Mota, J. M.; Collier, K. A.; Costa, R. L. B.; Taxter, T.; Kalyan, A.; Leite, C. A.; Chae, Y. K.; Giles, F. J.; Carneiro, B. A. A Comprehensive Review of Heregulins, HER3, and HER4 as Potential Therapeutic Targets in Cancer. *Oncotarget* 2017, *8* (51), 89284–89306. <https://doi.org/10.18632/oncotarget.18467>.
- (6) Falls, D. L. Neuregulins: Functions, Forms, and Signaling Strategies. *Exp. Cell Res.* 2003, *284* (1), 14–30. [https://doi.org/10.1016/s0014-4827\(02\)00102-7](https://doi.org/10.1016/s0014-4827(02)00102-7).
- (7) Sithanandam, G.; Anderson, L. M. The ERBB3 Receptor in Cancer and Cancer Gene Therapy. *Cancer Gene Ther.* 2008, *15* (7), 413–448. <https://doi.org/10.1038/cgt.2008.15>.
- (8) Schram, A. M.; Odintsov, I.; Espinosa-Cotton, M.; Khodos, I.; Sisso, W. J.; Mattar, M. S.; Lui, A. J. W.; Vojnic, M.; Shameem, S. H.; Chauhan, T.; Torrisi, J.; Ford, J.; O'Connor, M. N.; Geuijen,

- C. A. W.; Schackmann, R. C.; Bueren, J. J. L. van; Wasserman, E.; Stanchina, E. de; O'Reilly, E. M.; Ladanyi, M.; Drilon, A.; Somwar, R. Zenocutuzumab, a HER2xHER3 Bispecific Antibody, Is Effective Therapy for Tumors Driven by NRG1 Gene Rearrangements. *Cancer Discov.* 2022, *12* (5), candisc.1119.2021. <https://doi.org/10.1158/2159-8290.cd-21-1119>.
- (9) Seroogy, K. B.; Dickerson, J. W.; Cassella, S. N.; Zhang-Auberson, L. Handbook of Biologically Active Peptides (Second Edition). *Sect. XVIII: Neurotrophic Pept.* 2013, 1633–1638. <https://doi.org/10.1016/b978-0-12-385095-9.00223-2>.
- (10) Xu, Y.; Li, X.; Zhou, M. Neuregulin-1/ErbB Signaling: A Druggable Target for Treating Heart Failure. *Curr. Opin. Pharmacol.* 2009, *9* (2), 214–219. <https://doi.org/10.1016/j.coph.2008.11.004>.
- (11) Lenihan, D. J.; Anderson, S. A.; Lenneman, C. G.; Brittain, E.; Muldowney, J. A. S.; Mendes, L.; Zhao, P. Z.; Iaci, J.; Frohwein, S.; Zolty, R.; Eisen, A.; Sawyer, D. B.; Caggiano, A. O. A Phase I, Single Ascending Dose Study of Cimaglermin Alfa (Neuregulin 1 β 3) in Patients With Systolic Dysfunction and Heart Failure. *JACC: Basic Transl. Sci.* 2016, *1* (7), 576–586. <https://doi.org/10.1016/j.jacbts.2016.09.005>.
- (12) Jones, J. T.; Akita, R. W.; Sliwkowski, M. X. Binding Specificities and Affinities of Egf Domains for ErbB Receptors. *FEBS Lett.* 1999, *447* (2–3), 227–231. [https://doi.org/10.1016/s0014-5793\(99\)00283-5](https://doi.org/10.1016/s0014-5793(99)00283-5).
- (13) Bersell, K.; Arab, S.; Haring, B.; Kühn, B. Neuregulin1/ErbB4 Signaling Induces Cardiomyocyte Proliferation and Repair of Heart Injury. *Cell* 2009, *138* (2), 257–270. <https://doi.org/10.1016/j.cell.2009.04.060>.
- (14) Wallasch, C.; Weiss, F. U.; Niederfellner, G.; Jallal, B.; Issing, W.; Ullrich, A. Heregulin-dependent Regulation of HER2/Neu Oncogenic Signaling by Heterodimerization with

- HER3. *EMBO J.* 1995, *14* (17), 4267–4275. <https://doi.org/10.1002/j.1460-2075.1995.tb00101.x>.
- (15) Suter, T. M.; Cook-Bruns, N.; Barton, C. Cardiotoxicity Associated with Trastuzumab (Herceptin) Therapy in the Treatment of Metastatic *Breast Cancer*. *Breast* 2004, *13* (3), 173–183. <https://doi.org/10.1016/j.breast.2003.09.002>.
- (16) Jay, S. M.; Kurtagic, E.; Alvarez, L. M.; Picciotto, S. de; Sanchez, E.; Hawkins, J. F.; Prince, R. N.; Guerrero, Y.; Treasure, C. L.; Lee, R. T.; Griffith, L. G. Engineered Bivalent Ligands to Bias ErbB Receptor-Mediated Signaling and Phenotypes*. *J. Biol. Chem.* 2011, *286* (31), 27729–27740. <https://doi.org/10.1074/jbc.m111.221093>.
- (17) Li, Q.; Chen, Q.; Klauser, P. C.; Li, M.; Zheng, F.; Wang, N.; Li, X.; Zhang, Q.; Fu, X.; Wang, Q.; Xu, Y.; Wang, L. Developing Covalent Protein Drugs via Proximity-Enabled Reactive Therapeutics. *Cell* 2020, *182* (1), 85-97.e16. <https://doi.org/10.1016/j.cell.2020.05.028>.
- (18) Yu, B.; Li, S.; Tabata, T.; Wang, N.; Cao, L.; Kumar, G. R.; Sun, W.; Liu, J.; Ott, M.; Wang, L. Accelerating PERx Reaction Enables Covalent Nanobodies for Potent Neutralization of SARS-CoV-2 and Variants. *Chem* 2022, *8* (10), 2766–2783. <https://doi.org/10.1016/j.chempr.2022.07.012>.
- (19) Klauser, P. C.; Chopra, S.; Cao, L.; Bobba, K. N.; Yu, B.; Seo, Y.; Chan, E.; Flavell, R. R.; Evans, M. J.; Wang, L. Covalent Proteins as Targeted Radionuclide Therapies Enhance Antitumor Effects. *ACS Cent. Sci.* 2023, *9* (6), 1241–1251. <https://doi.org/10.1021/acscentsci.3c00288>.
- (20) Singh, J.; Petter, R. C.; Baillie, T. A.; Whitty, A. The Resurgence of Covalent Drugs. *Nat. Rev. Drug Discov.* 2011, *10* (4), 307–317. <https://doi.org/10.1038/nrd3410>.
- (21) Wang, N.; Yang, B.; Fu, C.; Zhu, H.; Zheng, F.; Kobayashi, T.; Liu, J.; Li, S.; Ma, C.; Wang, P. G.; Wang, Q.; Wang, L. Genetically Encoding Fluorosulfate-1 -Tyrosine To React with Lysine,

Histidine, and Tyrosine via SuFEx in Proteins in Vivo. *J Am Chem Soc* 2018, *140* (15), 4995–4999. <https://doi.org/10.1021/jacs.8b01087>.

(22) Zhang, K.; Sun, J.; Liu, N.; Wen, D.; Chang, D.; Thomason, A.; Yoshinaga, S. K. Transformation of NIH 3T3 Cells by HER3 or HER4 Receptors Requires the Presence of HER1 or HER2 (*). *J. Biol. Chem.* 1996, *271* (7), 3884–3890. <https://doi.org/10.1074/jbc.271.7.3884>.

(23) Liu, P.; Cleveland, T. E.; Bouyain, S.; Byrne, P. O.; Longo, P. A.; Leahy, D. J. A Single Ligand Is Sufficient to Activate EGFR Dimers. *Proc. Natl. Acad. Sci.* 2012, *109* (27), 10861–10866. <https://doi.org/10.1073/pnas.1201114109>.

(24) Diwanji, D.; Trenker, R.; Thaker, T. M.; Wang, F.; Agard, D. A.; Verba, K. A.; Jura, N. Structures of the HER2–HER3–NRG1 β Complex Reveal a Dynamic Dimer Interface. *Nature* 2021, *600* (7888), 339–343. <https://doi.org/10.1038/s41586-021-04084-z>.

(25) Zhang, X.; Gureasko, J.; Shen, K.; Cole, P. A.; Kuriyan, J. An Allosteric Mechanism for Activation of the Kinase Domain of Epidermal Growth Factor Receptor. *Cell* 2006, *125* (6), 1137–1149. <https://doi.org/10.1016/j.cell.2006.05.013>.

(26) Ward, M. D.; Leahy, D. J. Kinase Activator-Receiver Preference in ErbB Heterodimers Is Determined by Intracellular Regions and Is Not Coupled to Extracellular Asymmetry*. *J. Biol. Chem.* 2015, *290* (3), 1570–1579. <https://doi.org/10.1074/jbc.m114.612085>.

(27) Ostrem, J. M.; Peters, U.; Sos, M. L.; Wells, J. A.; Shokat, K. M. K-Ras(G12C) Inhibitors Allosterically Control GTP Affinity and Effector Interactions. *Nature* 2013, *503* (7477), 548–551. <https://doi.org/10.1038/nature12796>.

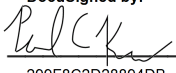
(28) Zhang, B.; Sun, J.; Yuan, Y.; Ji, D.; Sun, Y.; Liu, Y.; Li, S.; Zhu, X.; Wu, X.; Hu, J.; Xie, Q.; Wu, L.; Liu, L.; Cheng, B.; Zhang, Y.; Jiang, L.; Zhao, L.; Yu, F.; Song, W.; Wang, M.; Xu, Y.; Ma, S.; Fei, Y.; Zhang, L.; Zhou, D.; Zhang, X. Proximity-Enabled Covalent Binding of IL-2 to

IL-2R α Selectively Activates Regulatory T Cells and Suppresses Autoimmunity. *Signal Transduct Target Ther* 2023, 8 (1), 28. <https://doi.org/10.1038/s41392-022-01208-3>.

Publishing Agreement

It is the policy of the University to encourage open access and broad distribution of all theses, dissertations, and manuscripts. The Graduate Division will facilitate the distribution of UCSF theses, dissertations, and manuscripts to the UCSF Library for open access and distribution. UCSF will make such theses, dissertations, and manuscripts accessible to the public and will take reasonable steps to preserve these works in perpetuity.

I hereby grant the non-exclusive, perpetual right to The Regents of the University of California to reproduce, publicly display, distribute, preserve, and publish copies of my thesis, dissertation, or manuscript in any form or media, now existing or later derived, including access online for teaching, research, and public service purposes.

DocuSigned by:

299F8C2D28894DB... Author Signature

8/27/2023
Date